

# Acoustic Survey of a 3/8-Scale Automotive Wind Tunnel

---

*Earl R. Booth, Jr.*  
*Langley Research Center • Hampton, Virginia*

*Gary Romberg*  
*Chrysler Technology Center • Auburn Hills, Michigan*

*Larry Hansen*  
*Enviro-Acoustics Company • Minneapolis, Minnesota*

*Ron Lutz*  
*Sverdrup Technologies Corporation • Tullahoma, Tennessee*

The use of trademarks or names of manufacturers in this report is for accurate reporting and does not constitute an official endorsement, either expressed or implied, of such products or manufacturers by the National Aeronautics and Space Administration.

Available electronically at the following URL address: <http://techreports.larc.nasa.gov/ltrs/ltrs.html>

Printed copies available from the following:

NASA Center for AeroSpace Information  
800 Elkridge Landing Road  
Linthicum Heights, MD 21090-2934  
(301) 621-0390

National Technical Information Service (NTIS)  
5285 Port Royal Road  
Springfield, VA 22161-2171  
(703) 487-4650

## Summary

An acoustic survey that consists of insertion loss and flow noise measurements was conducted at key locations around the circuit of a 3/8-scale automotive acoustic wind tunnel. Descriptions of the test, the instrumentation, and the wind tunnel facility are included in the current report, along with data obtained in the test in the form of 1/3-octave-band insertion loss and narrowband flow noise spectral data.

## Introduction

Background noise in acoustic wind tunnel facilities consists of the summation of flow-induced noise sources not caused by the test object itself and nonflow-induced noise sources caused by mechanical and auxiliary systems. Measurements of this noise in the test section are usually included as a matter of course in most acoustic test reports. Although background noise in the test section is important for comparison with test results, the noise is usually generated elsewhere in the tunnel circuit. To date, comprehensive flow and auxiliary system noise data that are gathered around the circuit of acoustic wind tunnel facilities are rarely published. Providing these data for open study will lead to a better understanding of flow noise generation processes which, in turn, will lead to better acoustic wind tunnels. This report is intended to address the gap in the existing literature and to encourage similar data sets to be published from other acoustic test facilities. The data are presented herein with minimal analysis.

The acoustic survey was a collaboration between the National Aeronautics and Space Administration (NASA), Chrysler Technology Center (CTC), Enviro-Acoustics Company Inc., and Sverdrup Technologies, Inc. Each participant in the test envisioned different uses for the resulting data. The NASA participants were interested in having the data provide an experimental database to compare with computational and analytical design methods for designing an acoustic wind tunnel. The proposed National Wind Tunnel Complex (NWTC) will incorporate acoustic testing capabilities and data from this investigation to support the design effort for NWTC facilities. Chrysler built the 3/8-scale automotive wind tunnel as the pilot for a full-scale automotive wind tunnel that will be used primarily for acoustic testing of new automobiles. For Chrysler this test was one of many designed to enhance understanding of this facility in order to improve the capabilities of both the present 3/8-scale facility and especially the future full-scale facility. Enviro-Acoustics manufactured several portions of the acoustic treatment for the pilot facility, such as the boundary-layer removal system and the acoustically treated turning vanes, and intended this test primarily as

a hardware verification test. Finally, Sverdrup Technologies designed the facility based on design specifications from Chrysler and will use the test results to verify that design specifications were met for the pilot tunnel. Each participant in the test recognized and understood the motivations and objectives of the other participants, and each brought various unique contributions and capabilities to the testing effort. The resulting collaborative test effort produced data to fulfill all test requirements and thus to provide a model for future NASA-Industry collaborative efforts.

## Symbols and Abbreviations

$A_{TS}$	test section area (also contraction nozzle exit area), 33 ft <sup>2</sup>
$A/A_{TS}$	ratio of local TScross-sectional area to test section area
B.L.S.	boundary-layer removal system
bw	bandwidth, Hz
$\Delta p_{fan}$	pressure rise produced by the drive fan, lb/ft <sup>2</sup>
$l/d$	ratio length to depth
$M$	Mach number
OASPL	overall sound pressure level, dB re 20 $\mu$ Pa
$p_0$	test section static pressure, lb/in <sup>2</sup>
$q$	dynamic pressure, lb/ft <sup>2</sup>
SPL	sound pressure level, dB re 20 $\mu$ Pa
$T$	temperature inside test section, °F

## Description of 3/8-Scale Automotive Wind Tunnel

The 3/8-scale automotive wind tunnel is a closed-circuit atmospheric pressure automotive wind tunnel. The overall tunnel circuit layout is shown in figure 1. The test section, measuring 4.4 ft high by 7.5 ft wide, can be converted from an open jet test section bounded by a floor with tops and sides open, as shown in the figure, to a slotted-wall test section configuration. In the slotted-wall configuration, 30-percent open-area ratio-ventilated sidewalls and ceiling surround the test section. The floor is nonventilated for both configurations. The tunnel is capable of producing a top speed on the order of 200 mph ( $M = 0.23$ ) in either the slotted or open jet test section configurations. The acoustic calibration measurements were performed with the test section in the open jet configuration.

The test section is enclosed in a plenum chamber that is 9.38 ft high by 16.88 ft wide by 36.25 ft long. The ratio of plenum area to test section cross-sectional area is 4.8. In the open jet configuration, a flow collector is located

17 ft downstream from the contraction exit plane. The collector consists of two sides and a ceiling, each angled  $15^\circ$  from the tunnel centerline. The collector is ventilated by 1-ft-long air vents that are halfway down the length of the collector and at the collector exit. The air vent at the exit of the collector separates the collector from the entrance to the first diffuser.

In addition to the test section and plenum, the wind tunnel circuit consists of low half-angle diffusers, a constant cross-sectional flow area from turn 3 to the contraction, a 6.3:1 contraction ratio nozzle, a honeycomb, and a single turbulence screen. Major wind tunnel circuit elements are briefly described in the following paragraphs.

The first diffuser is 27.75 ft long with a  $2.28^\circ$  equivalent half-angle. Turn 1 has an area ratio  $A/A_{TS}$  of 1.97. The cross-leg diffuser that connects turns 1 and 2 is 14.26 ft long with an equivalent half-angle of  $2.21^\circ$ . Turn 2 has an area ratio of 2.48. The turning vanes are the large, double-circular arc type with a gap-to-chord ratio of 0.41 and were designed based on the concept presented in reference 1. The chord of the turning vanes is 2.65 ft for turns 1 and 2 and 4.98 ft for turns 3 and 4. The positive pressure surfaces of the turning vanes in all four turns have perforated surfaces and are filled with acoustic absorbing material. A debris screen is mounted to the leading edge of the turning vanes in turn 2 to protect the fan from foreign objects carried by the airstream.

The fan section, just downstream of turn 2, has an area ratio  $A/A_{TS}$  of 2.26. The main fan is an axial-type variable-speed system driven by an internal electric motor rated at 1000 hp. The fan diameter is 11.44 ft on a 6-ft diameter hub. The fan has 10 blades and 13 stators and is controllable from 0 to 875 rpm. The fan is housed in an aero-dynamically faired nacelle which is supported by aero-dynamically faired supports. The fan motor is cooled by air circulation through the support struts. Air is drawn from above the tunnel by a cooling fan to the motor and out through the sides of the fan section through vents in the tunnel shell. Operation of the drive motor cooling fan was thought to be a major source of flow noise prior to this test.

The backleg diffuser is 63.97 ft long and has an equivalent half-angle of  $2.96^\circ$ . Turns 3 and 4 both have an area ratio of 6.3. A flow heat exchanger is located in the low-speed cross leg between turns 3 and 4. The cooler is a two-row vertical-staggered round-tube configuration with circular fins. A constant cooling water flow is maintained through the cooler in a counterflow fashion by using a circulation pump, piping, and mixing valves. Chilled water is mixed in as required to maintain a constant airflow temperature, as sensed by instrumentation located near the turbulence screen. This system can

maintain the operating temperature between  $70^\circ\text{F}$  and  $90^\circ\text{F}$  over all operating speeds.

The flow-conditioning section is located upstream of the contraction and consists of an aluminum honeycomb and a stainless-steel turbulence reduction screen. The honeycomb has 3/16-in-wide cells and is 3 in. deep, giving a cell  $l/d$  of 16. The screen is constructed of 0.015-in-diameter woven wire cloth with a wire spacing of 0.064 in. (16 mesh). The screen open area ratio is 58 percent.

A boundary-layer-removal-system (B.L.S.) inlet scoop is located 2.75 ft downstream of the contraction exit plane on the test section floor. This system, when active, removes the boundary layer from the floor of the test section and reinjects the flow into the diffuser. The system is acoustically treated to prevent an increase in test section background noise from B.L.S. operation. The system includes acoustically treated flow removal ducts, flow plenum, flow reinjection ducting, and a flow reinjection slot in the first diffuser floor. The boundary-layer system is driven by a centrifugal fan equipped with a variable-speed drive and an air exhaust to the building exterior. The boundary-layer system is controlled by adjusting the boundary-layer-removal fan speed until the differential pressure measured across the inlet scoop upper lip is zero. Reference 2 presents a complete description of the facility.

## Test Description

The data included herein encompass three parts of the test program carried out in the 3/8-scale automotive wind tunnel: (1) insertion loss measurements of various wind tunnel components, (2) background noise measurements caused by the operation of the boundary-layer removal system and the drive fan cooling motor, and (3) flow noise measurements at key locations around the wind tunnel circuit.

The insertion loss measurement tests were performed to determine the acoustic absorption characteristics of various wind tunnel components (such as the turning vanes) in the absence of flow. The tests were performed by generating a diffuse acoustic field on one side of the component and by comparing simultaneous measurements made on the source side and the transmitted side of the component, as shown schematically in figure 2(a). A photograph of the test setup for insertion loss measurement in turn 3 is presented in figure 2(b).

Measurements of background noise caused by operation of the B.L.S. and the cooling fan for the drive motor were performed to assess the contribution to test section background noise made by these systems. The data were measured in the center of the test section with no flow in

the tunnel for a range of B.L.S. motor rpm's and with the cooling fan for the drive motor either on or off.

Flow noise measurements were made at several representative locations around the wind tunnel circuit shown in figure 1. In order to ensure that placement of the microphone in the flow did not adversely affect noise level in the test section, a reference microphone was placed outside the flow adjacent to the test section, shown as position 0 in figure 1. No changes in the reference test section noise level resulted from microphone hardware in the flow at any of the test locations. In figure 3 a photograph of the flow noise test setup in the test section shows both the in-flow microphone at position 1 and the reference microphone at position 0.

## Instrumentation

Data were measured with a B&K 1/2-in. microphone, type 4166, for the source side measurement in the insertion loss tests and the reference microphone measurements in the flow noise tests. Data for the transmitted (data) signal measurement in the insertion loss tests and flow noise measurement around the circuit were measured with a B&K 1-in. microphone, type 4144. With the exception of the 1-in. microphone for the flow test, all microphones were outfitted with standard B&K grid caps and foam windscreens. For the flow noise test, the 1-in. microphone was outfitted with a standard B&K nose cone. The data were recorded on a Nagra portable tape recorder at a tape speed of 7.5 in/sec, which resulted in a usable frequency range of 35 Hz to 20 kHz from the recorded data. Data were also measured on-line by using a B&K model 2133 Spectral Analyzer, which provided 1/12-octave-band on-line data plots during the test. Although the on-line data are not presented in this report, the overall sound pressure values from the on-line data agree with the narrowband data presented in this report to within 1.0 dB.

After the test, the data were digitized from the recorded tapes by using a NASA digital data acquisition system. The data were sampled for 8 sec at a rate of 40000 samples/sec and were low-pass filtered at 20 kHz to prevent aliasing of the data. Data were then written to computer disk for subsequent analysis. The flow noise data were analyzed with a Fourier transform in 18 independent blocks of 16 384 data points to provide 2.441-Hz-bandwidth data for frequencies up to 20 kHz for the flow noise data. The insertion loss data were further processed into the 1/3-octave-band format, since insertion loss testing is more commonly presented in that format.

During posttest data processing, it was discovered that the on-line data system had contaminated the flow noise data in the frequency range of 15 to 17 kHz. Since

the contamination does not represent a physical noise source in the 3/8-scale automotive wind tunnel, these data have been corrected by interpolating the spectral data across the affected frequency range.

## Presentation of Data

Tables 1, 2, and 3 serve as a directory for locating data at specific conditions. Table 1 lists figures 4 through 12 for insertion loss data as a function of location. Since the wind tunnel drive fan is normally assumed to be the largest contributor to test section background noise, the insertion loss data were usually acquired in the direction away from the fan; that is, the generating side was usually closer to the drive fan than to the transmitted side of the component that was being evaluated. An exception to this rule is the data presented in figure 8. Here the insertion loss of turn 3 was evaluated in the direction toward the fan for comparison with figure 7(a), where data were acquired in the direction away from the fan. Insertion loss data are presented in the form of 1/3-octave-band sound pressure level as a function of frequency band. The data presented are the difference in sound power between the generation and transmitted sides of the component that is measured. Data for frequencies less than 178 Hz (200-Hz 1/3-octave band), where acoustic wavelengths are greater than tunnel characteristic dimensions, were disregarded because of expected contamination by standing-wave phenomenon. Since the microphones used on the transmitted and generation sides were different, a calibration test in which both microphones were located on the generation side of turn 1 was used to assess a microphone correction function that represented microphone sensitivity differences, as shown in figure 4. All insertion loss data are corrected with this microphone correction function.

Table 2 lists data (figs. 13 and 14) for background noise measurements in the test section. The noise was caused by operation of the boundary-layer removal system and the cooling fan for the drive motor when there was no flow in the tunnel. Data for these measurements were processed in the same manner as the flow noise measurements described below.

Table 3 lists figures 15 through 29 for flow noise data as a function of location and tunnel dynamic pressure. Other relevant wind tunnel operating conditions are also included in table 3. Data are presented for each measurement location for test section dynamic pressure levels of 20, 40, 60, and 70 lb/ft<sup>2</sup>. Reference test section data are presented once, in figure 15, since these data were independent of the in-flow microphone position. Data are presented in the form of sound pressure level as a function of frequency with a bandwidth of 2.441 Hz. Both test section background noise data and tunnel

circuit flow noise data are presented in three frequency range plots: (1) up to 20 kHz to provide a global view of the data; (2) up to 5 kHz; and (3) up to 1000 Hz to provide details of low frequency data, where the amplitudes were the greatest.

Although an extensive analysis of all these data is beyond the scope of this report, a brief discussion of some of the interesting aspects of the data is provided here. First, as shown in figures 5 and 6, the turning vanes in turns 1 and 2 generally provided between 5 and 10 dB attenuation for frequencies above 300 Hz. Treated turning vanes are not expected to provide much, if any, attenuation for low frequencies, where the acoustic wavelength is much greater than the turning vane chord. Correspondingly, turns 3 and 4, as shown in figures 7(a) and 10, attenuated transmitted acoustic energy somewhat better into slightly lower frequency ranges because of their larger chords. As expected, not much insertion loss was measured in the heat exchanger (fig. 9) and in the honeycomb and screens (fig. 11). Figure 12 shows the contraction provided significant attenuation for frequencies greater than 300 Hz, primarily due to reflection of acoustic energy by the contraction back into the upstream direction. This result suggests that attenuation of noise from the settling chamber to the test section may be reduced by increasing the contraction ratio. Static insertion loss, as measured here, is expected to be greater than the actual attenuation experienced during tunnel operation because of flow convection effects.

Prior to this test, auxiliary systems were thought to contribute significantly to test section background noise. Figures 13 and 14 show that background noise from any of the auxiliary systems is actually of a much smaller magnitude than the flow noise in the test section, measured at a dynamic pressure of 20 lb/sec<sup>2</sup>, as shown in figures 16(a) and 17(a). Interestingly, the flow noise measured in the test section was greater with the boundary-layer system turned off for dynamic pressures of 60 lb/sec<sup>2</sup> and 70 lb/sec<sup>2</sup>, as shown in figures 16(c), 17(c), 16(d), and 17(d). A possible explanation is that improved stability of the test section flow was caused by removal of the boundary layer on the floor during the

high-speed tests. Significantly, drive fan blade harmonics, shown most clearly immediately downstream of the fan station (fig. 24) as the series of tones between 300 and 900 Hz, are not evident upstream of turn 1, as shown in figure 20, but are detectable downstream of the fan at all measurement locations to the contraction, as shown in figures 25 through 29. These data indicate that the fan tones traveled towards the test section via the downstream route, even though the acoustic turning vanes in turns 3 and 4 offer much more acoustic treatment area than is in the turning vanes in turns 1 and 2. Fortunately, the attenuation offered by the contraction (fig. 12), coupled with the acceleration of the flow and the resulting increase of flow noise level, kept fan tones from being evident in the test section.

## Concluding Remarks

An acoustic calibration of a 3/8-scale automotive wind tunnel was performed by a group composed of members from government and industry. Through collaboration this test provided data to meet all the test objectives of each test partner. Data from the test were presented to document flow noise levels and insertion losses that are provided by various flow-conditioning devices around the acoustic wind tunnel circuit, to fill a gap in the existing literature concerning flow noise in acoustic test facilities, and to serve as a database to validate design methods for future wind tunnel facilities.

NASA Langley Research Center  
Hampton, VA 23681-0001  
July 17, 1996

## References

1. Gelder, T. F.; Moore, R. D.; Sanz, J. M.; and McFarland, E. R.: Wind Tunnel Turning Vanes of Modern Design. AIAA-86-0044, Jan. 1986.
2. Romberg, Gary F.; Gunn, James A.; and Lutz, Ronald G.: *The Chrysler 3/8-Scale Pilot Wind Tunnel*. SAE Paper 94-0416, Mar. 1994.

Table 1. Figures for Insertion Loss Data as Function of Wind Tunnel Circuit Location

Figure	Source microphone	Data microphone	Location
4	B	B	Microphone differences
5	B	A	Turn 1
6	D	C	Turn 2
7(a)	E	F	Turn 3
7(b)	E	F	Turn 3 inside corner
7(c)	E	F	Turn 3 outside corner
8	F	E	Turn 3 upstream
9	G	H	Heat exchanger
10	J	K	Turn 4
11	L	M	Screen and honeycomb
12	M	N	Contraction

Table 2. Figures for Background Noise Caused by Operation of B.L.S. and Drive Motor Cooling Fan

Figure	Code	Location	B.L.S. fan speed, rpm	Cooling fan
13(a)	TS1	Test section	500	Off
13(b)	TS1	Test section	1000	Off
13(c)	TS1	Test section	1500	Off
14(a)	TS1	Test section	0	On
14(b)	TS1	Test section	500	On
14(c)	TS1	Test section	1000	On
14(d)	TS1	Test section	1500	On

Table 3. Figures for Flow Noise Data and Relevant Operating Conditions

Figure	Code	Location	$q$ , lb/ft <sup>2</sup>	$p_0$ , lb/in <sup>2</sup>	$T$ , °F	Fan speed, rpm	Fan $\Delta p_{fan}$ , lb/ft <sup>2</sup>	B.L.S.
15(a)	TS0	Reference	19.945	14.300	67.72	383.14	2.930	On
15(b)	TS0	Reference	40.136	14.300	68.73	543.46	5.840	On
15(c)	TS0	Reference	60.268	14.300	70.64	667.71	8.850	On
15(d)	TS0	Reference	69.595	14.300	71.83	721.52	10.340	On
16(a)	TS1	Test section	19.945	14.300	67.72	383.14	2.930	On
16(b)	TS1	Test section	40.136	14.300	68.73	543.46	5.840	On
16(c)	TS1	Test section	60.268	14.300	70.64	667.71	8.850	On
16(d)	TS1	Test section	69.595	14.300	71.83	721.52	10.340	On
17(a)	TS1	Test section	20.196	14.300	70.69	388.13	3.030	Off
17(b)	TS1	Test section	40.293	14.400	72.46	545.64	5.890	Off
17(c)	TS1	Test section	60.570	14.300	73.05	668.18	8.830	Off
17(d)	TS1	Test section	70.515	14.300	72.70	721.54	10.300	Off
18(a)	TS2	Collector plane	19.663	14.300	69.06	382.76	2.930	On
18(b)	TS2	Collector plane	40.128	14.300	69.71	545.63	5.940	On
18(c)	TS2	Collector plane	60.083	14.210	71.40	665.15	8.720	On
18(d)	TS2	Collector plane	70.187	14.300	72.20	721.62	10.300	On
19(a)	A	1st diffuser	19.870	14.310	68.37	383.63	2.920	On
19(b)	A	1st diffuser	39.951	14.300	69.06	545.59	5.870	On
19(c)	A	1st diffuser	60.176	14.300	71.17	667.80	8.790	On
19(d)	A	1st diffuser	69.894	14.300	72.16	719.77	10.310	On
20(a)	A	1st diffuser	20.123	14.310	73.02	386.04	2.960	Off
20(b)	A	1st diffuser	40.521	14.300	74.66	548.97	5.900	Off
20(c)	A	1st diffuser	60.503	14.300	73.70	669.67	8.800	Off
20(d)	A	1st diffuser	70.872	14.300	73.18	724.39	10.400	Off
21(a)	C	1st cross leg	19.856	14.400	69.48	384.83	2.960	On
21(b)	C	1st cross leg	39.883	14.390	69.80	544.57	5.860	On
21(c)	C	1st cross leg	59.806	14.300	68.13	664.64	8.740	On
21(d)	C	1st cross leg	69.855	14.370	72.66	722.27	10.310	On
22(a)	C	1st cross leg	20.378	14.390	72.33	386.52	2.930	Off
22(b)	C	1st cross leg	40.425	14.380	73.39	545.83	5.850	Off
22(c)	C	1st cross leg	61.033	14.340	74.08	670.28	8.870	Off
22(d)	C	1st cross leg	70.538	14.340	73.59	721.03	10.290	Off
23(a)	D	Before fan	19.959	14.230	68.66	384.14	2.930	On
23(b)	D	Before fan	40.005	14.300	69.48	547.85	5.910	On
23(c)	D	Before fan	59.961	14.300	71.02	667.69	8.790	On
23(d)	D	Before fan	70.050	14.300	71.99	720.68	10.280	On
24(a)	D'	After fan	19.889	14.300	67.26	383.73	2.970	On
24(b)	D'	After fan	40.005	14.300	68.48	547.85	5.910	On
24(c)	D'	After fan	59.961	14.300	71.02	667.69	8.790	On
24(d)	D'	After fan	70.050	14.300	71.99	720.68	10.280	On
25(a)	E	Before turn 3	19.889	14.300	67.26	383.73	2.970	On
25(b)	E	Before turn 3	40.008	14.300	67.87	542.45	5.810	On
25(c)	E	Before turn 3	59.797	14.300	69.67	664.97	8.760	On
25(d)	E	Before turn 3	69.933	14.300	73.71	720.35	10.270	On
26(a)	G	After turn 3	19.856	14.300	69.97	383.67	2.980	On
26(b)	G	After turn 3	39.869	14.300	69.90	543.51	5.860	On
26(c)	G	After turn 3	59.976	14.300	71.10	665.02	8.790	On
26(d)	G	After turn 3	70.239	14.300	72.59	719.85	10.270	On
27(a)	J	Before turn 4	19.912	14.300	68.82	383.93	2.980	On
27(b)	J	Before turn 4	39.725	14.300	69.31	542.50	5.810	On
27(c)	J	Before turn 4	59.891	14.300	71.26	666.25	8.730	On
27(d)	J	Before turn 4	70.115	14.300	72.38	718.99	10.270	On
28(a)	L	Settling chamber	19.751	14.300	69.49	383.00	2.950	On
28(b)	L	Settling chamber	40.167	14.300	69.78	543.58	5.840	On
28(c)	L	Settling chamber	59.959	14.300	71.00	664.66	8.720	On
28(d)	L	Settling chamber	70.576	14.300	72.16	722.68	10.370	On
29(a)	M	Contraction	19.725	14.300	69.46	383.87	2.940	On
29(b)	M	Contraction	40.038	14.300	69.66	545.14	5.880	On
29(c)	M	Contraction	59.898	14.300	70.99	666.74	8.830	On
29(d)	M	Contraction	70.177	14.300	72.05	721.42	10.360	On

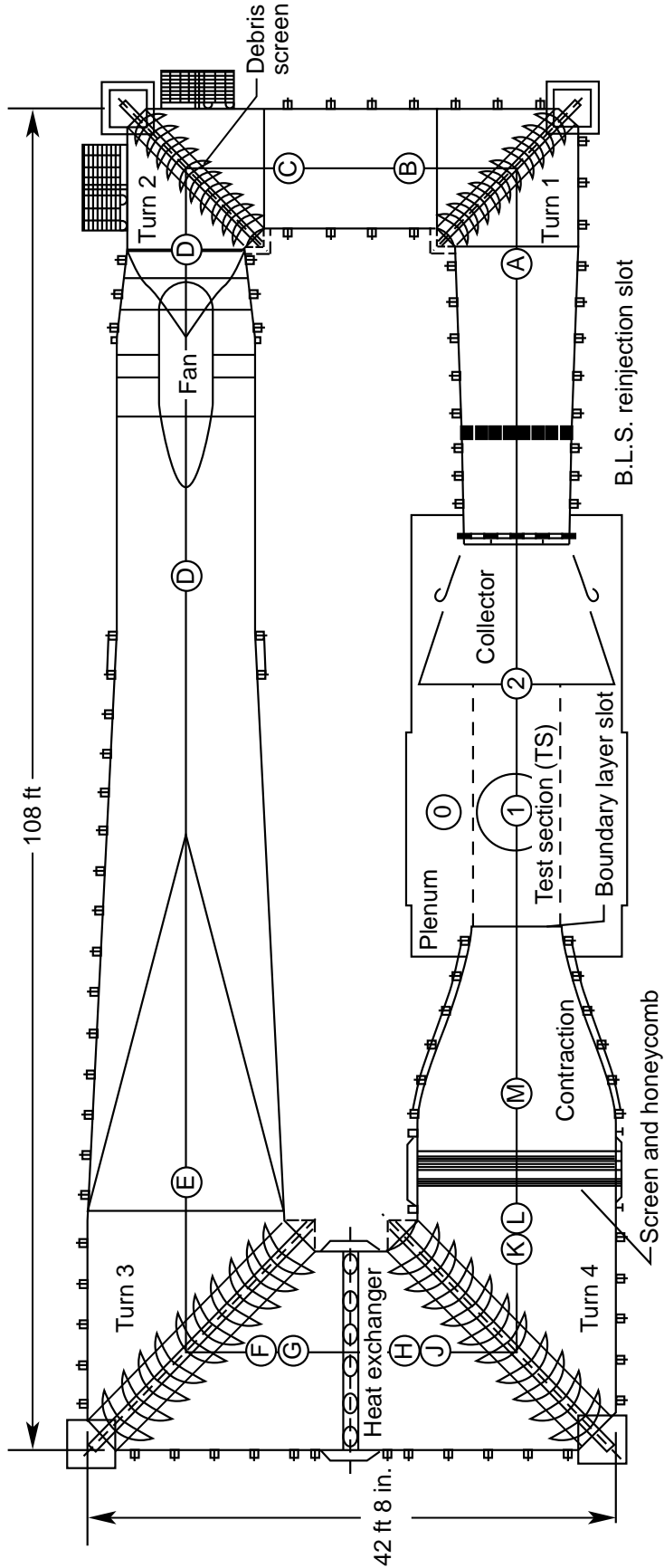
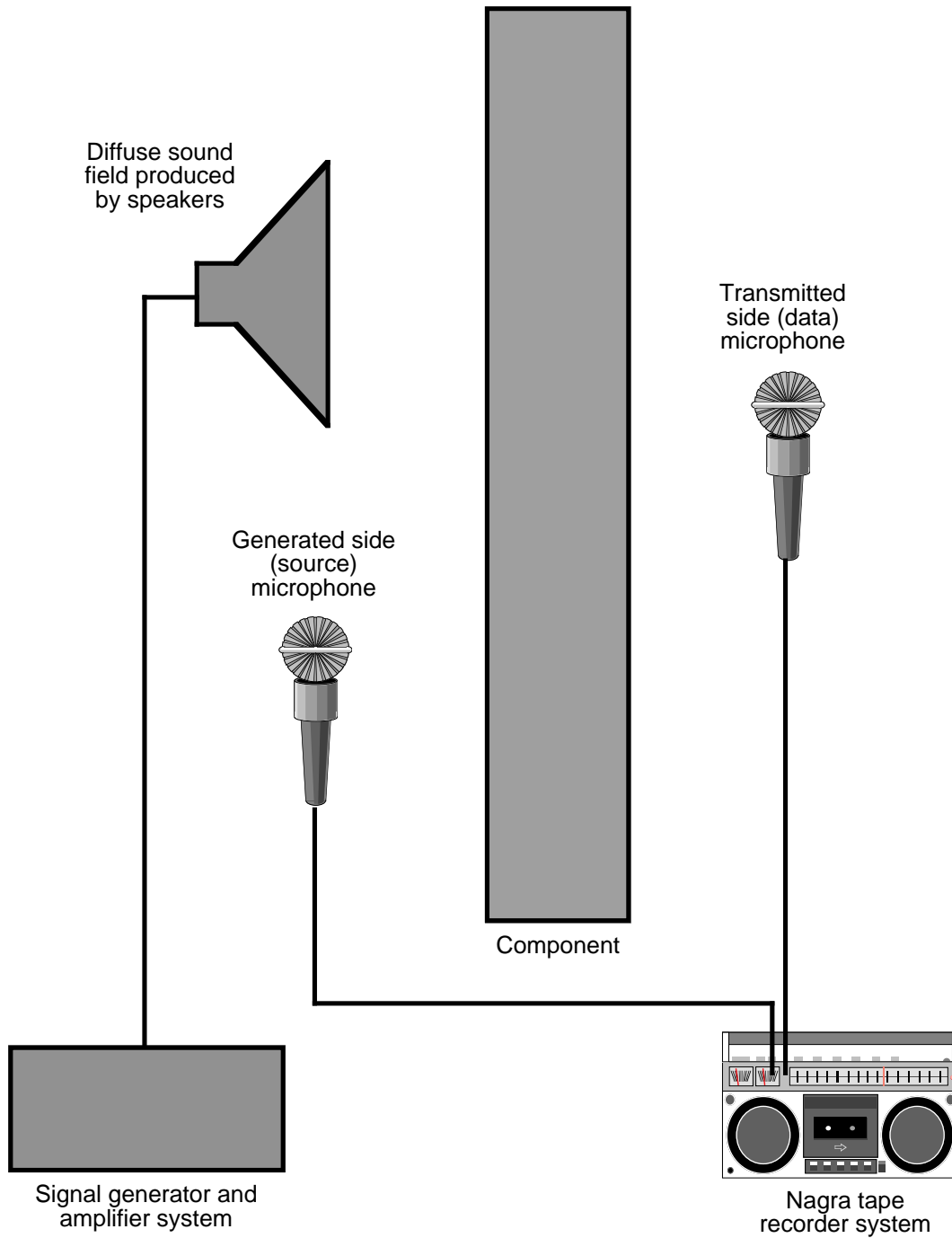
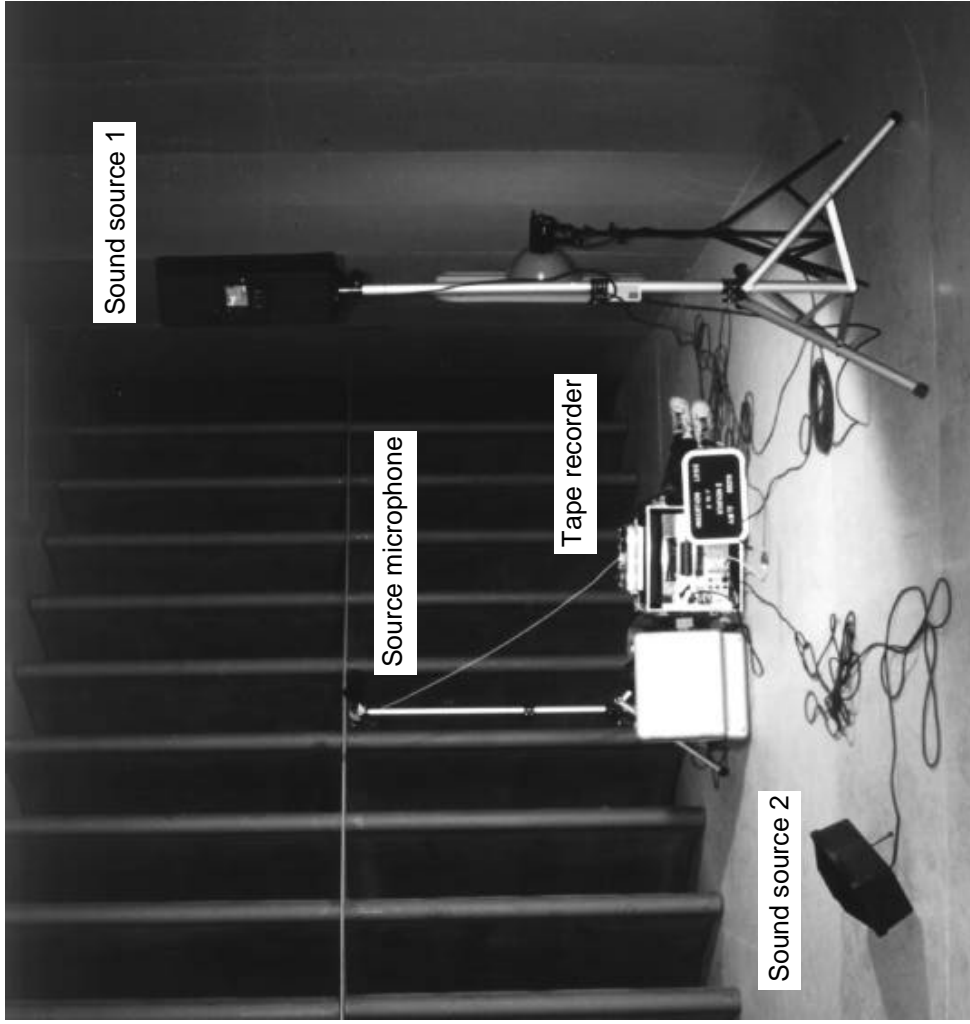
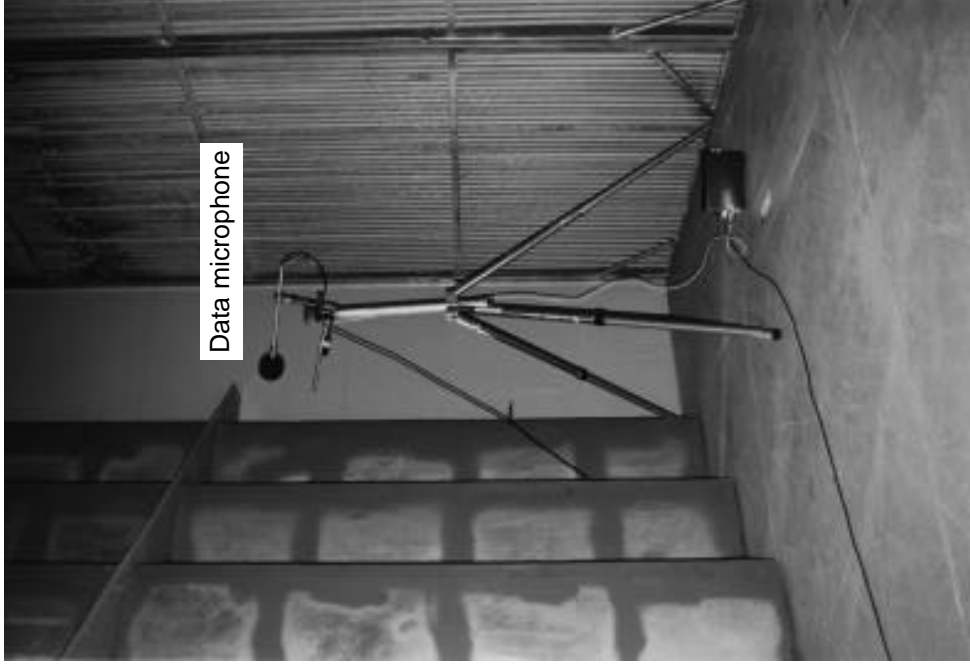


Figure 1. Layout of wind tunnel showing microphone locations.



(a) Sketch of test setup.

Figure 2. Insertion loss test.



(b) Photograph showing typical source and monitor equipment for insertion loss test.

Figure 2. Concluded.



Figure 3. Data and reference microphones in test section for flow noise test.



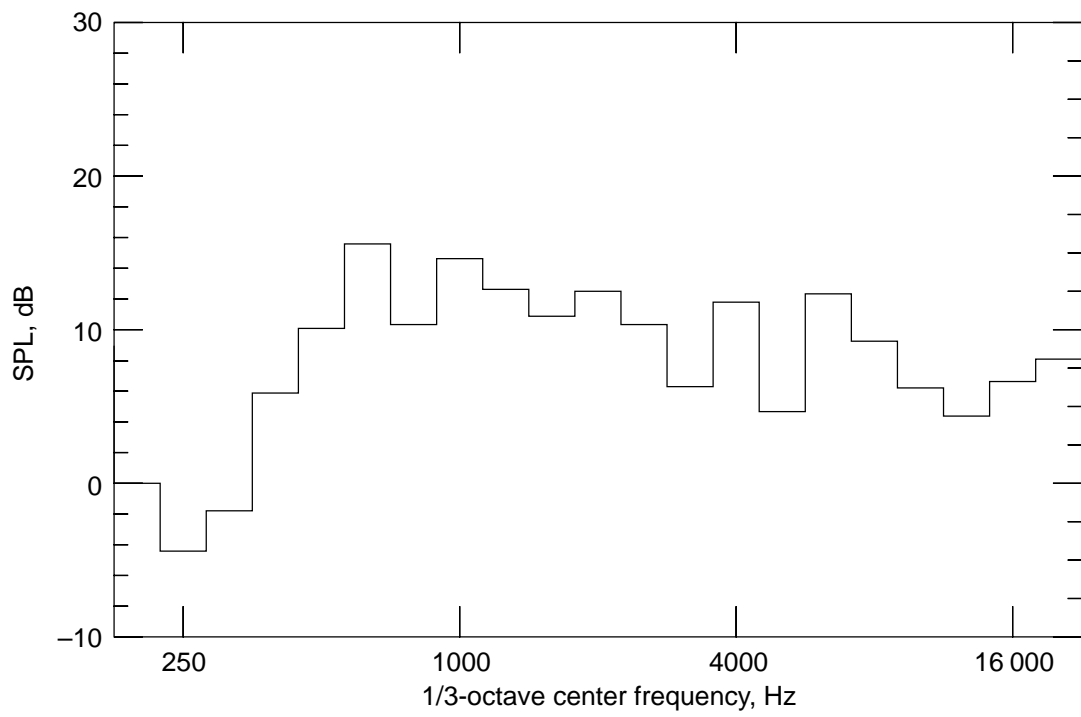
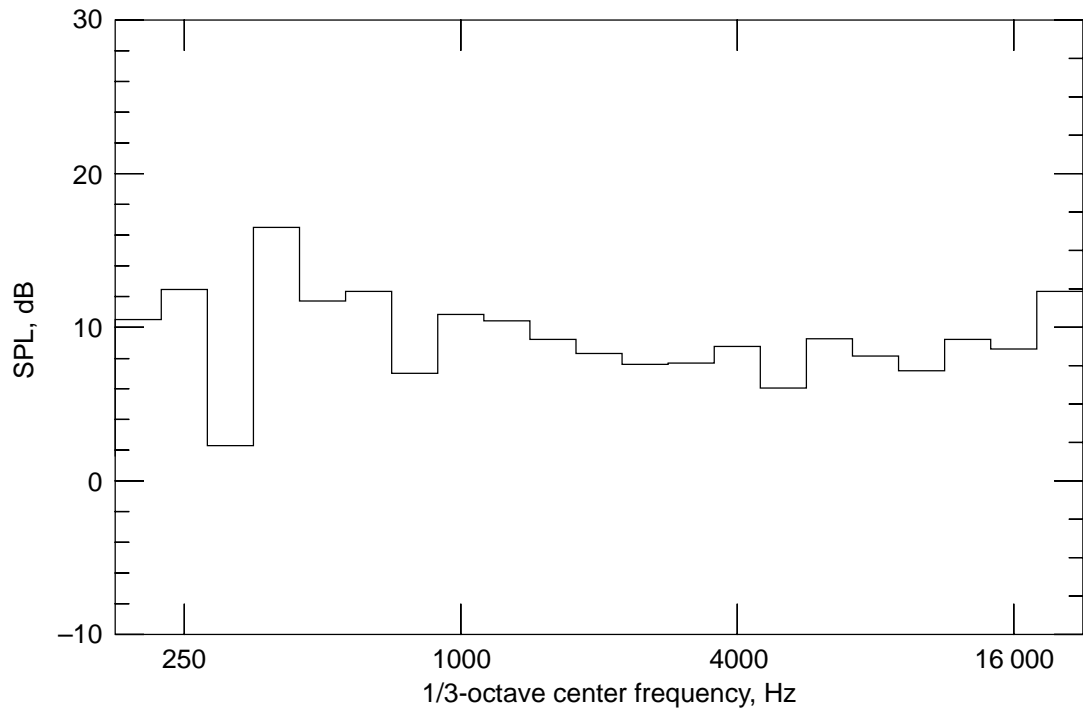
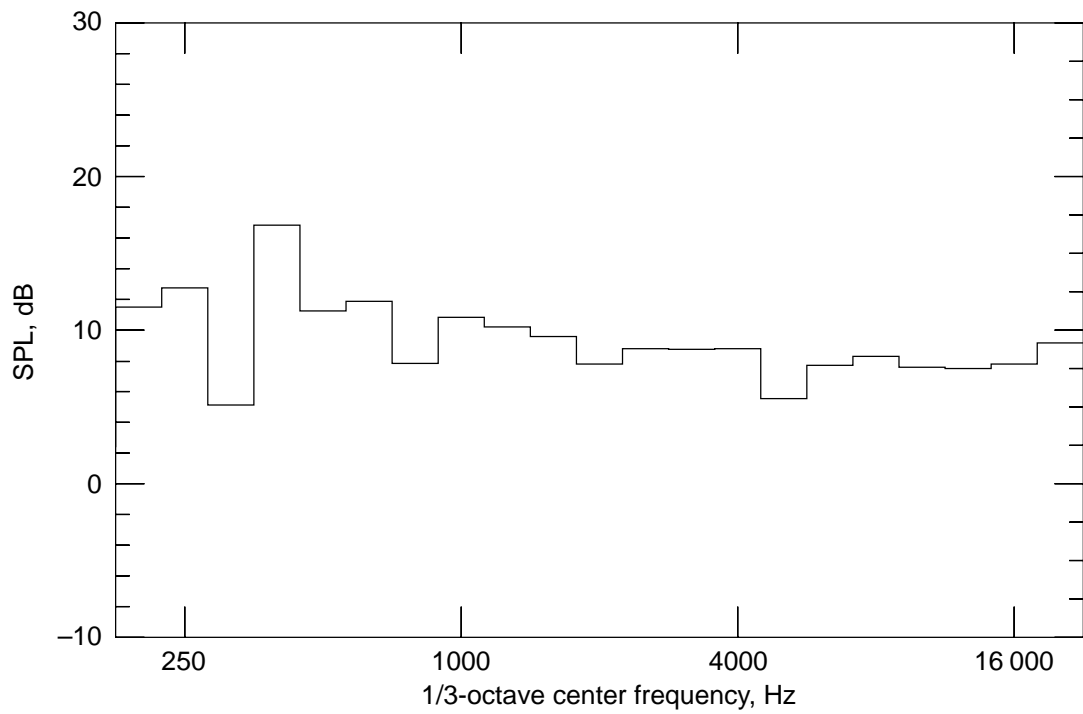


Figure 6. Insertion loss caused by turn 2.

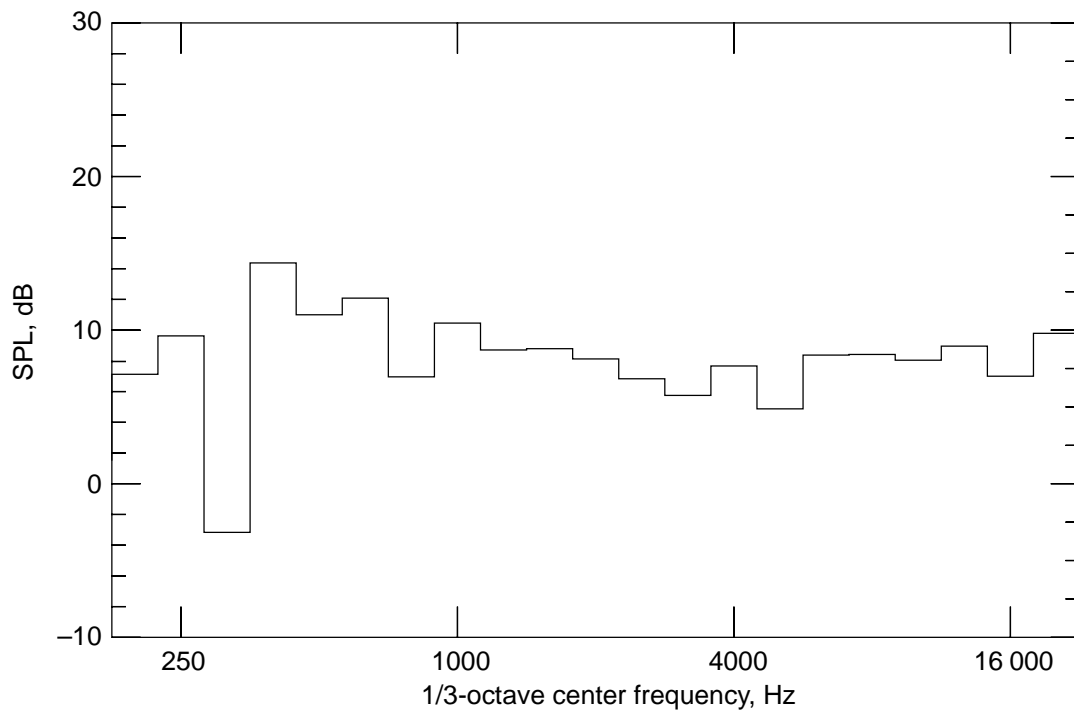


(a) Centerline position.



(b) Inside corner.

Figure 7. Insertion loss caused by turn 3.



(c) Outside corner.

Figure 7. Concluded.

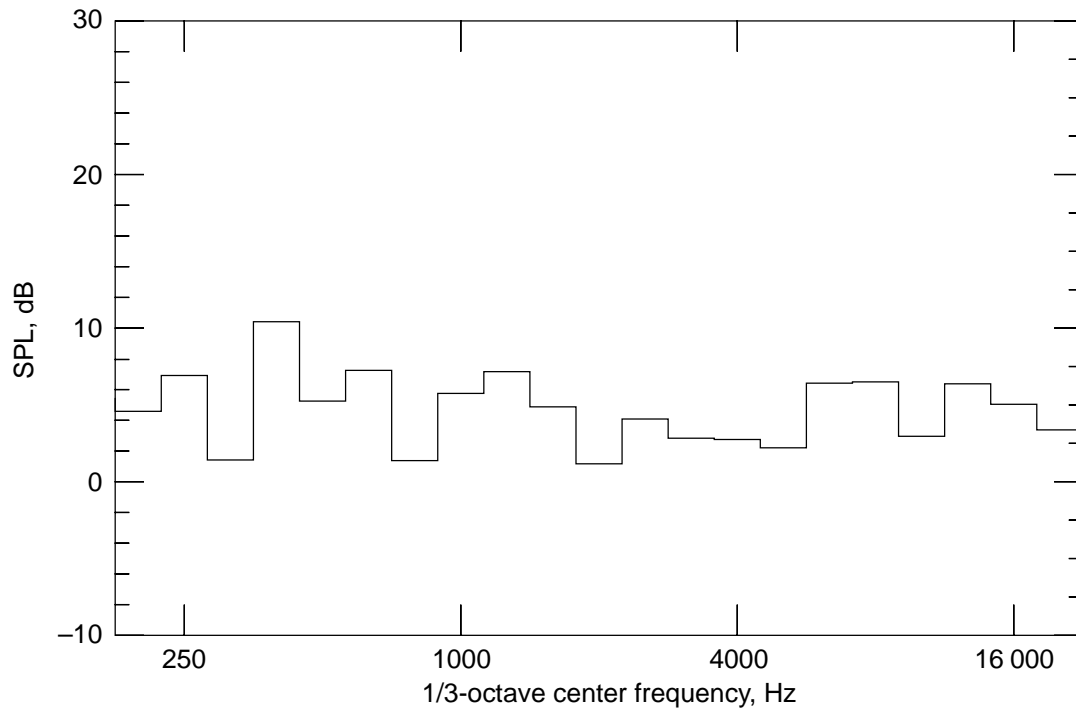


Figure 8. Insertion loss caused by turn 3 in upstream direction.

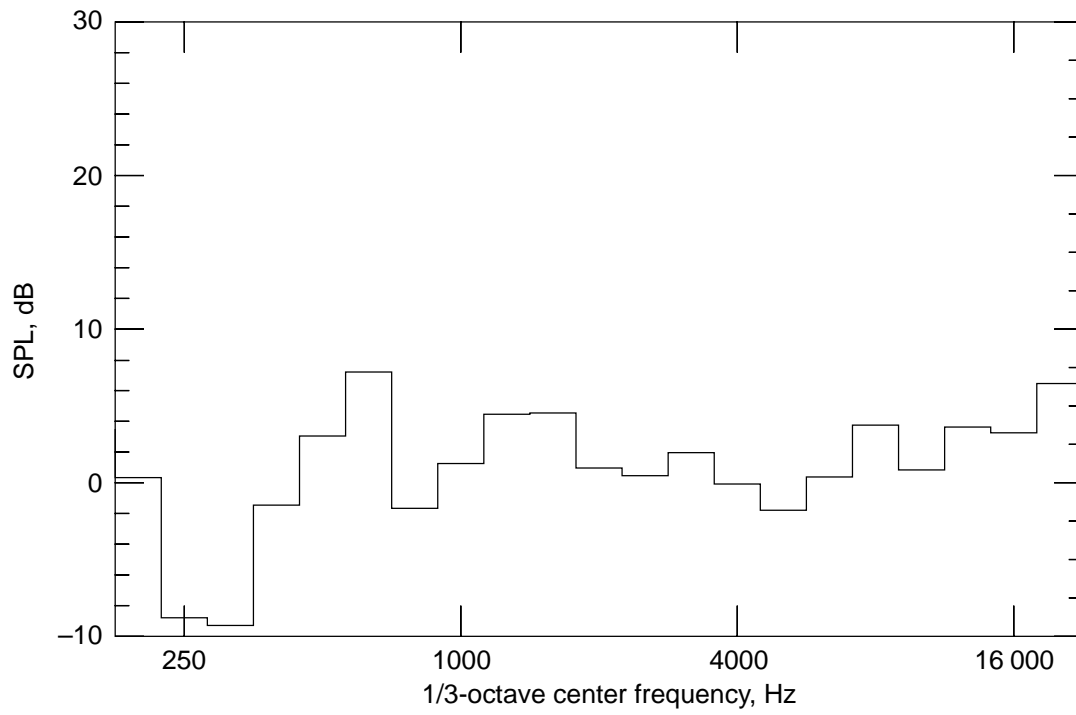


Figure 9. Insertion loss caused by heat exchanger.

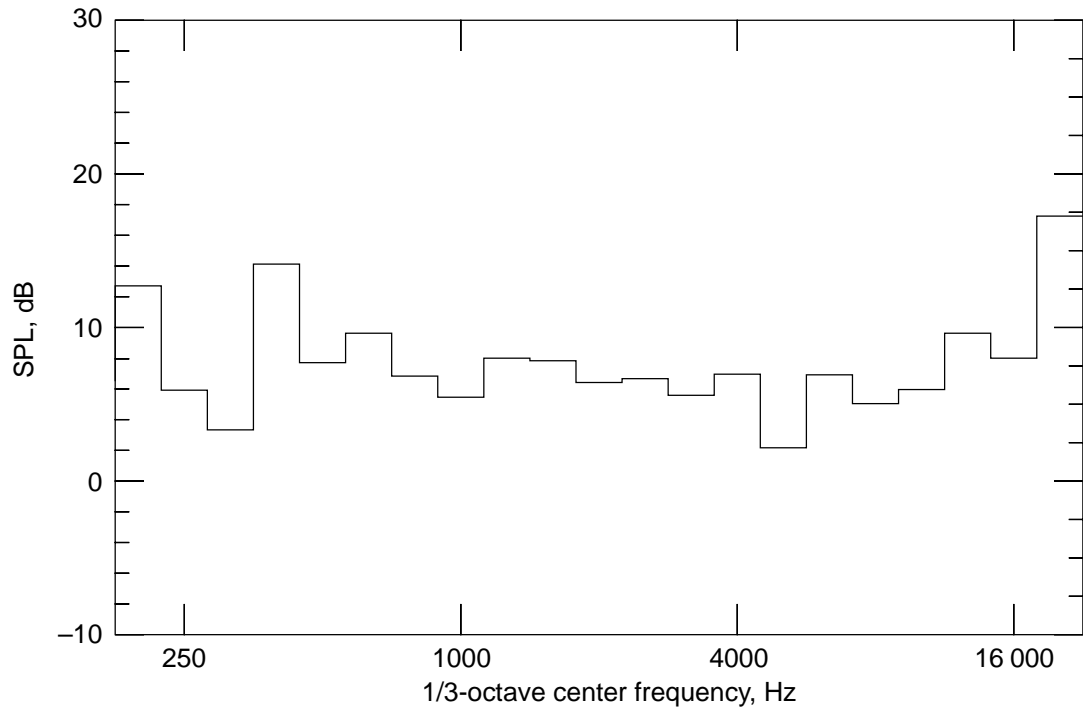


Figure 10. Insertion loss caused by turn 4.

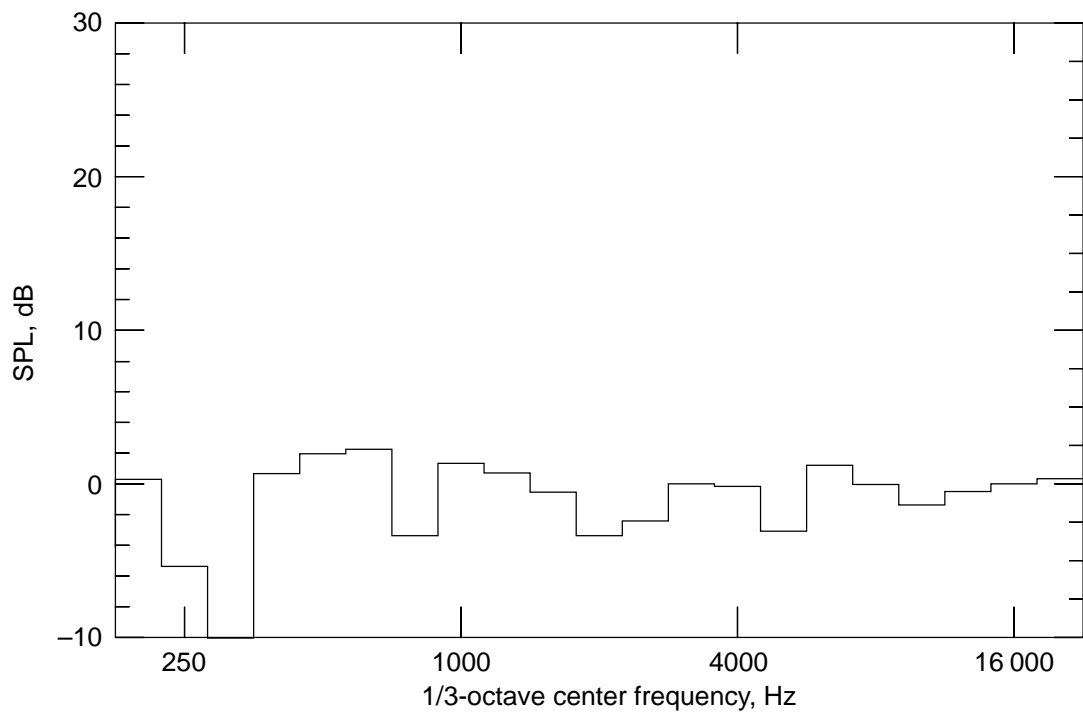


Figure 11. Insertion loss caused by screen and honeycomb.

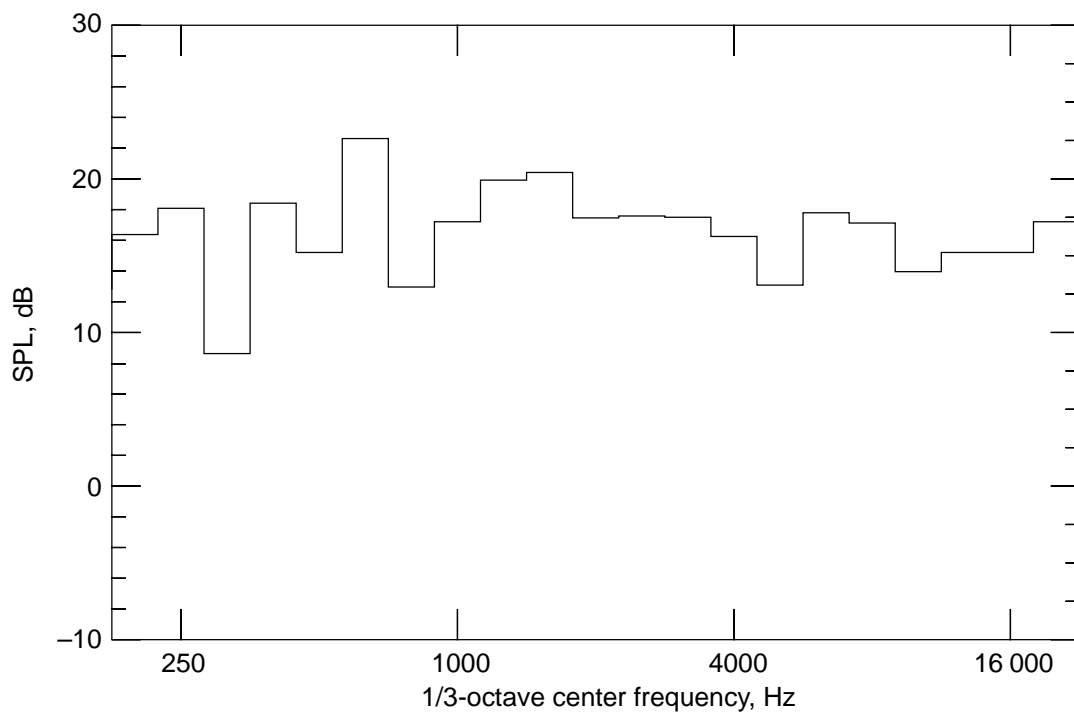
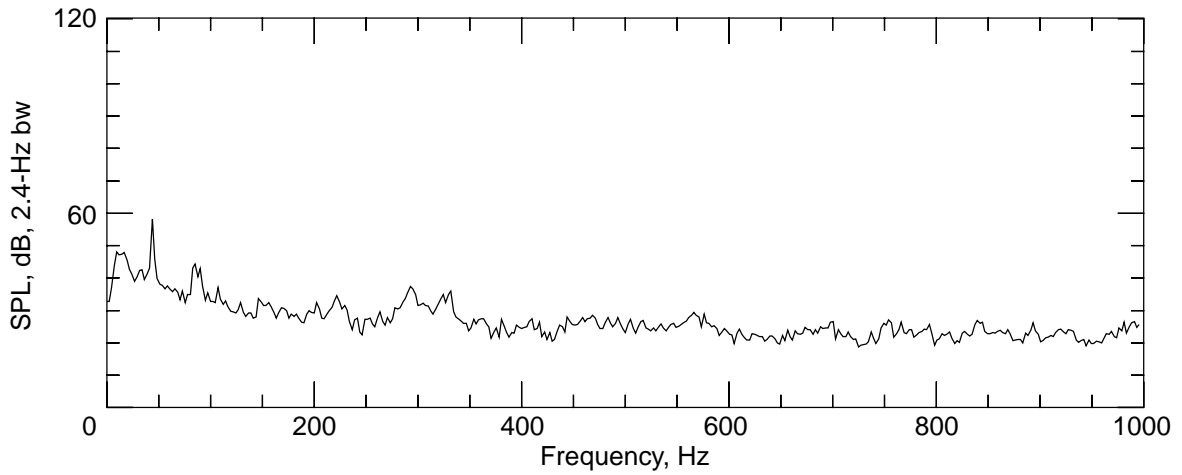
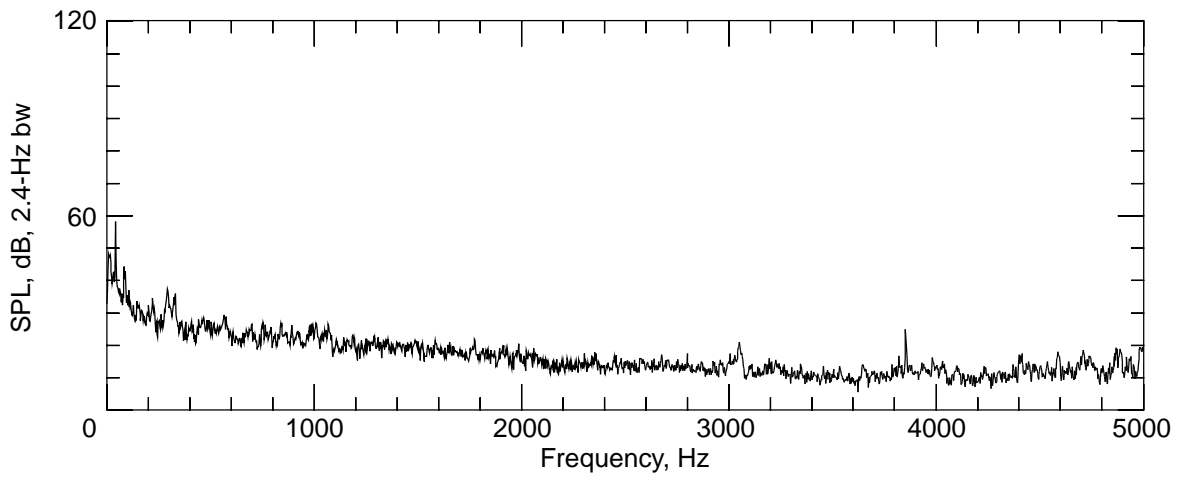
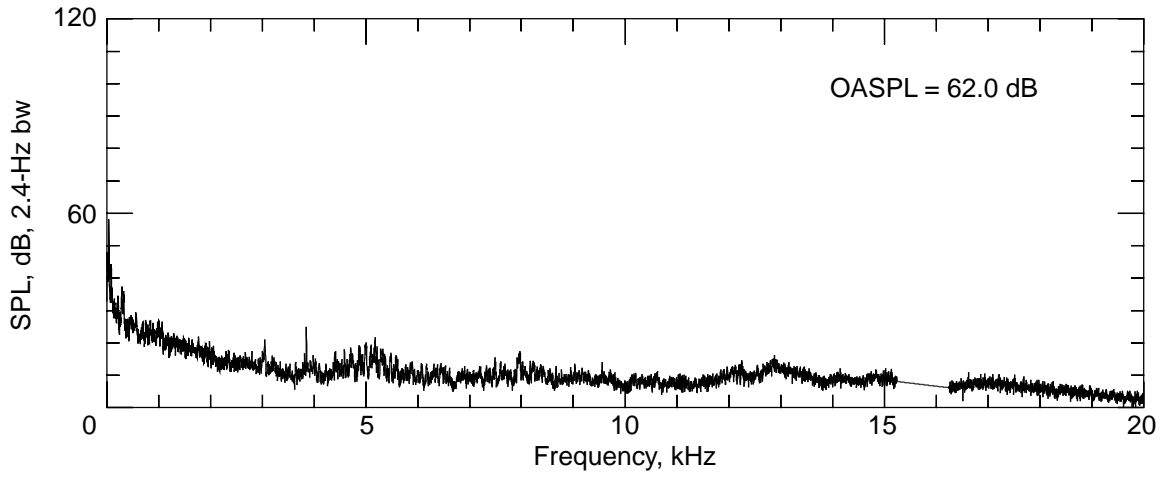
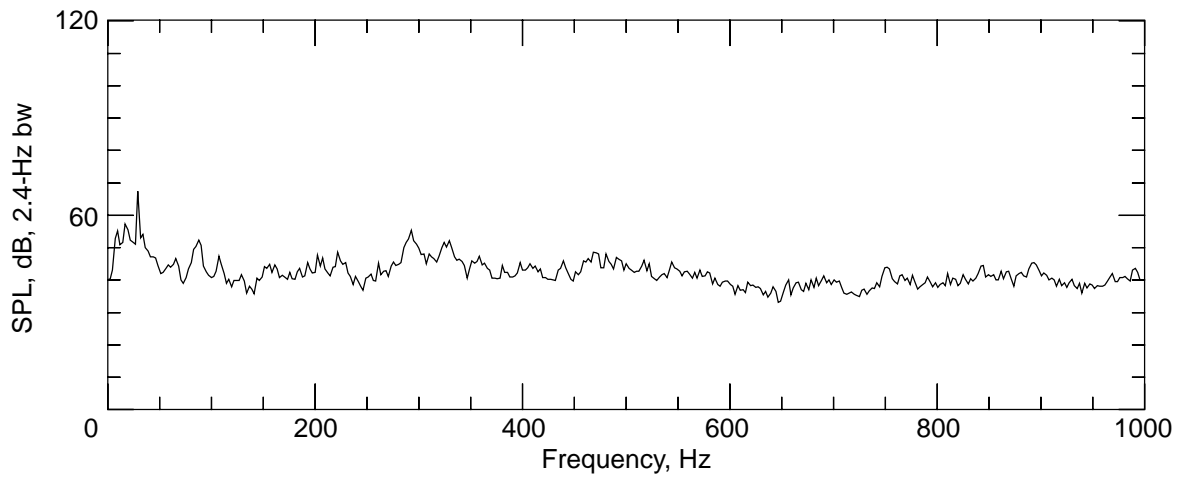
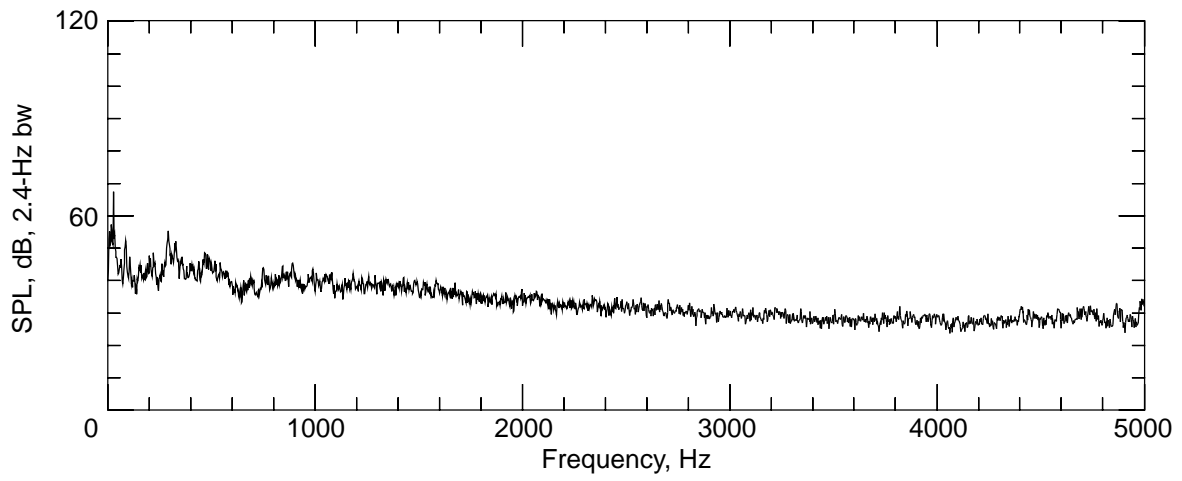
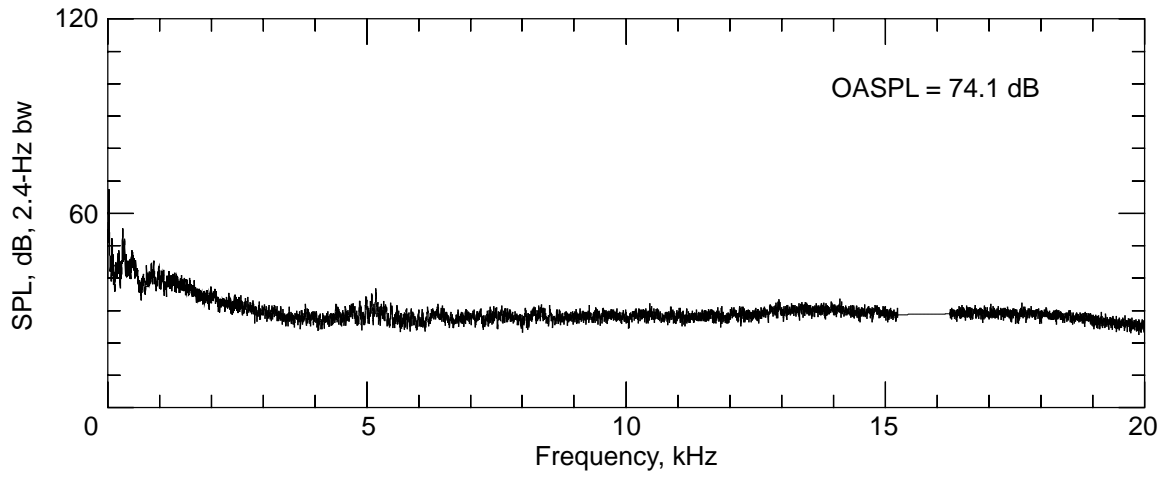


Figure 12. Insertion loss caused by contraction.



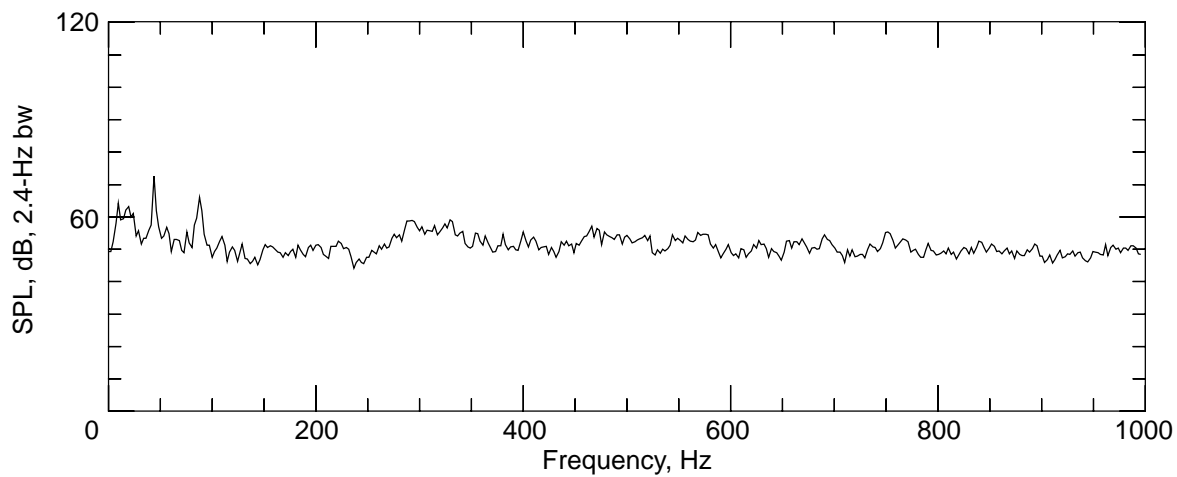
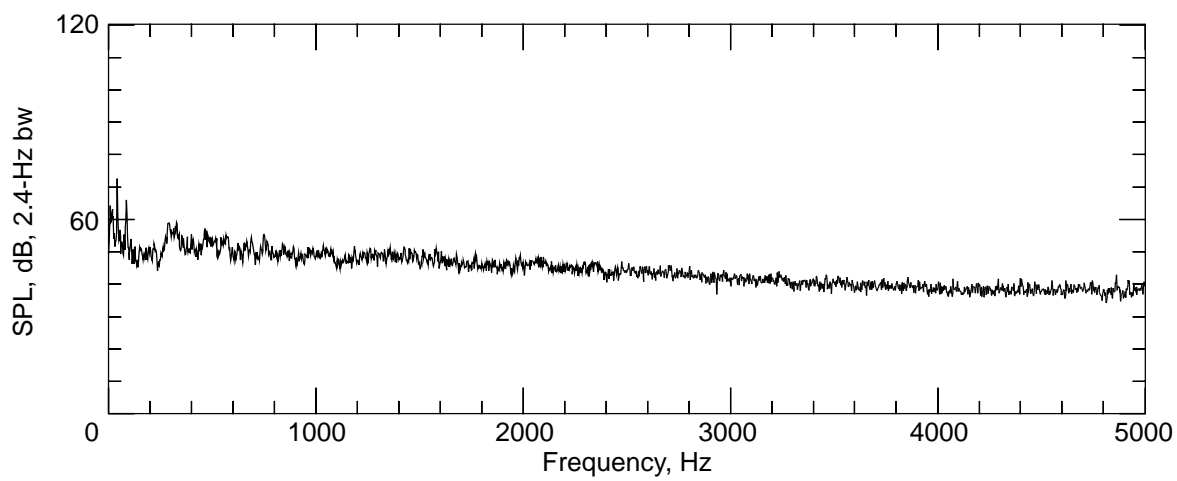
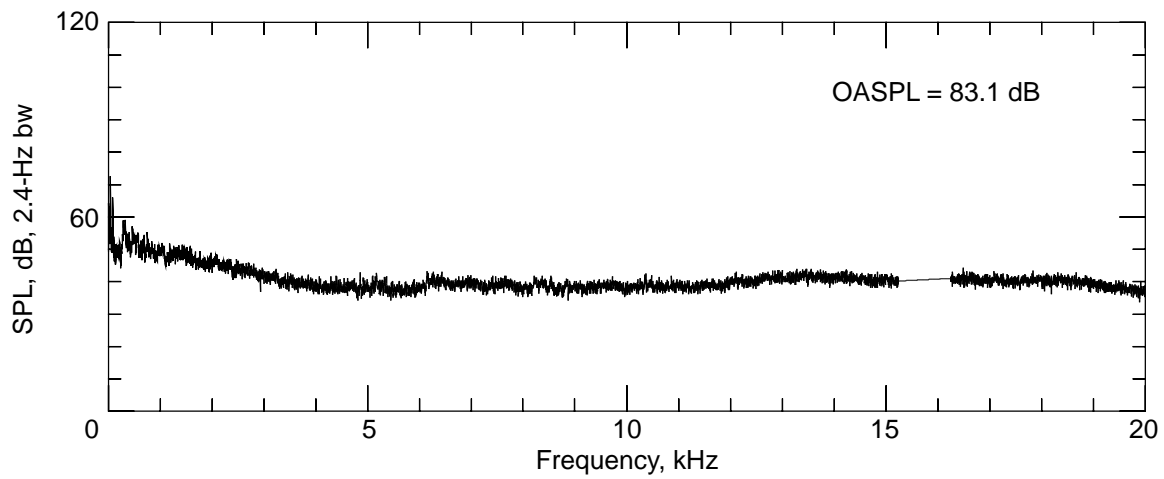
(a) Boundary layer fan operating at 500 rpm.

Figure 13. Background noise in test section caused by B.L.S. only.



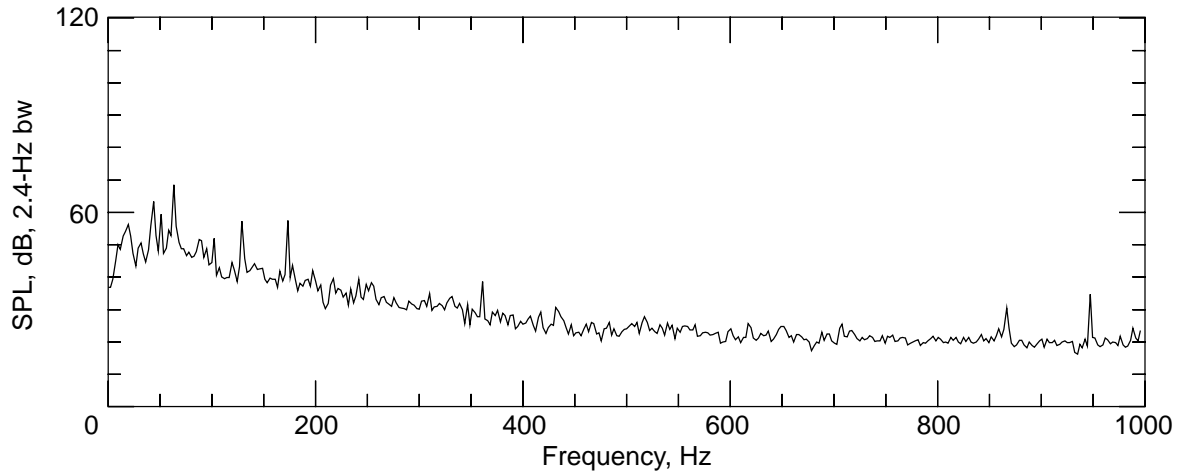
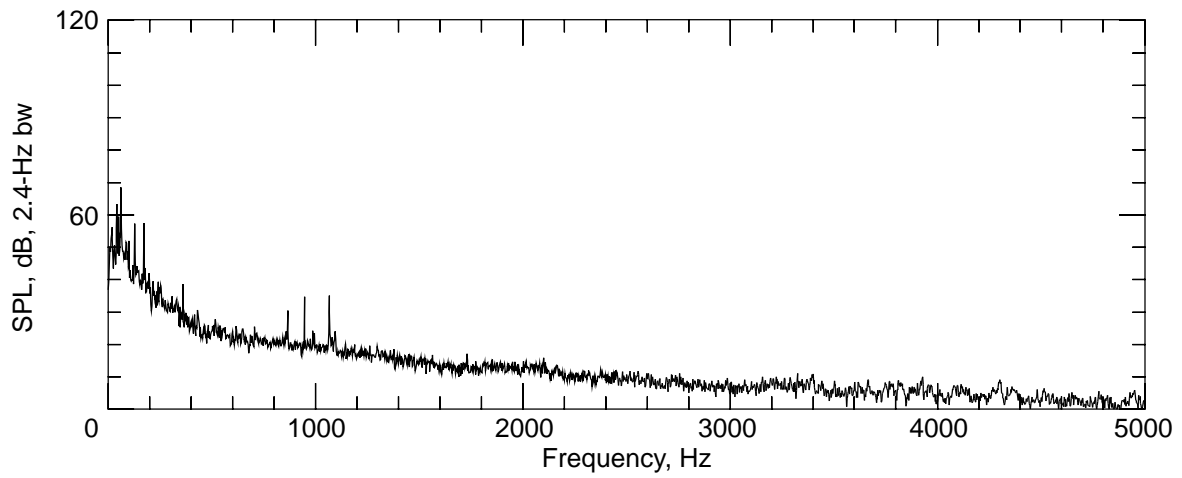
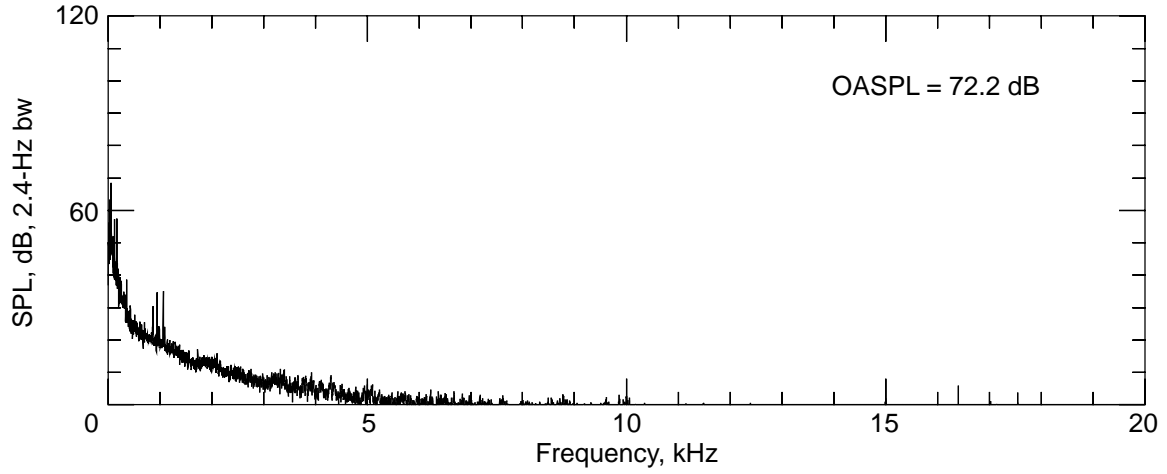
(b) Boundary layer fan operating at 1000 rpm.

Figure 13. Continued.



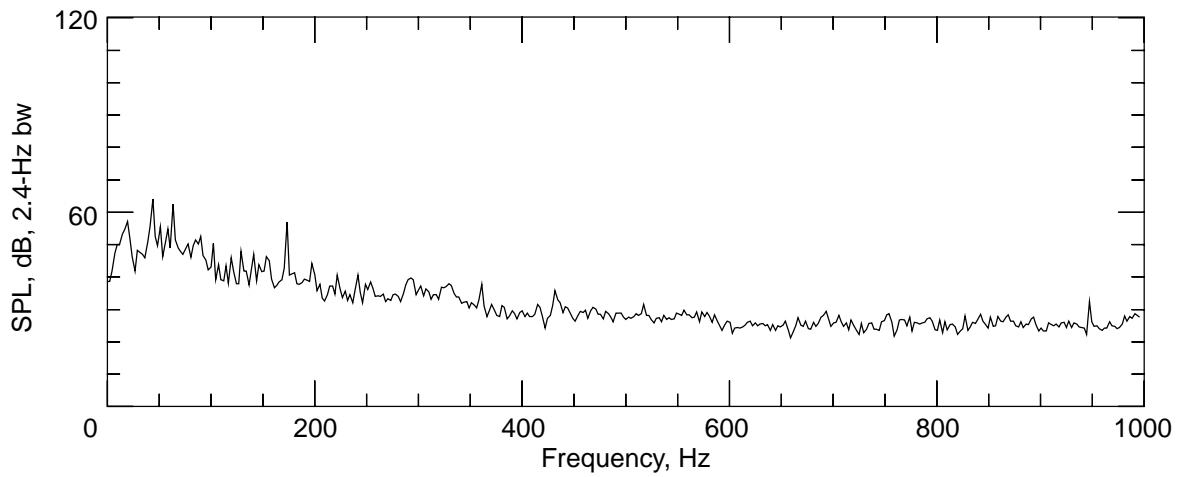
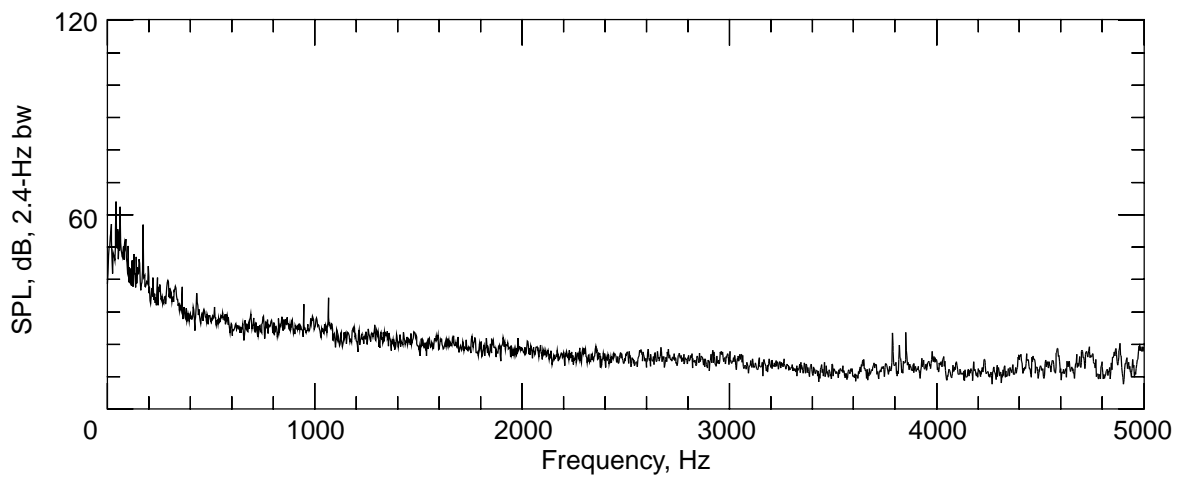
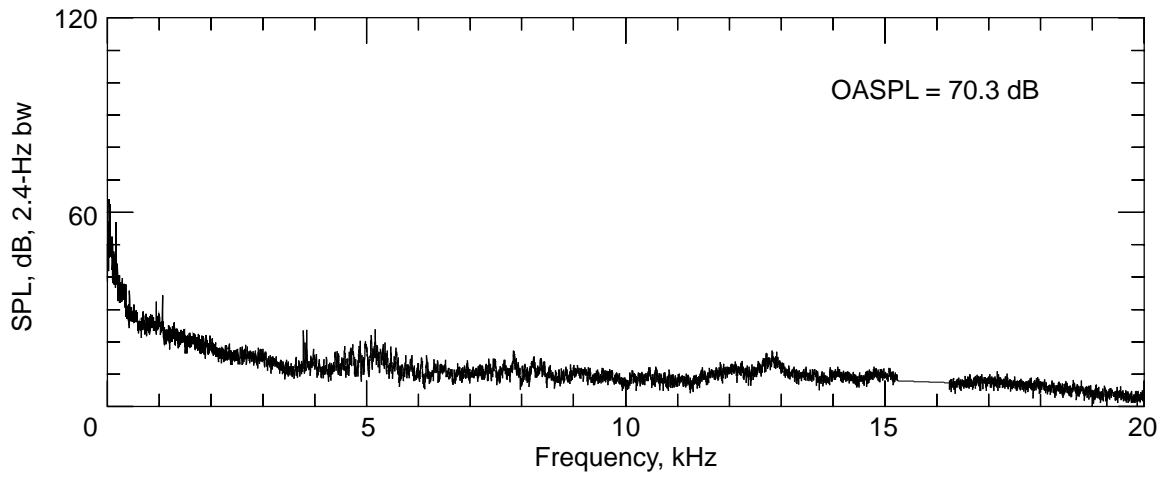
(c) Boundary layer fan operating at 1500 rpm.

Figure 13. Concluded.



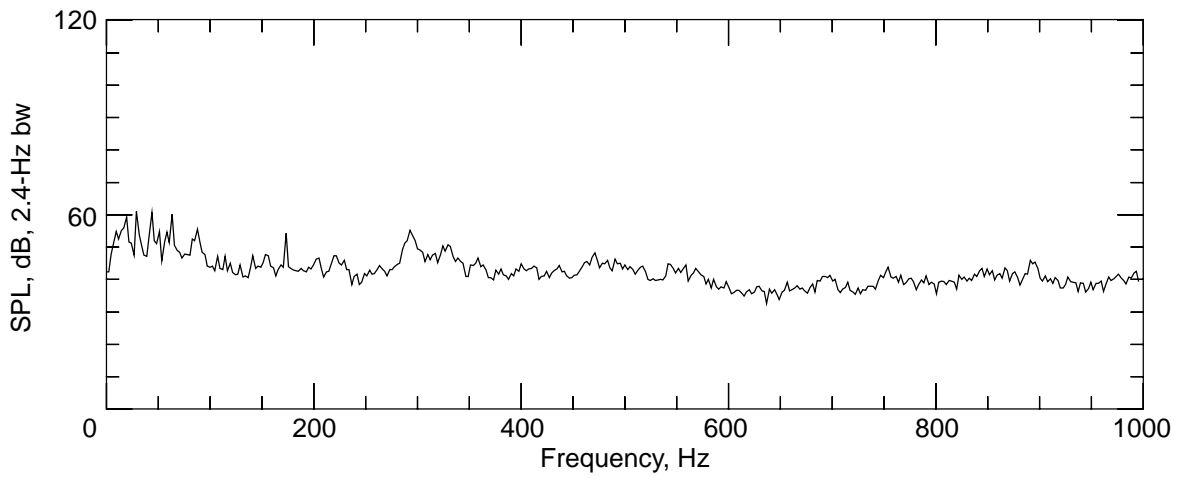
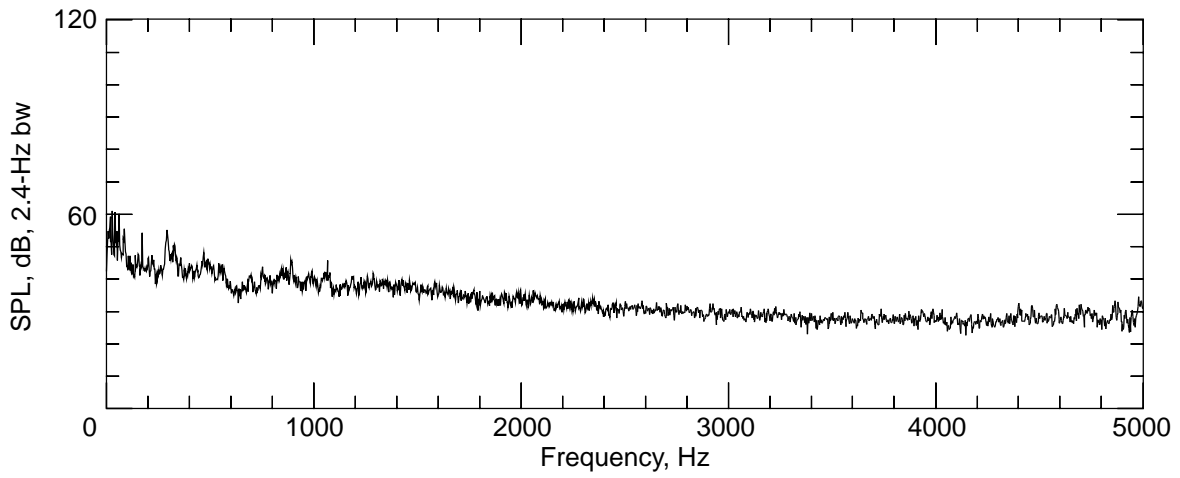
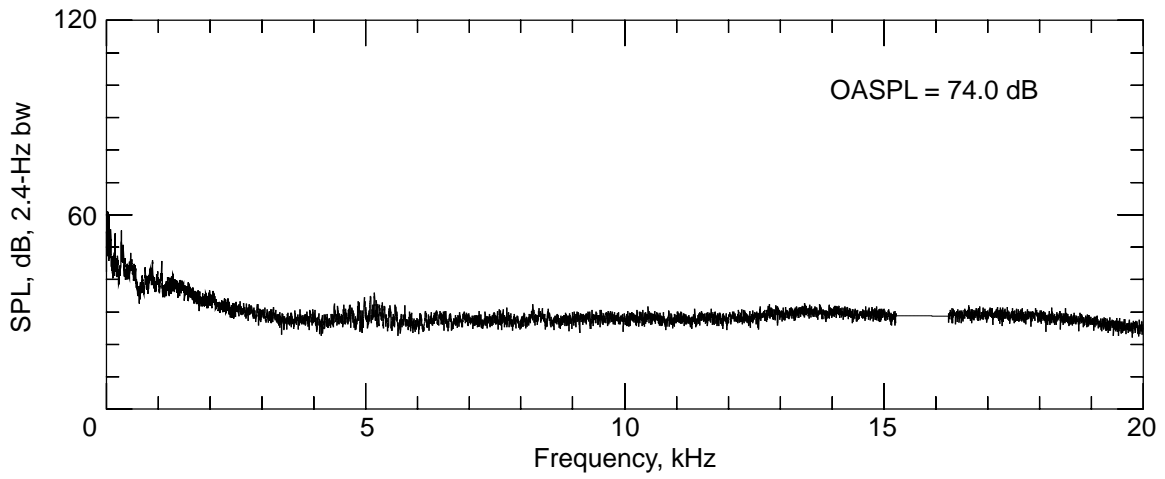
(a) Boundary layer fan not operating.

Figure 14. Background noise in test section caused by main drive cooling fan and B.L.S.



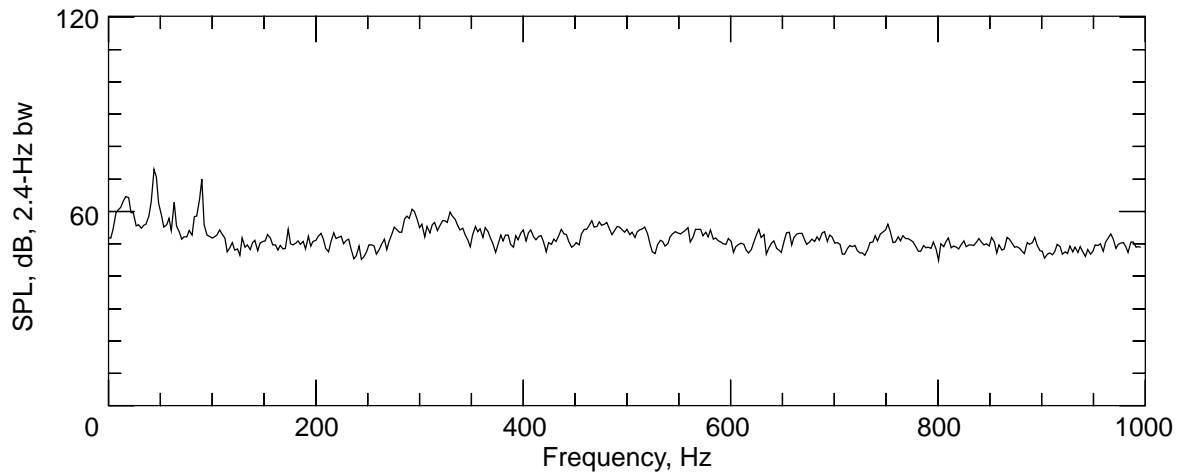
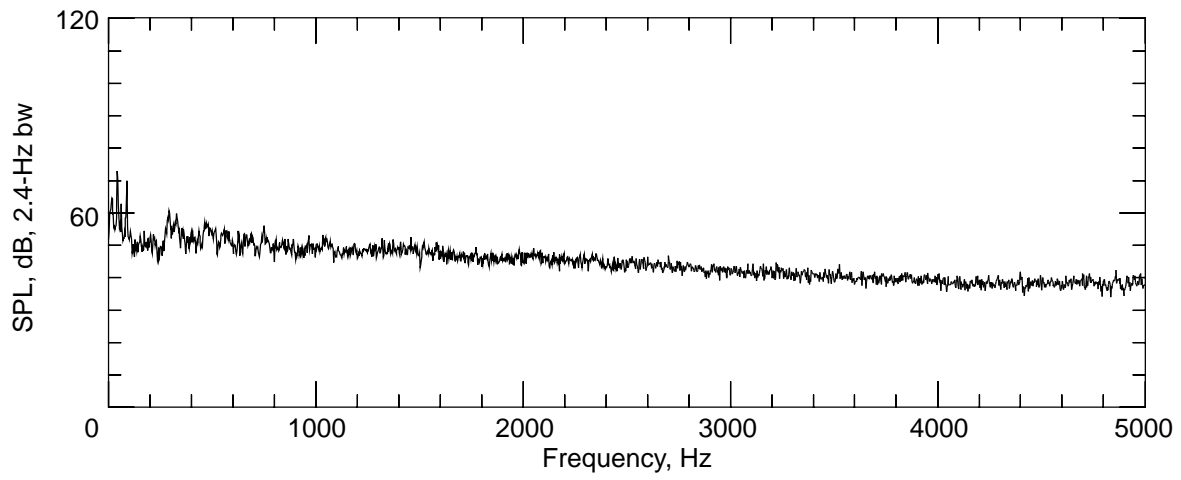
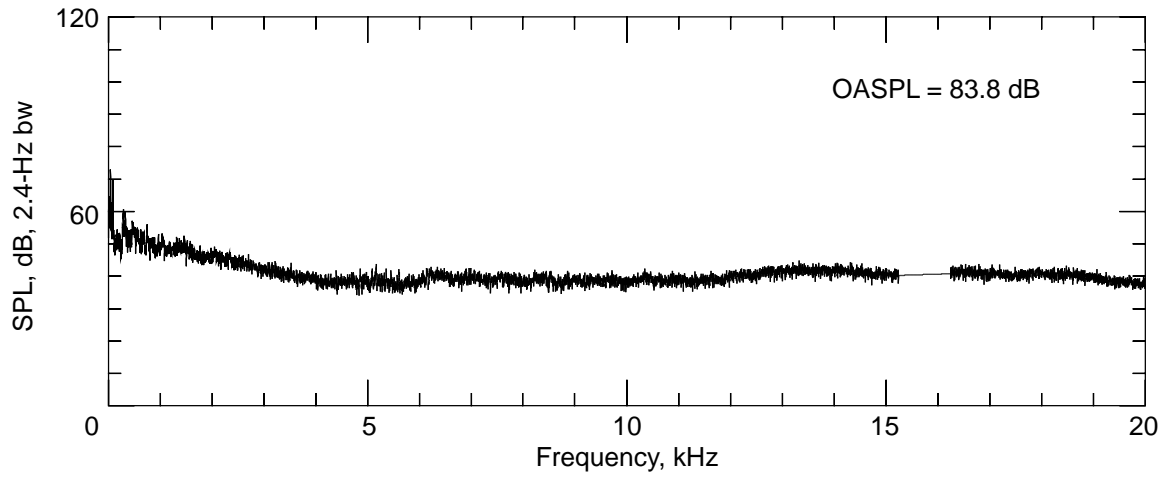
(b) Boundary layer fan operating at 500 rpm.

Figure 14. Continued.



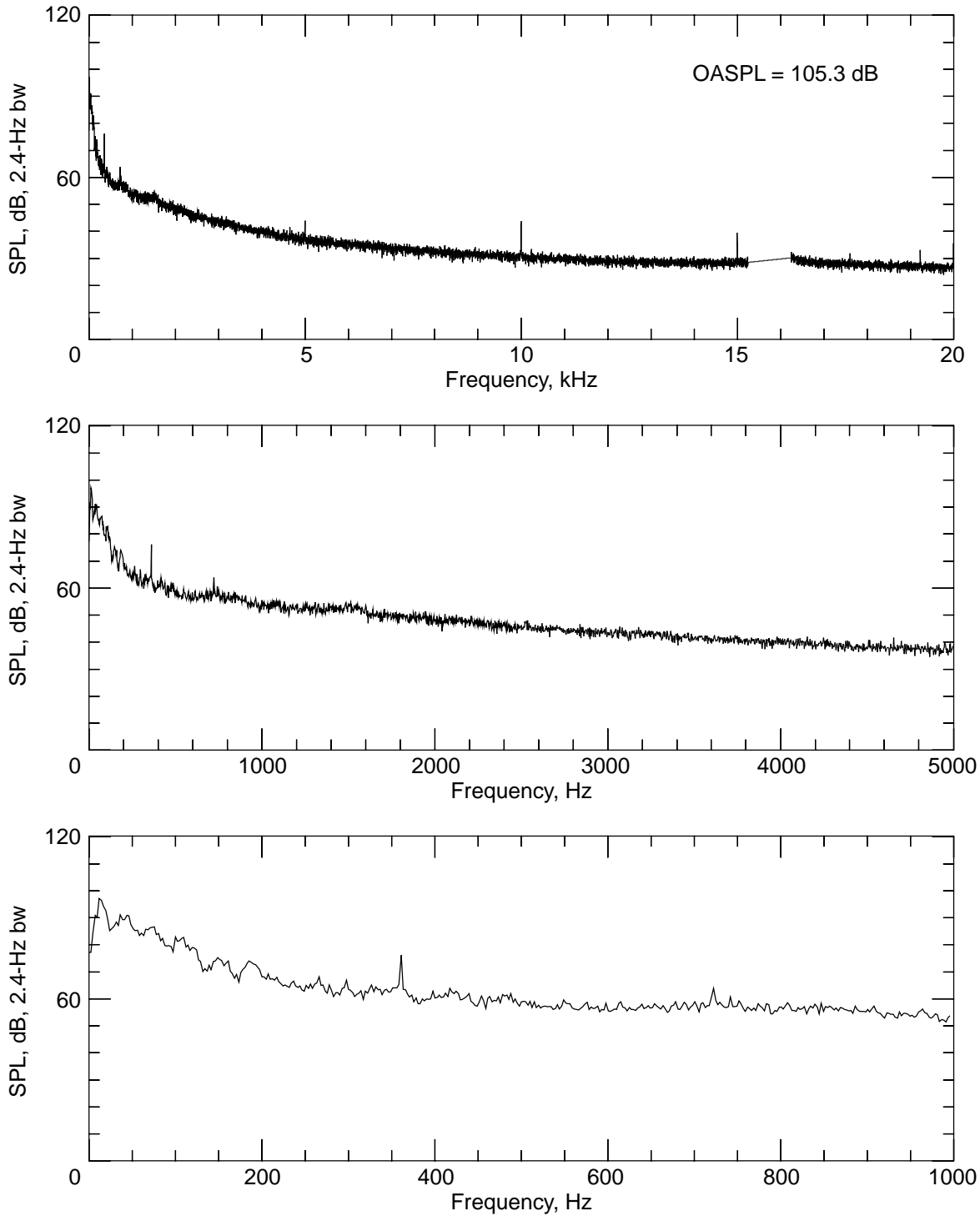
(c) Boundary layer fan operating at 1000 rpm.

Figure 14. Continued.



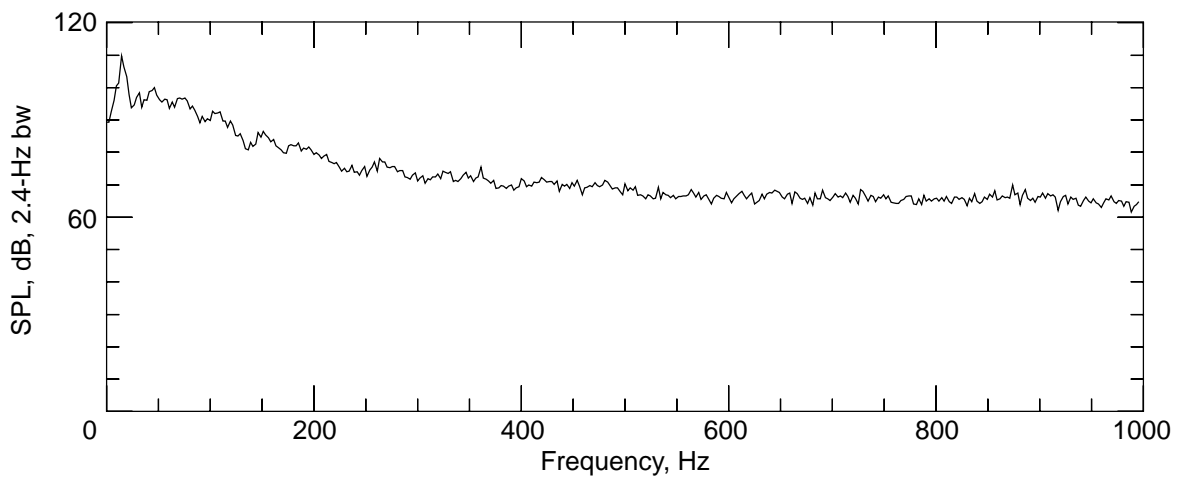
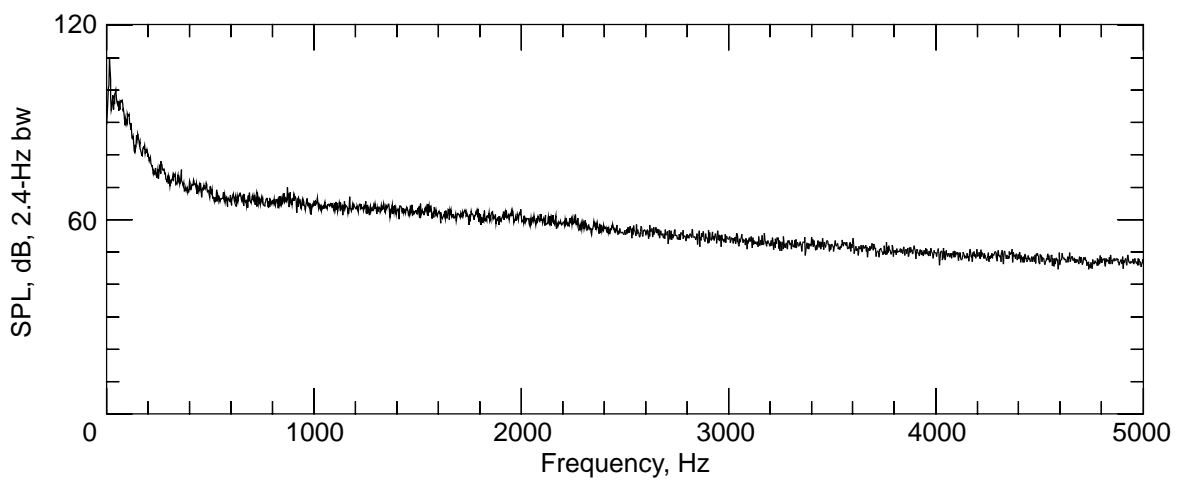
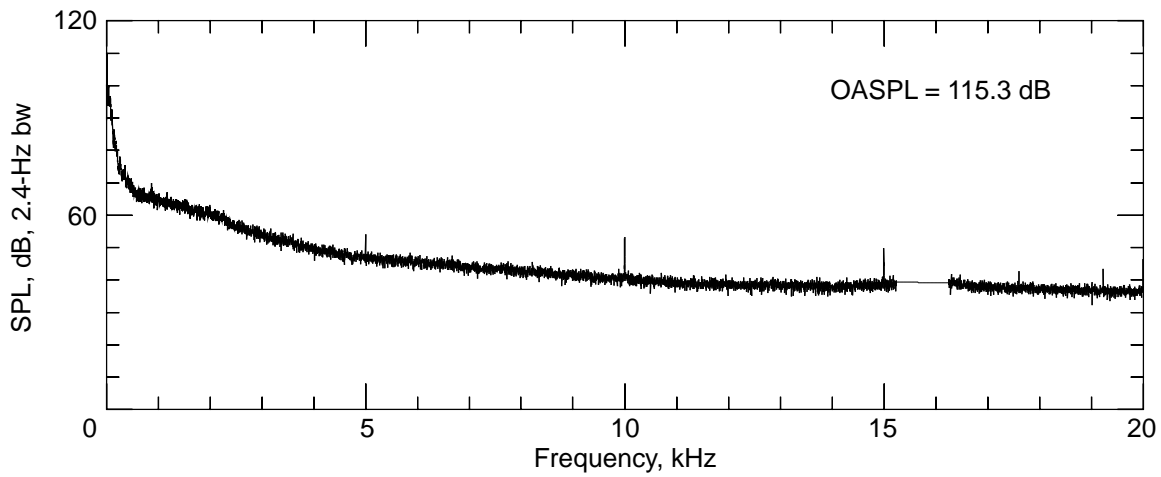
(d) Boundary layer fan operating at 1500 rpm.

Figure 14. Concluded.



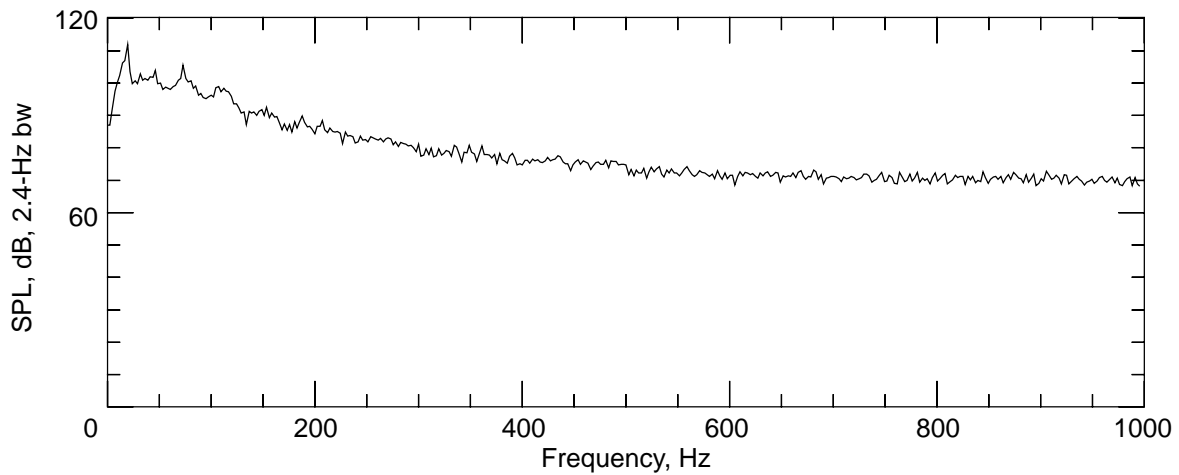
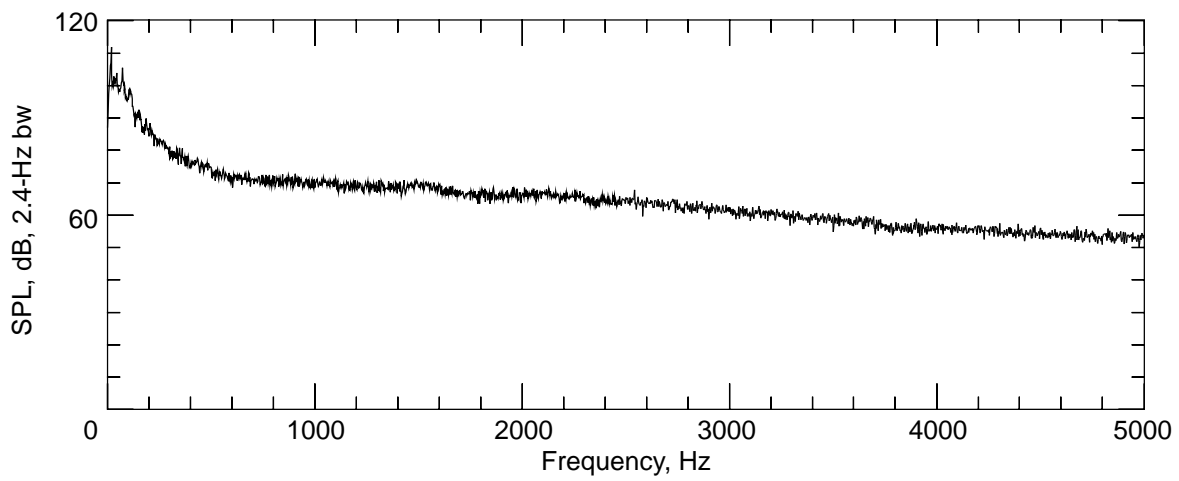
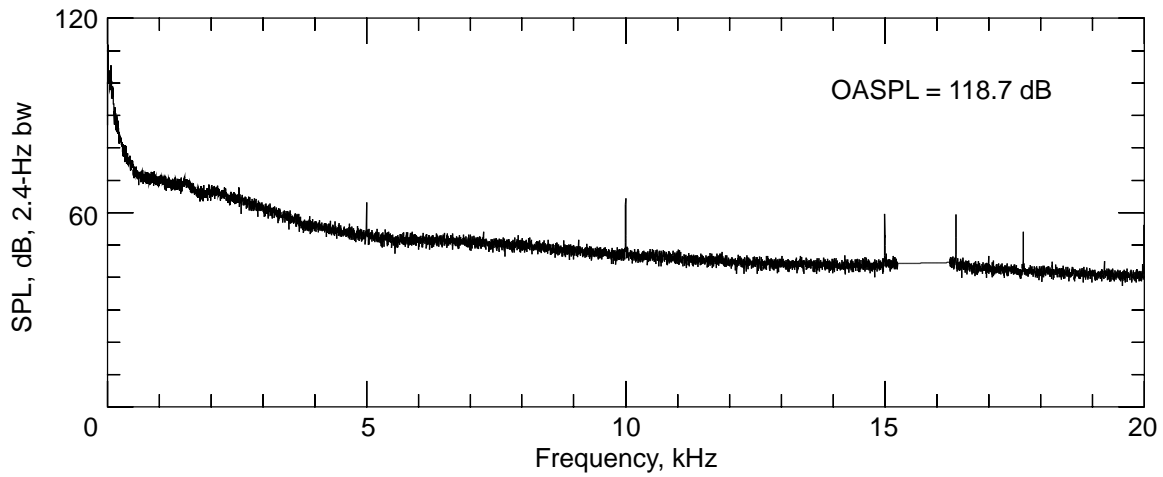
(a) Dynamic pressure = 20 lb/ft<sup>2</sup>.

Figure 15. Flow noise measurement by reference microphone.



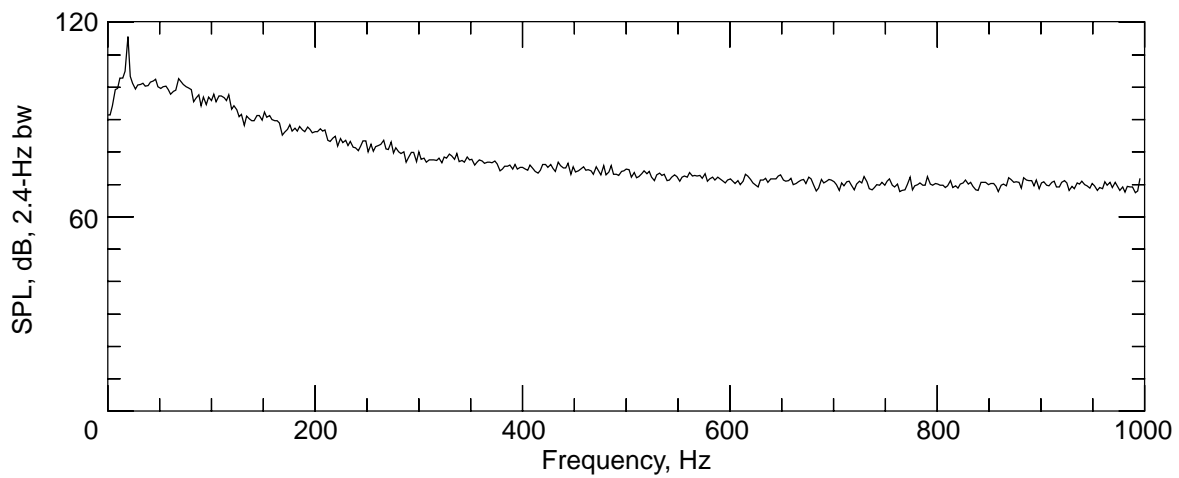
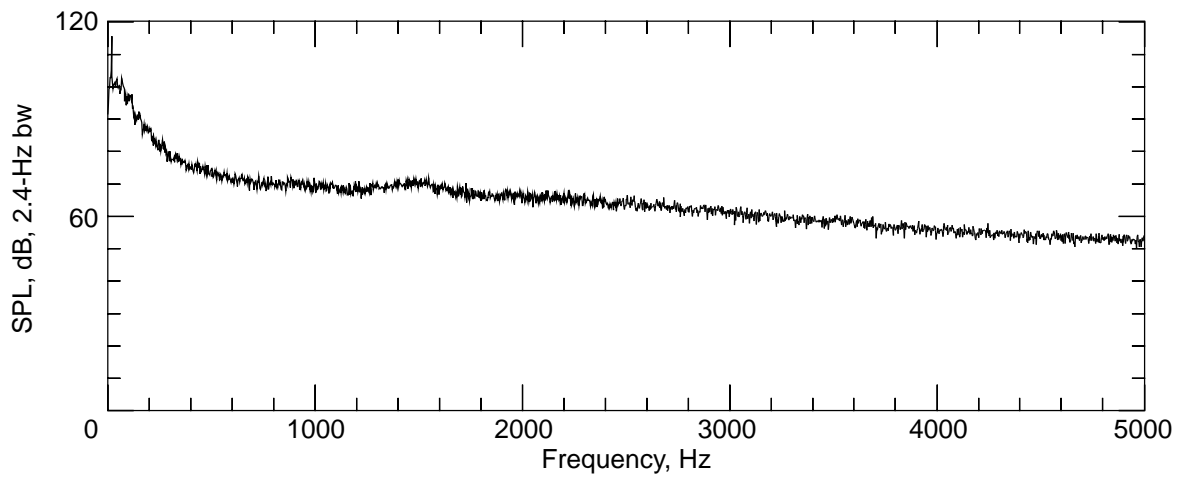
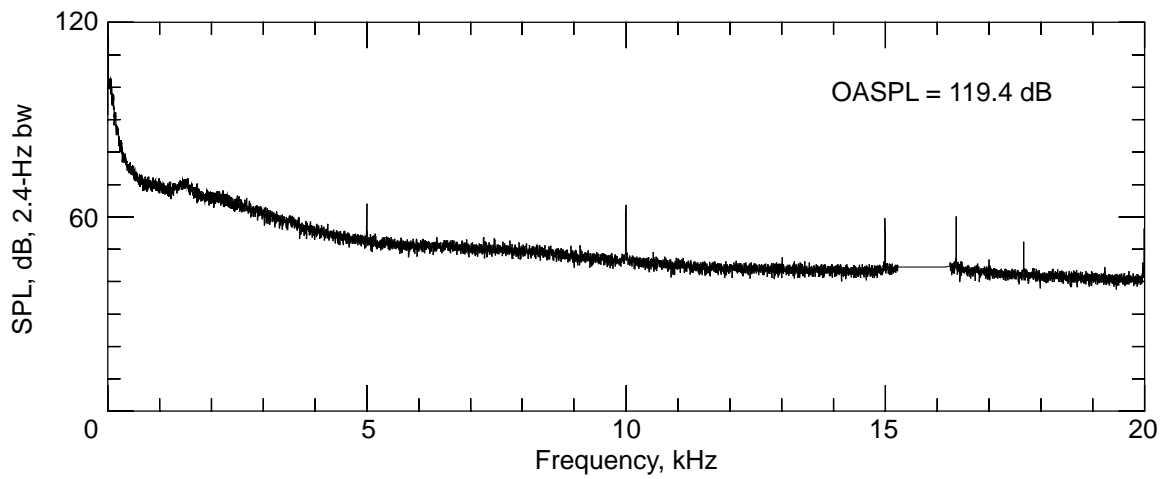
(b) Dynamic pressure = 40 lb/ft<sup>2</sup>.

Figure 15. Continued.



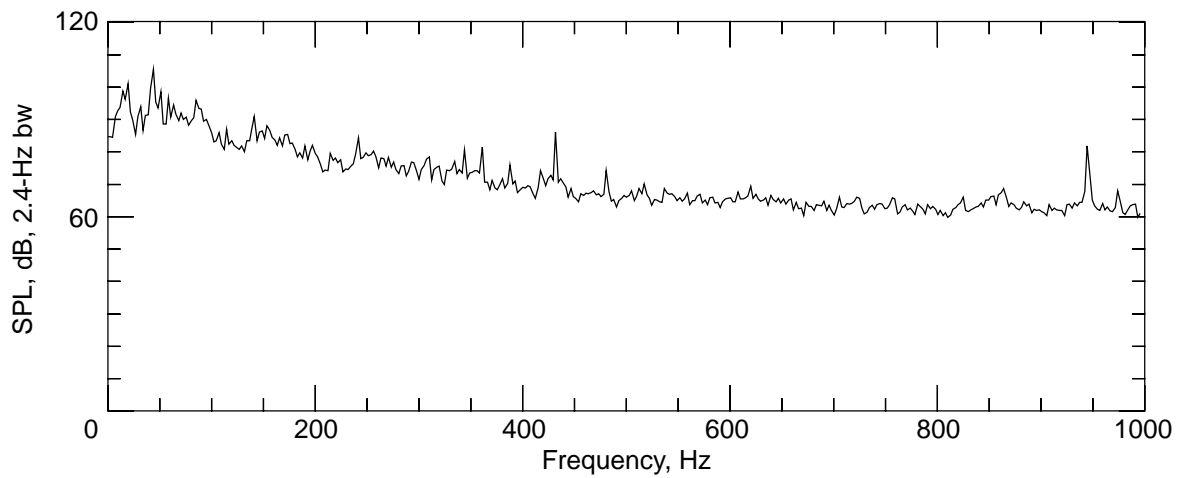
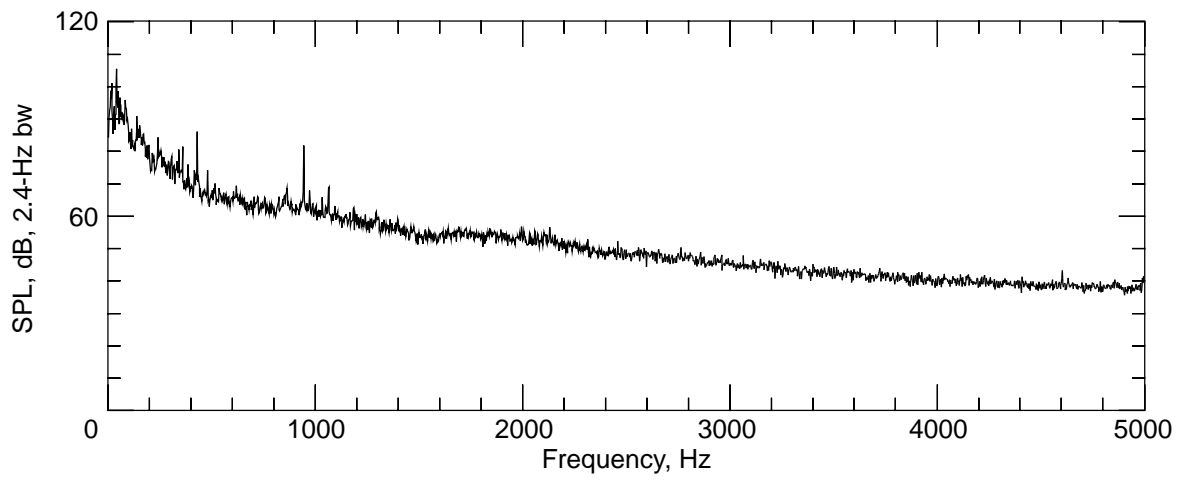
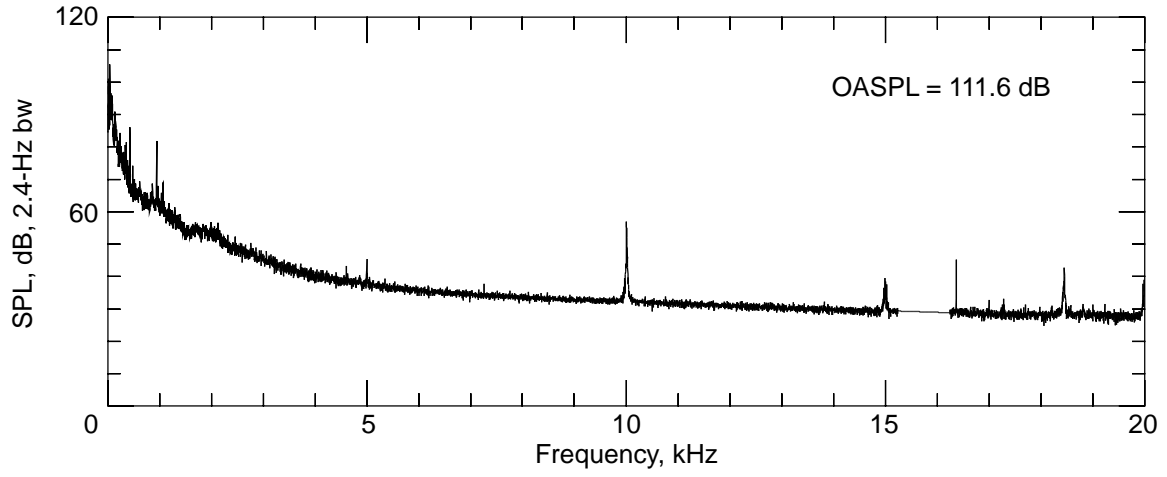
(c) Dynamic pressure = 60 lb/ft<sup>2</sup>.

Figure 15. Continued.



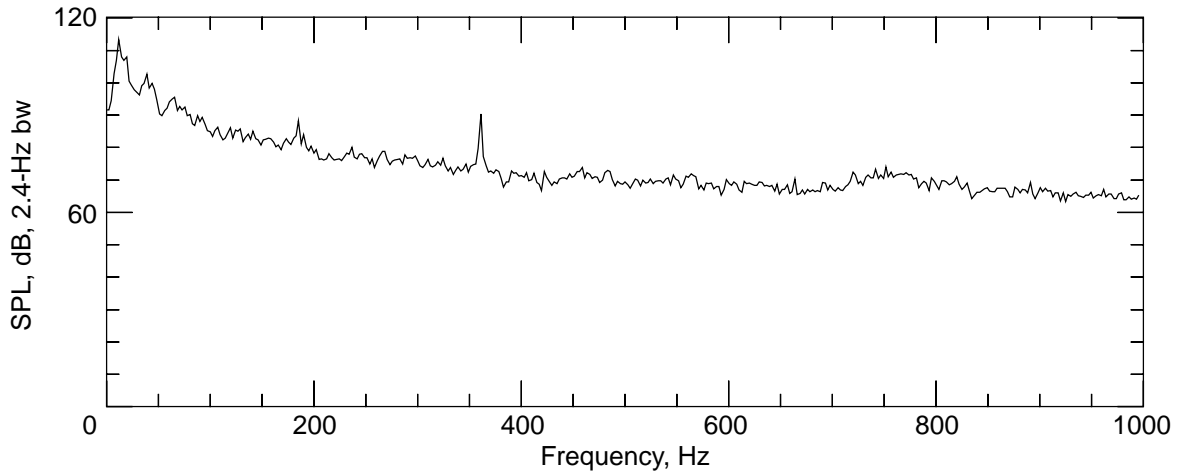
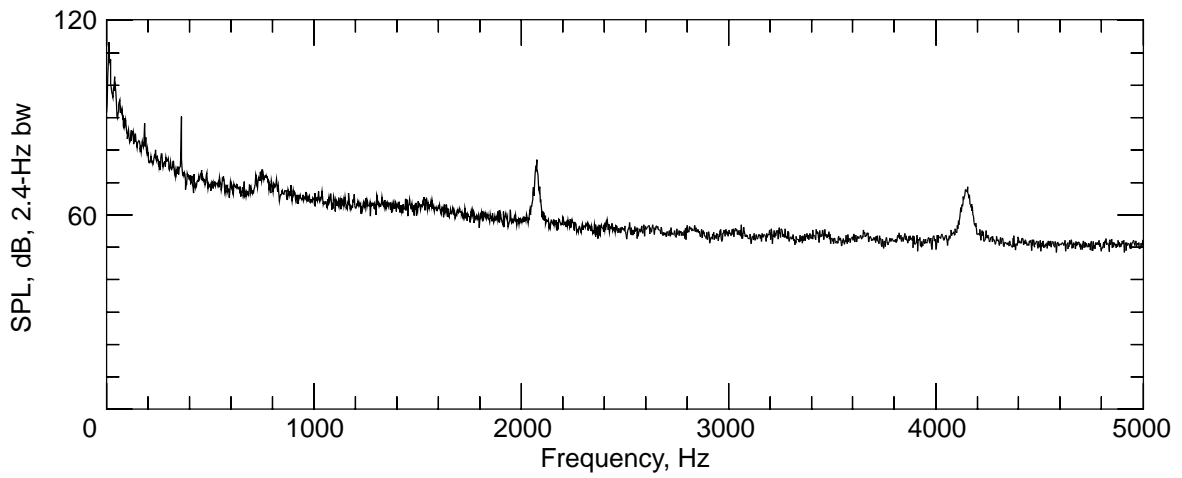
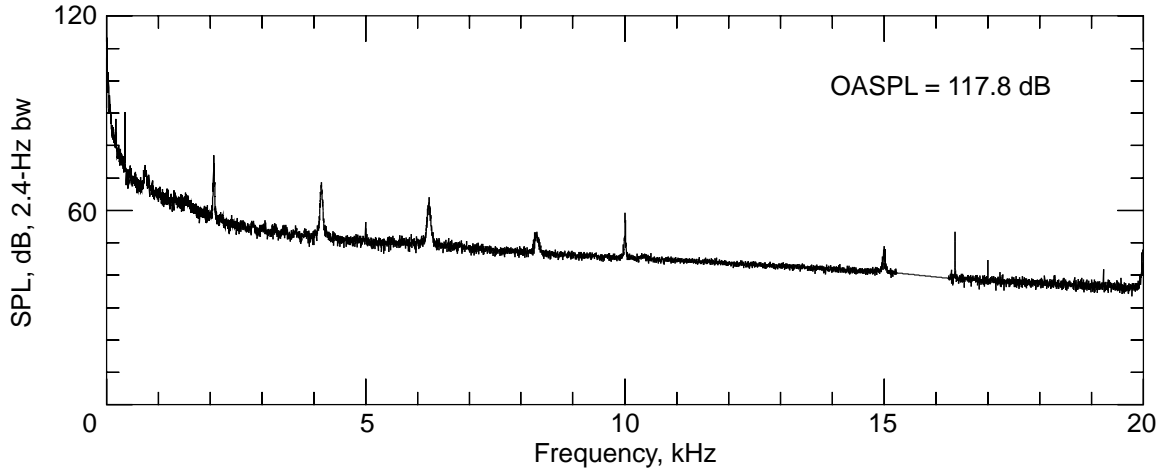
(d) Dynamic pressure = 70 lb/ft<sup>2</sup>.

Figure 15. Concluded.



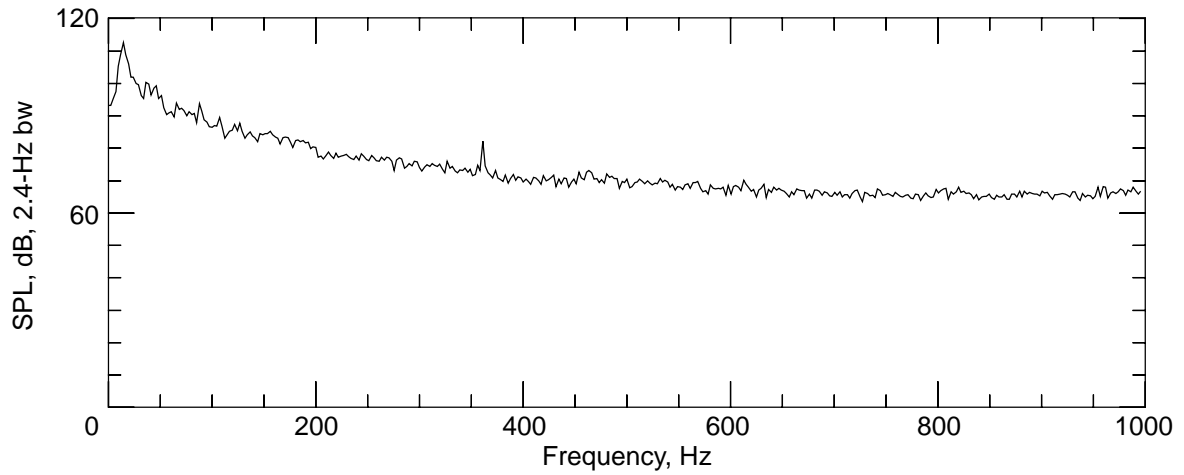
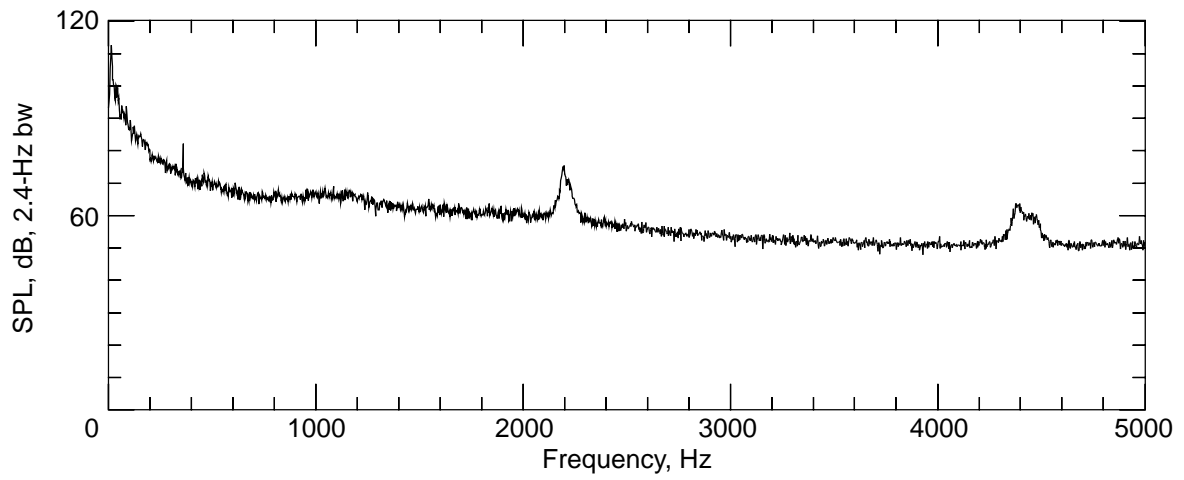
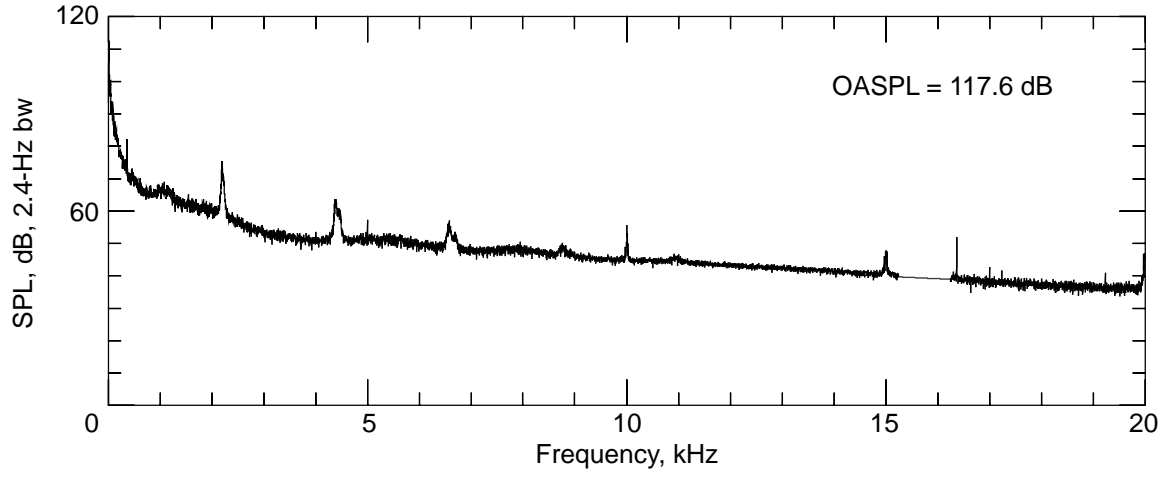
(a) Dynamic pressure = 20 lb/ft<sup>2</sup>.

Figure 16. Flow noise measurement in test section with B.L.S. on.



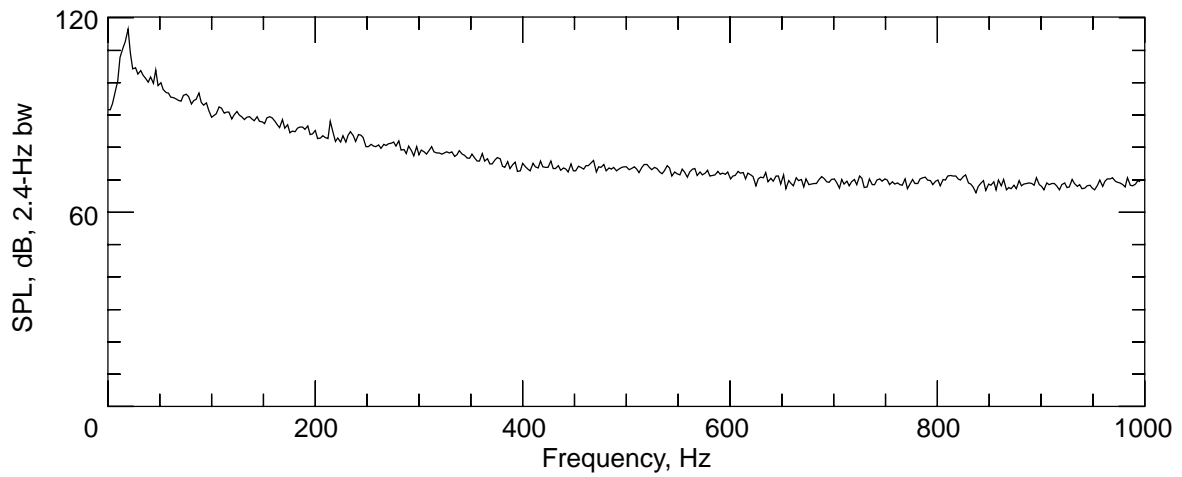
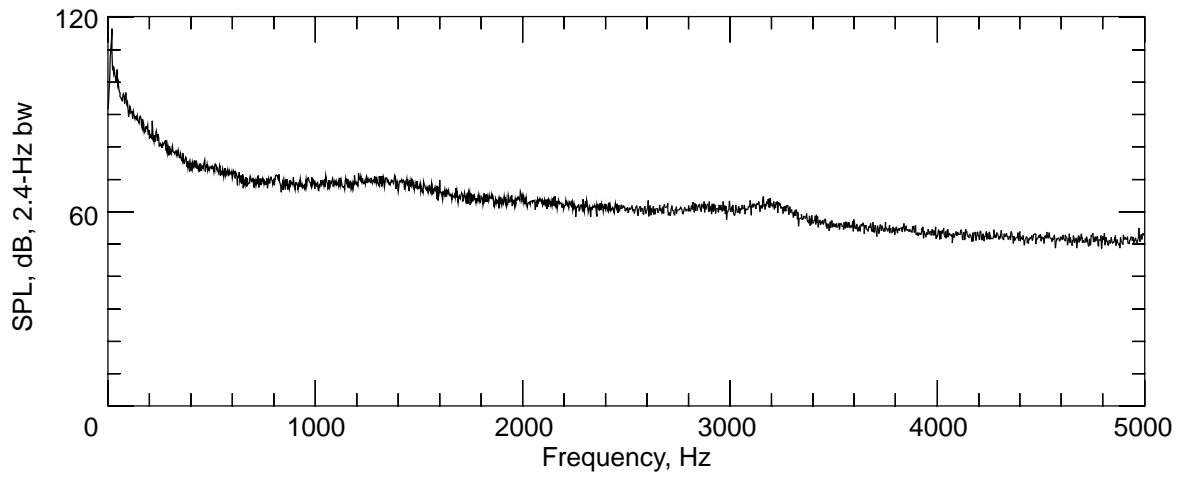
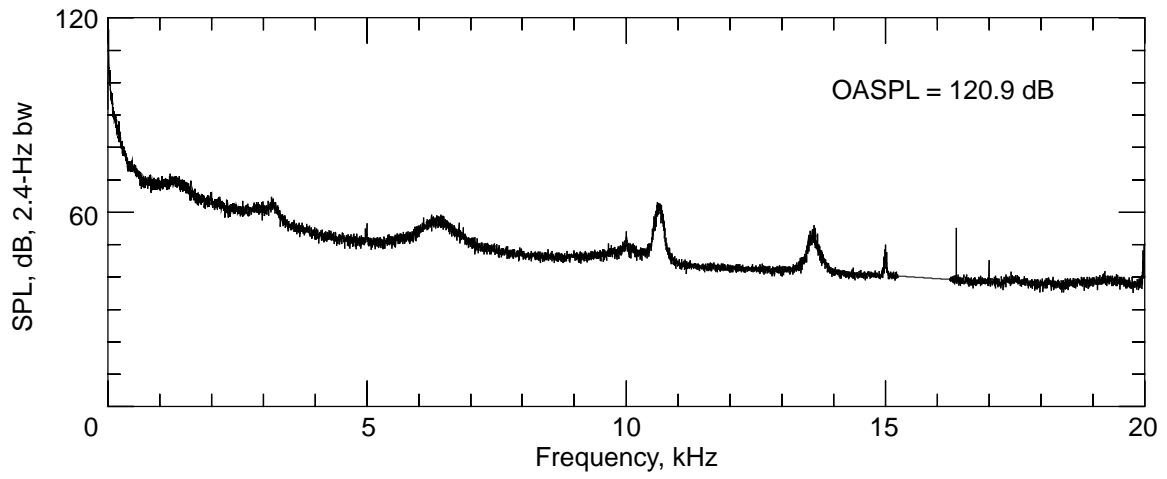
(b) Dynamic pressure = 40 lb/ft<sup>2</sup>.

Figure 16. Continued.



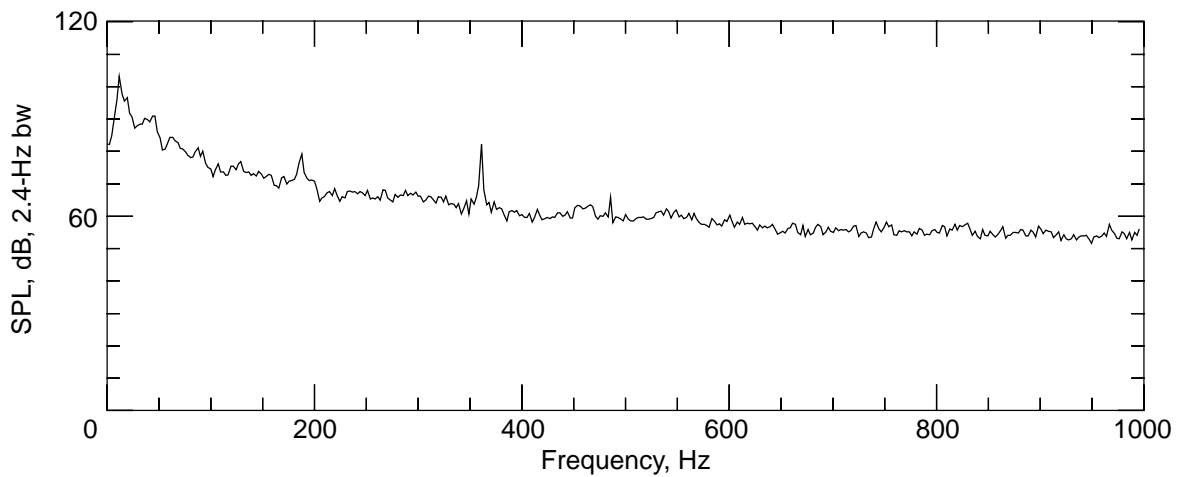
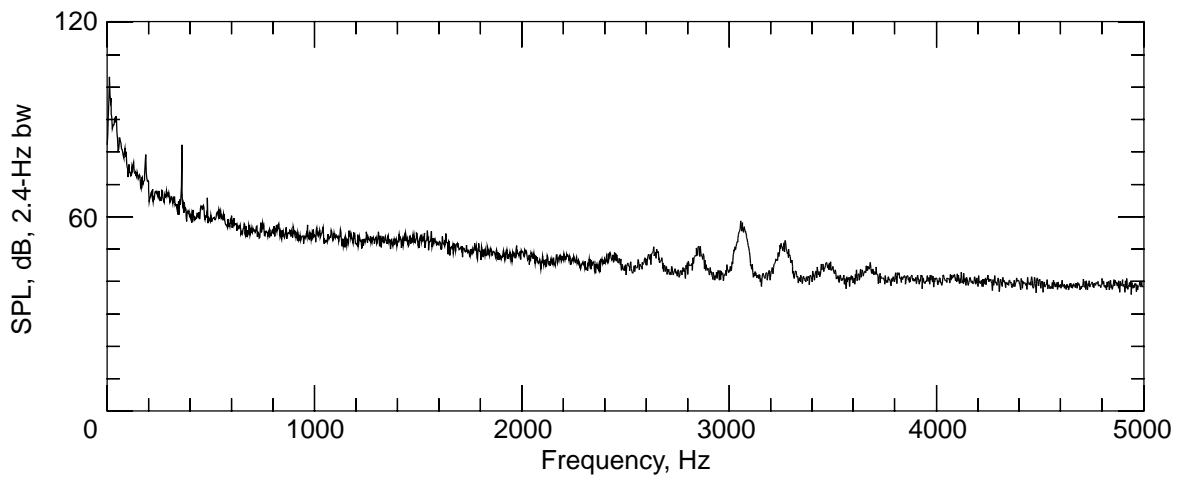
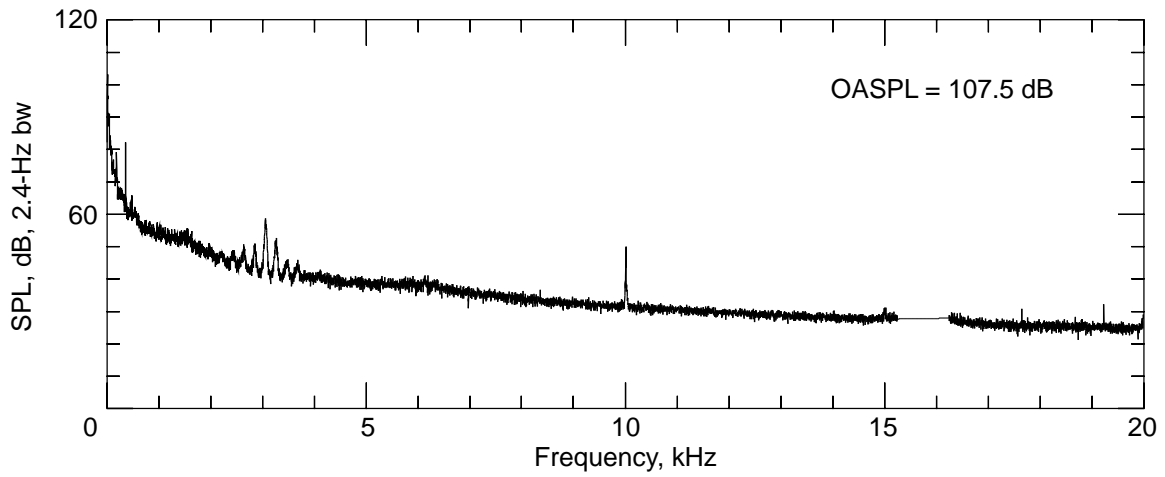
(c) Dynamic pressure = 60 lb/ft<sup>2</sup>.

Figure 16. Continued.



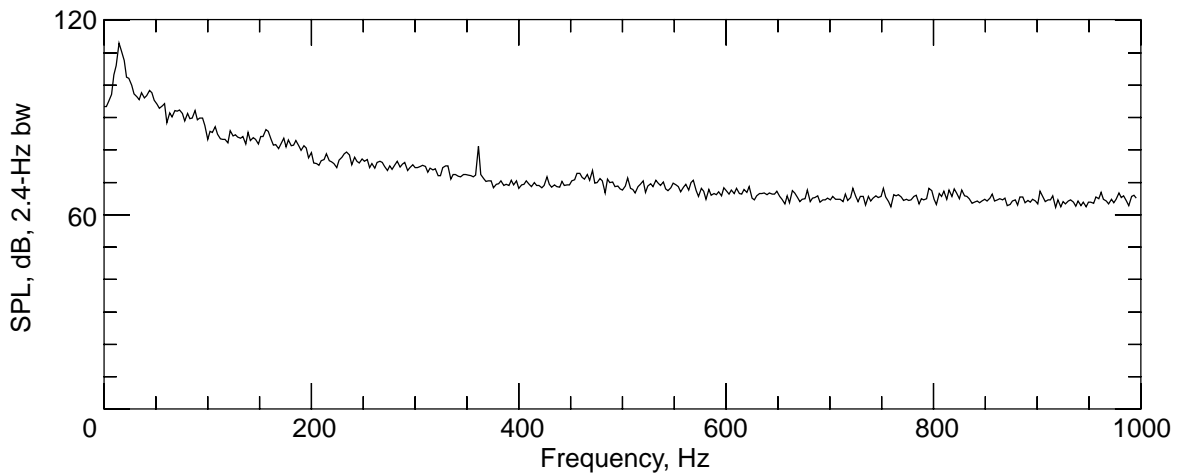
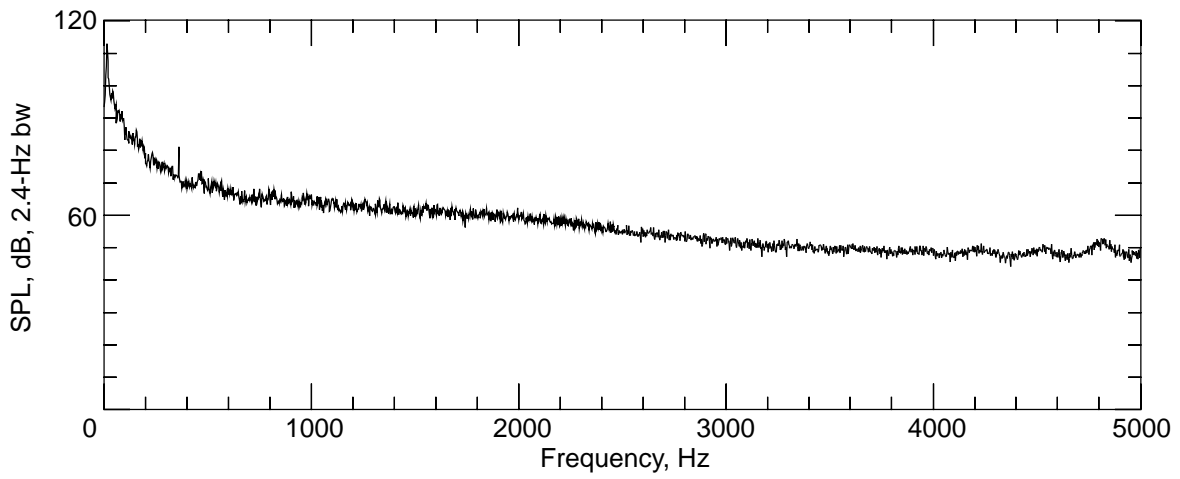
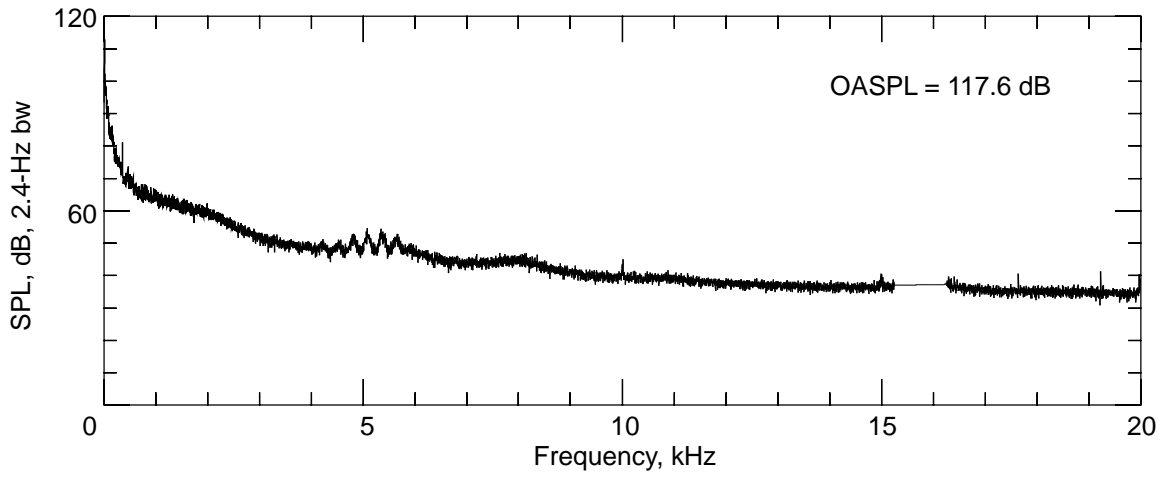
(d) Dynamic pressure = 70 lb/ft<sup>2</sup>.

Figure 16. Concluded.



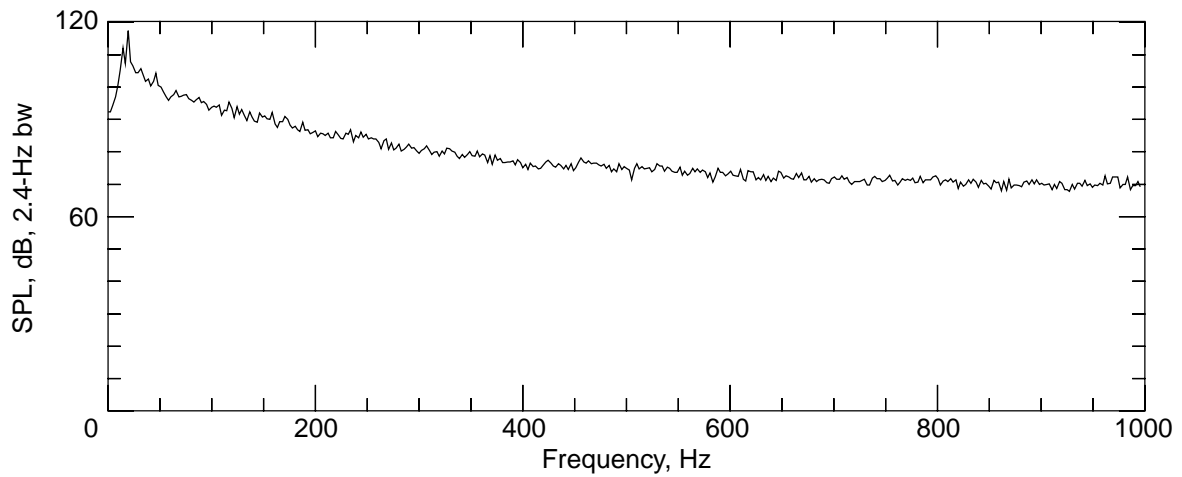
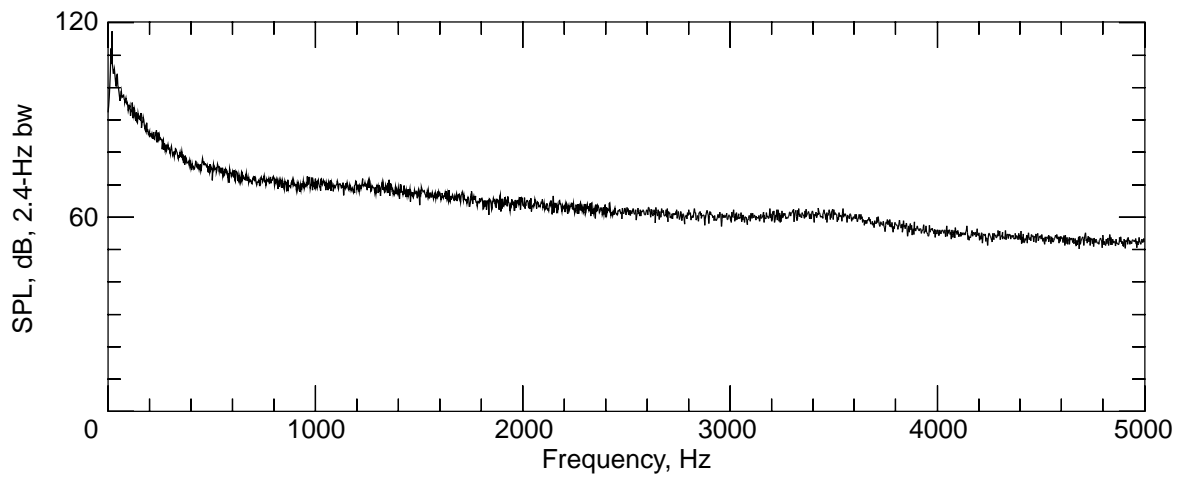
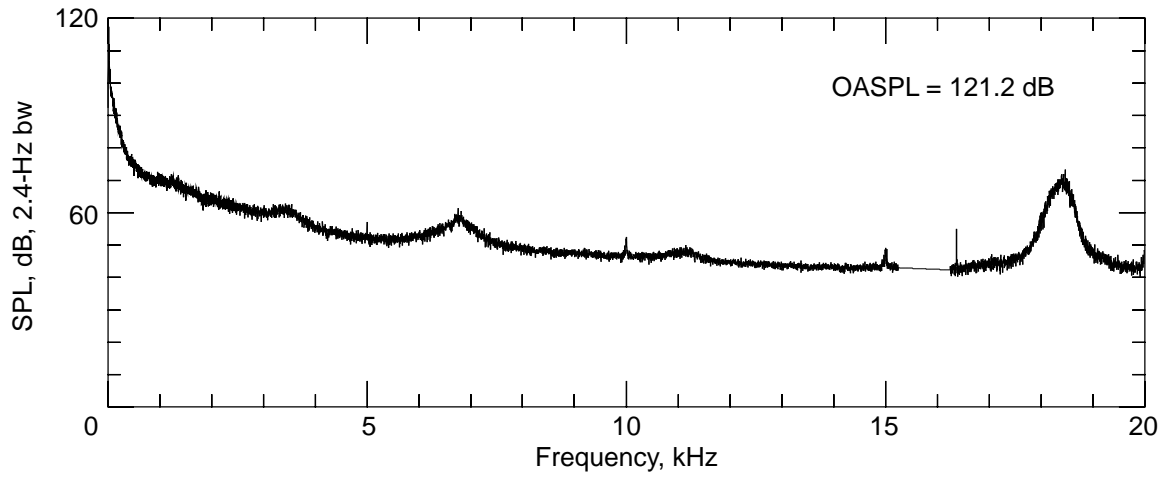
(a) Dynamic pressure = 20 lb/ft<sup>2</sup>.

Figure 17. Flow noise measurement in test section with B.L.S. off.



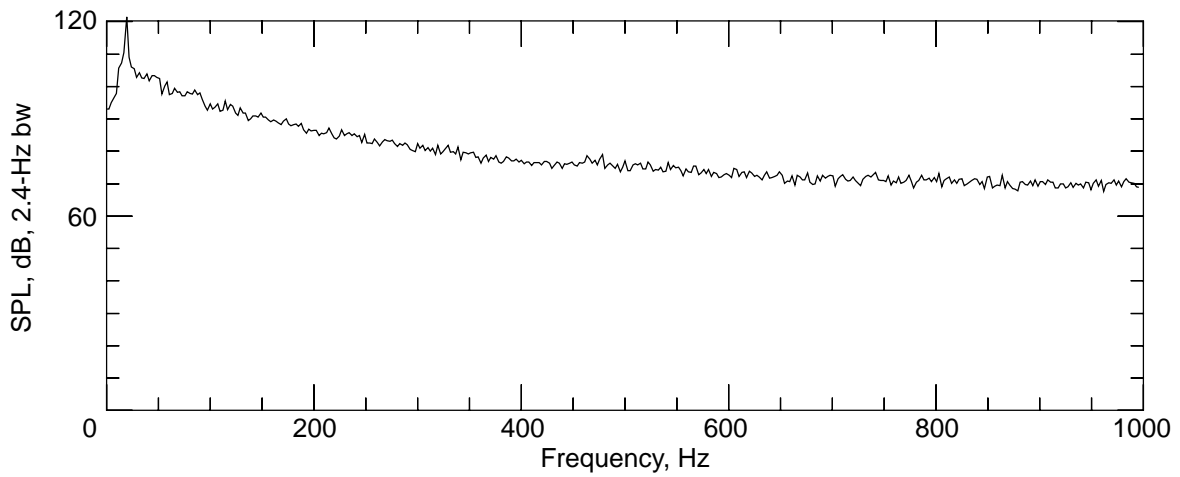
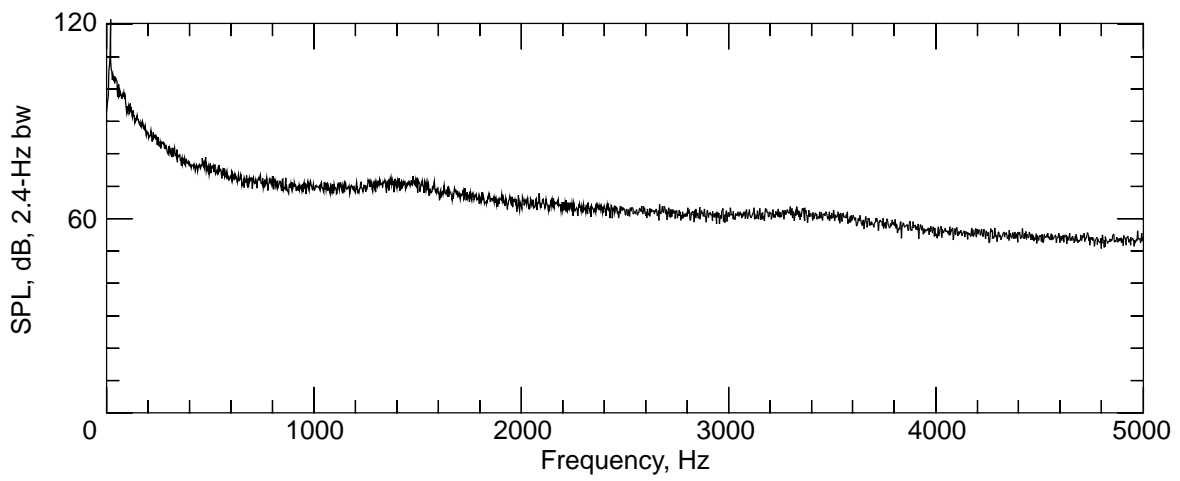
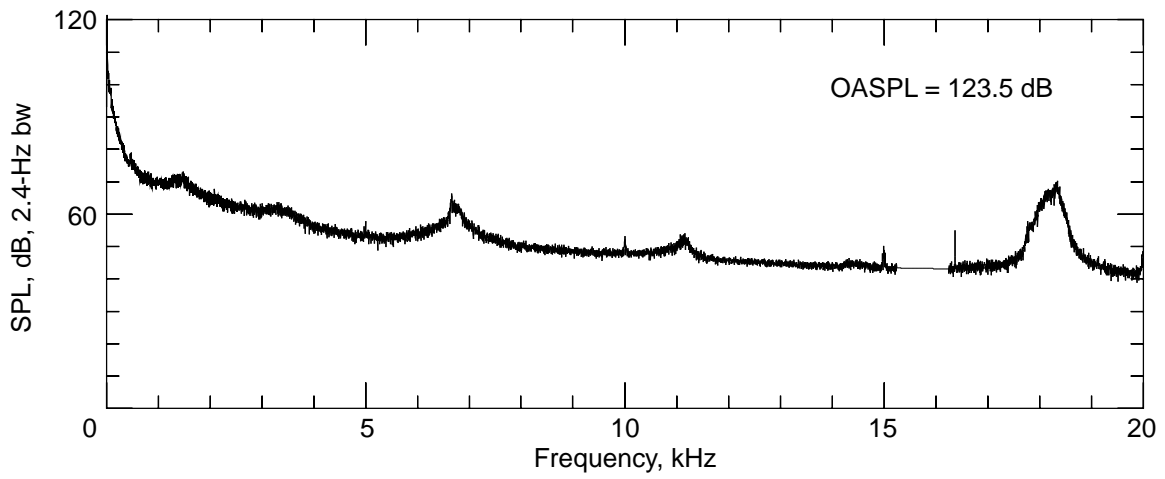
(b) Dynamic pressure = 40 lb/ft<sup>2</sup>.

Figure 17. Continued.



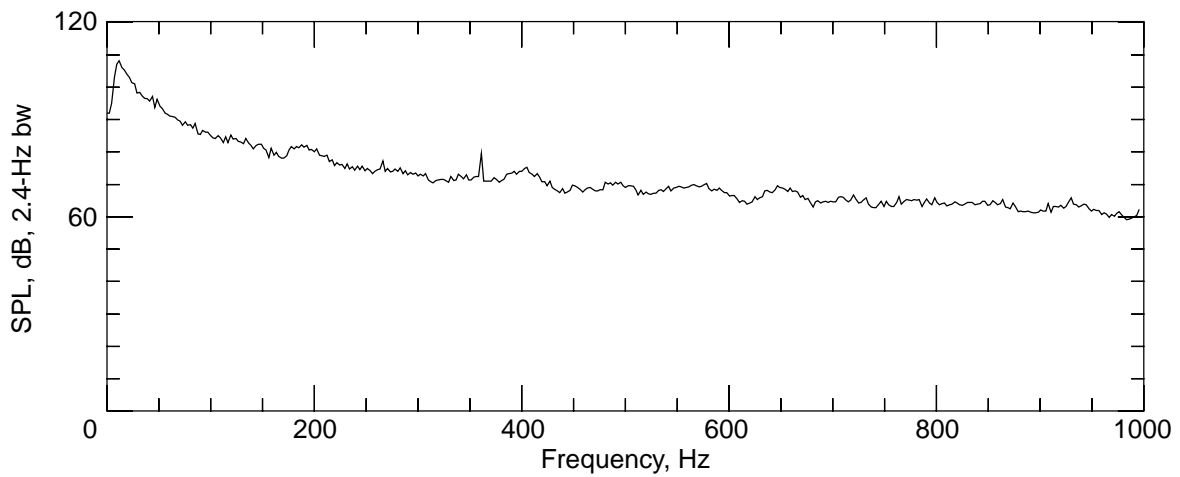
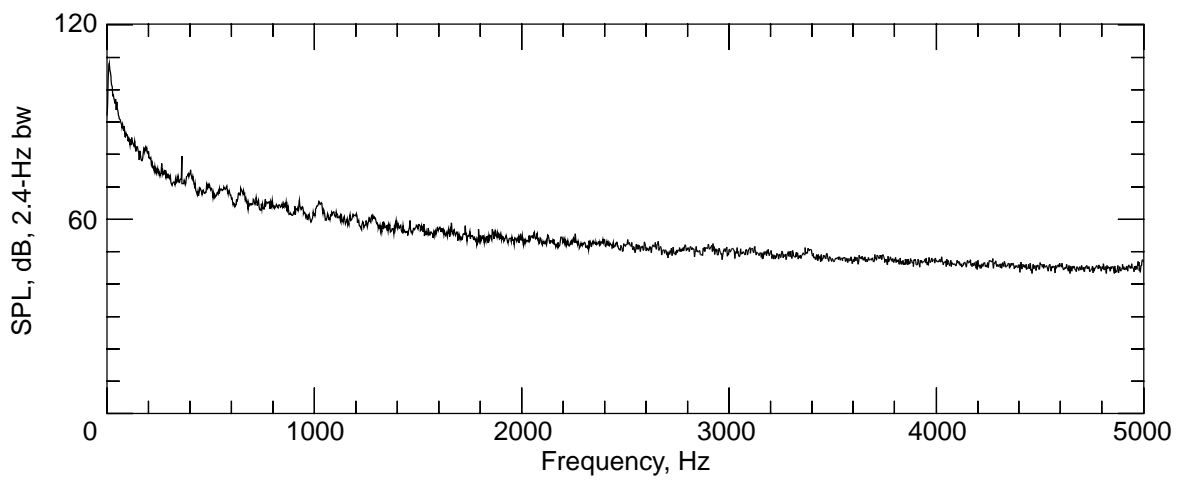
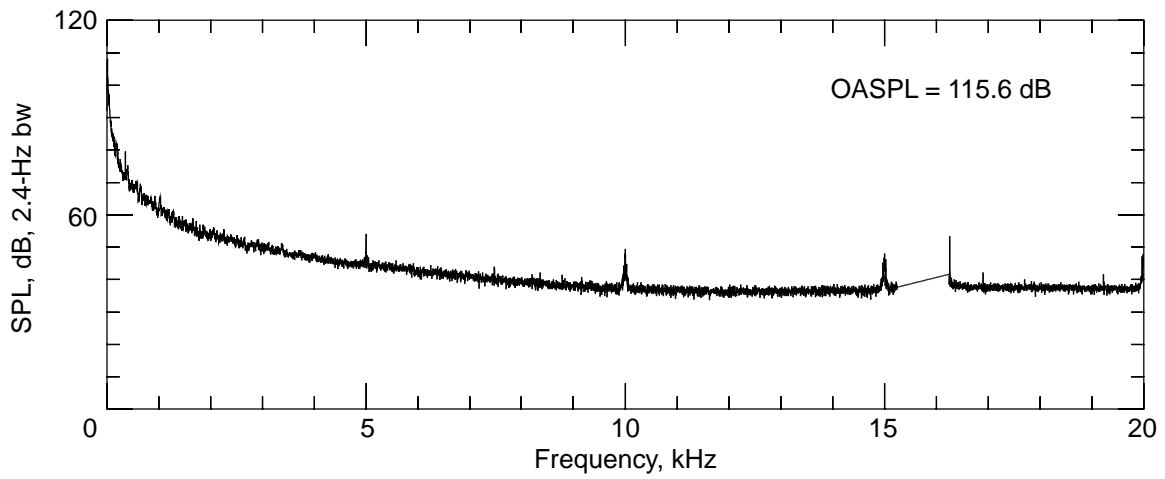
(c) Dynamic pressure = 60 lb/ft<sup>2</sup>.

Figure 17. Continued.



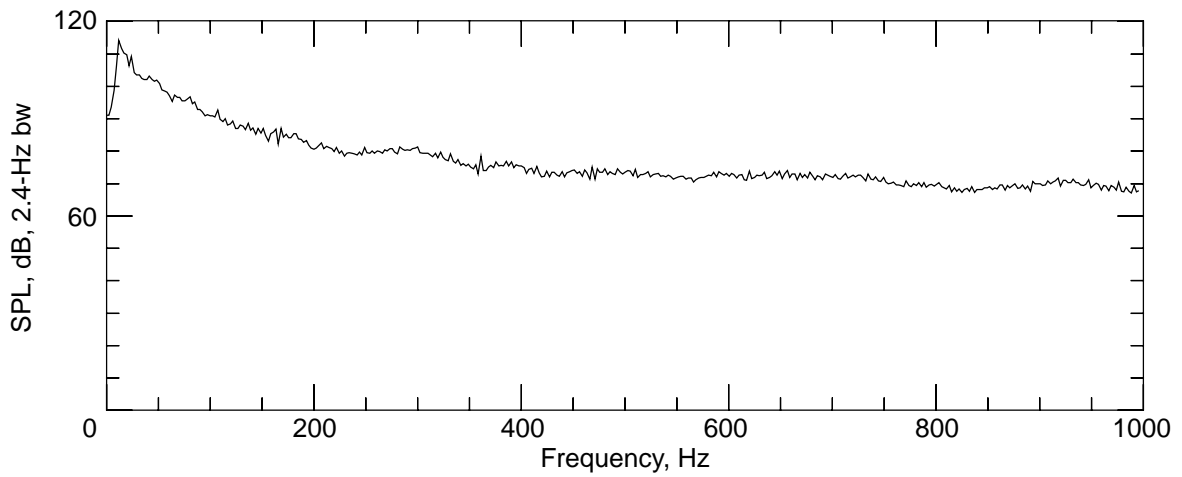
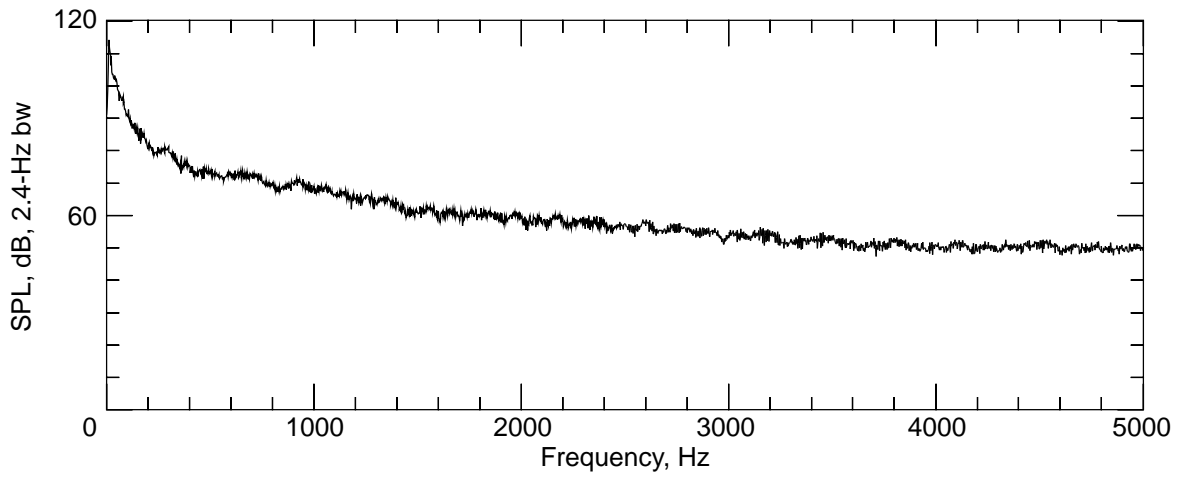
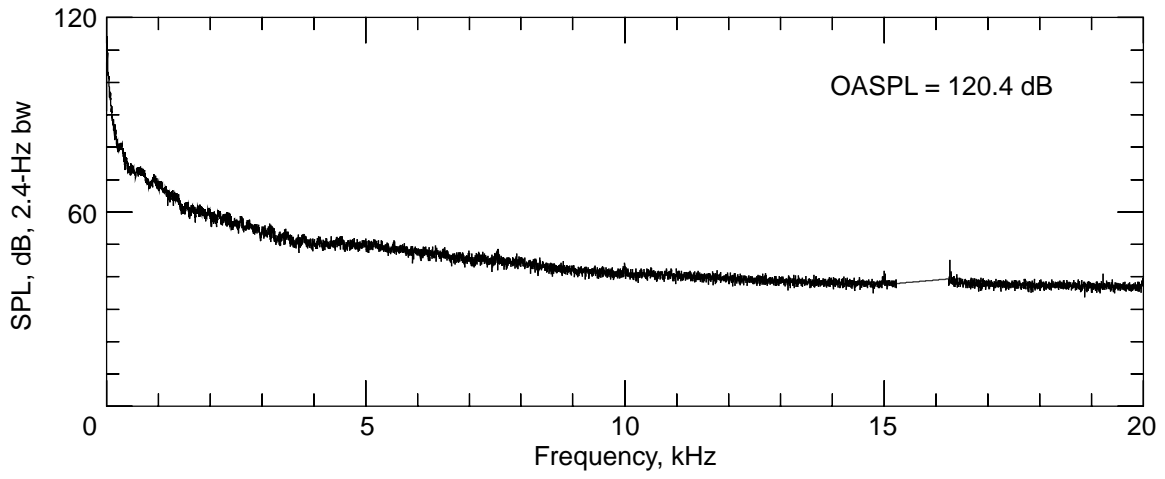
(d) Dynamic pressure = 70 lb/ft<sup>2</sup>.

Figure 17. Concluded.



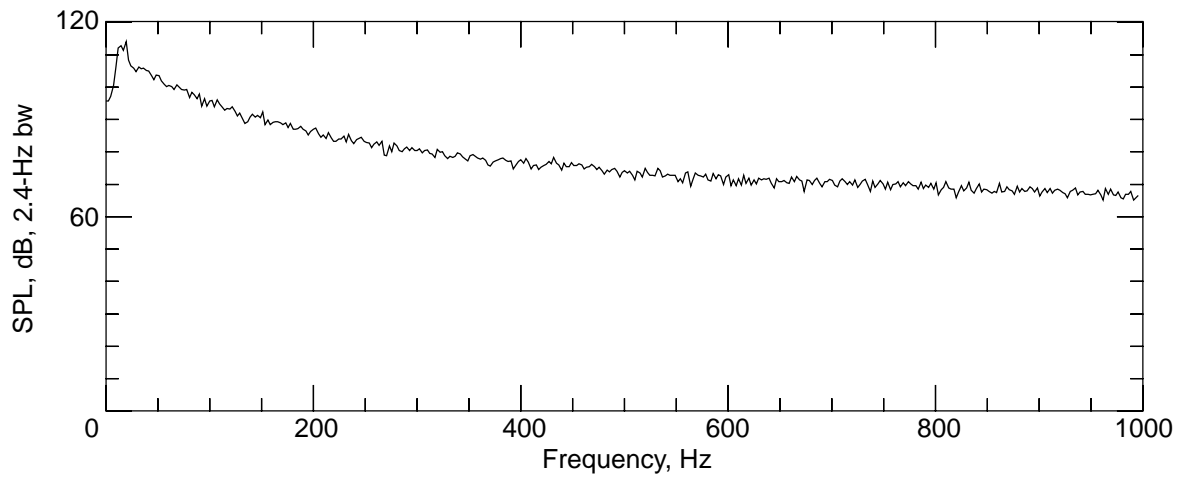
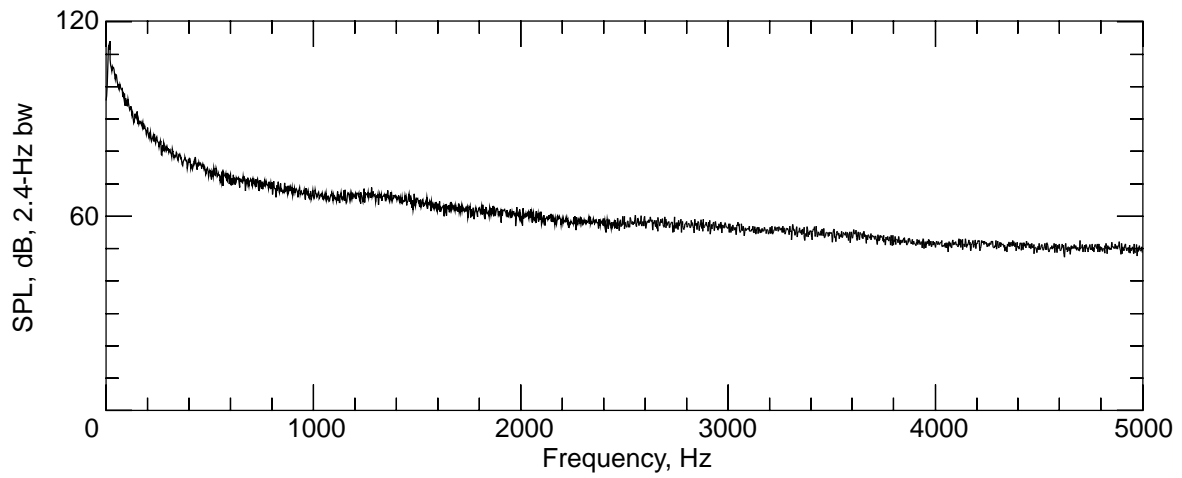
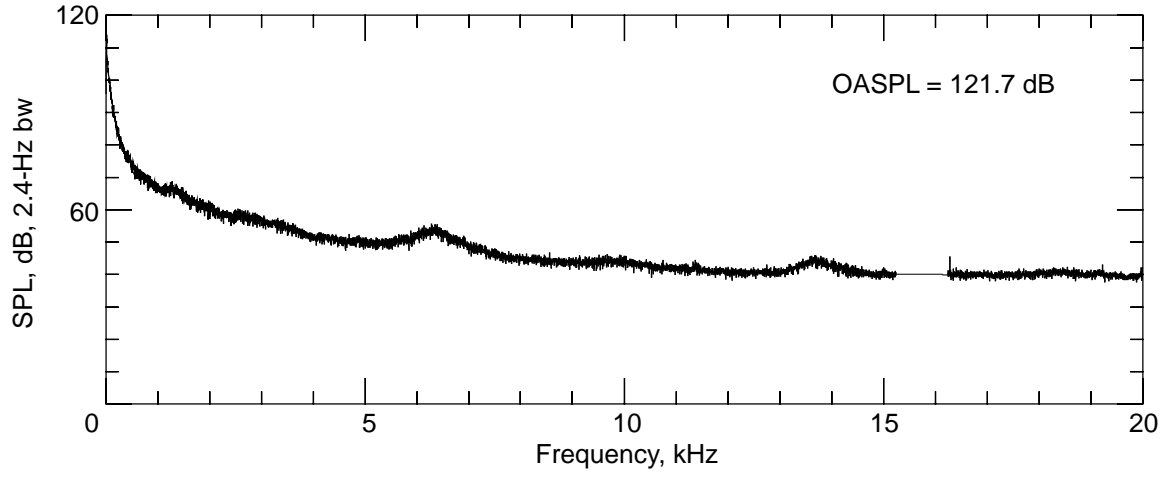
(a) Dynamic pressure = 20 lb/ft<sup>2</sup>.

Figure 18. Flow noise measurement in entrance of collector.



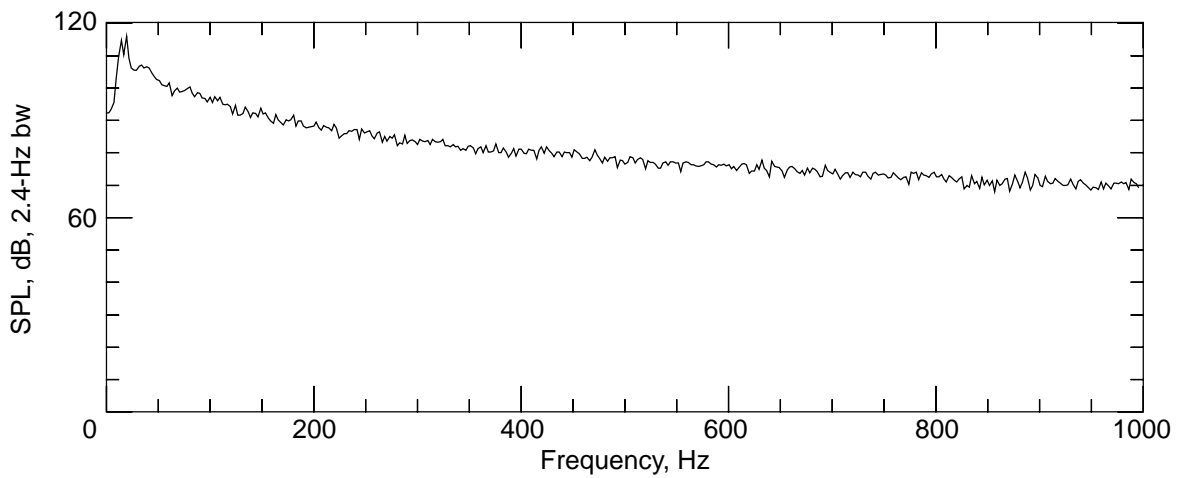
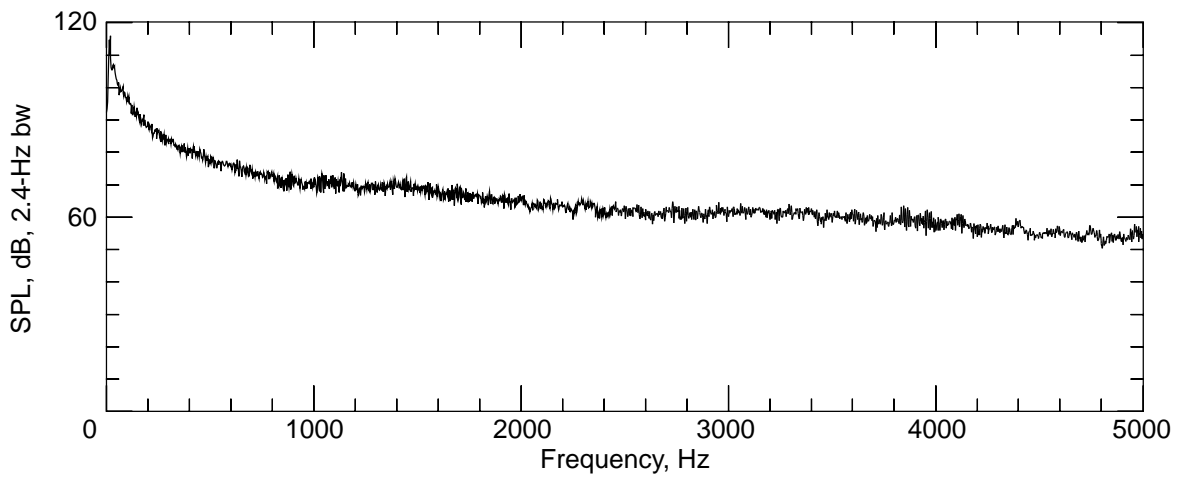
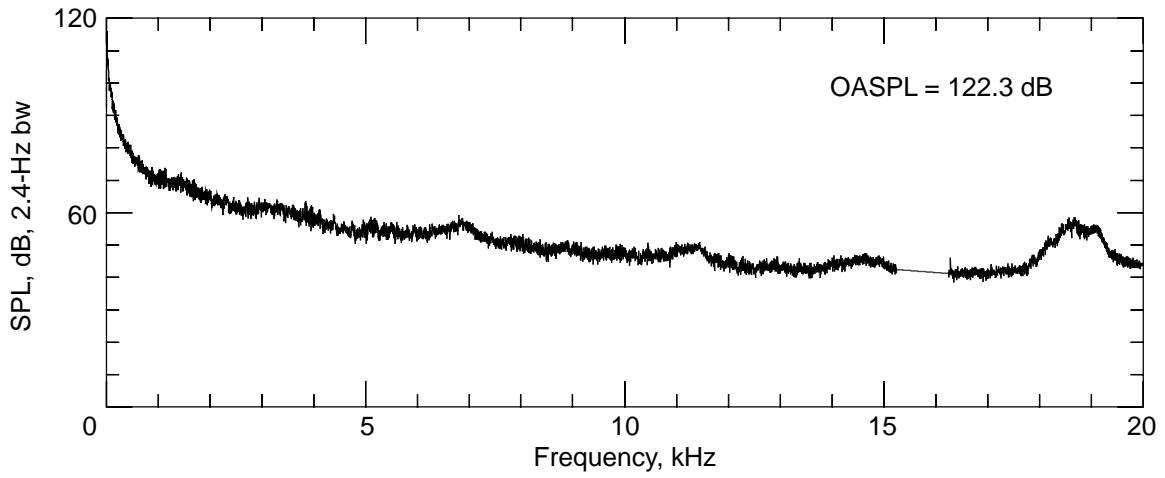
(b) Dynamic pressure = 40 lb/ft<sup>2</sup>.

Figure 18. Continued.



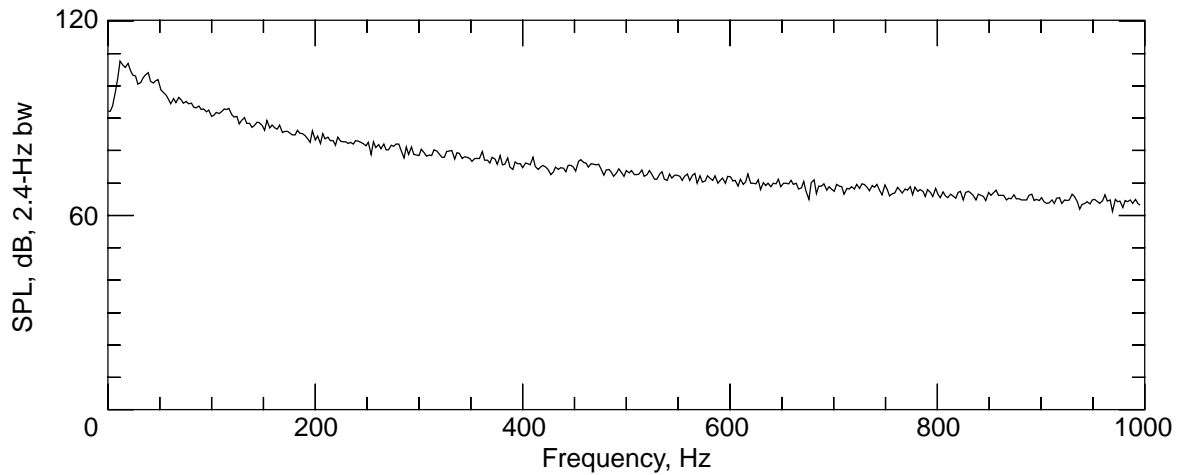
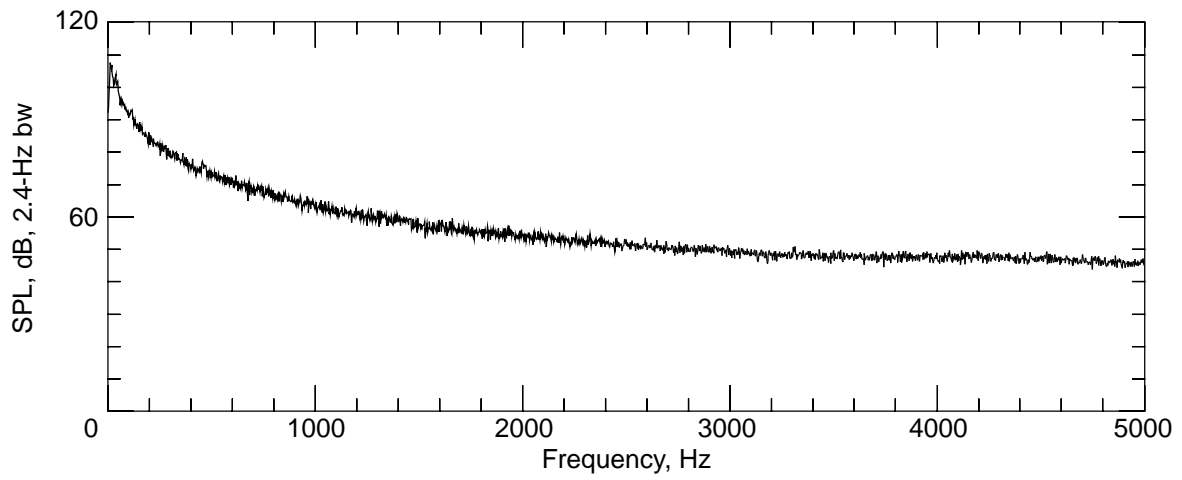
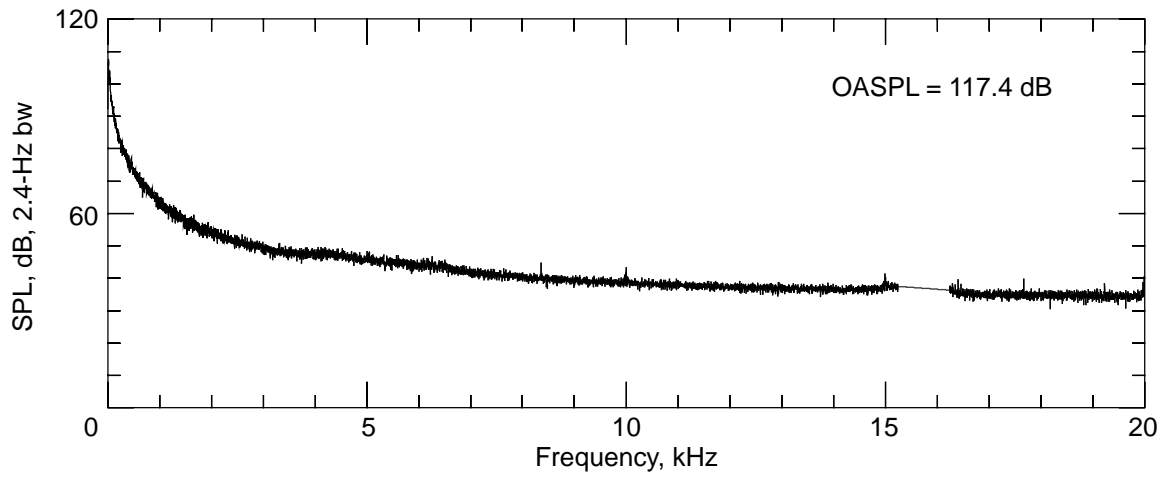
(c) Dynamic pressure = 60 lb/ft<sup>2</sup>.

Figure 18. Continued.



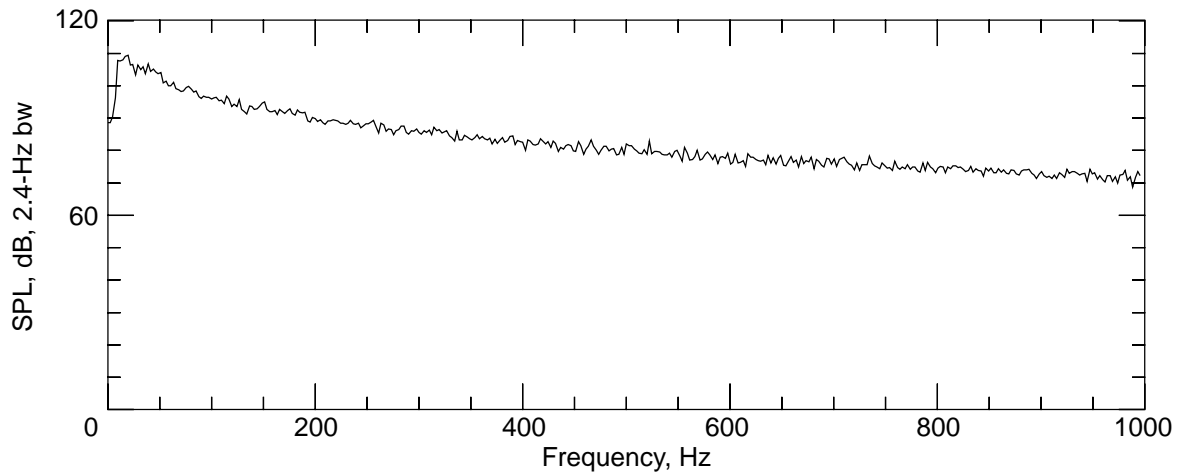
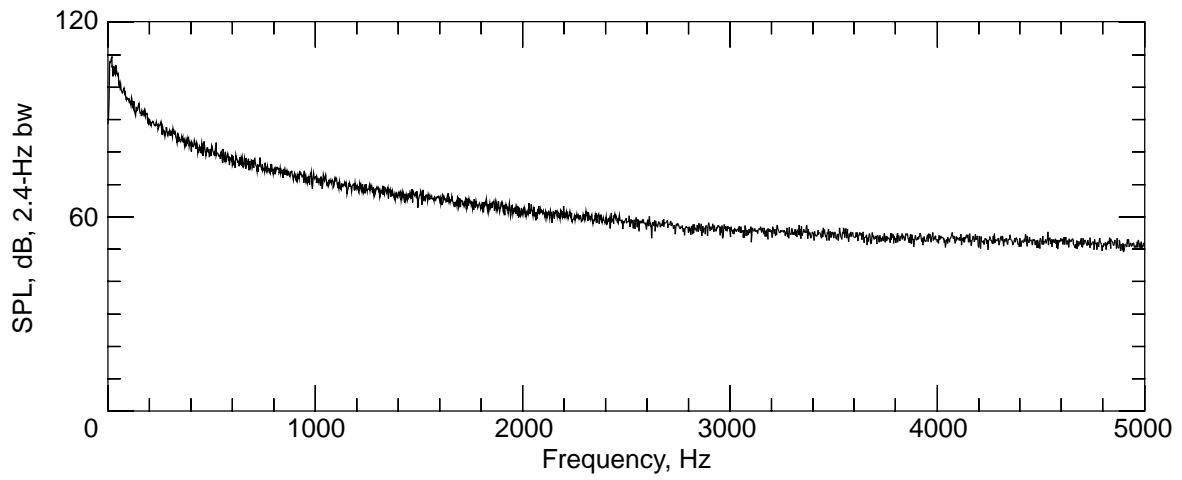
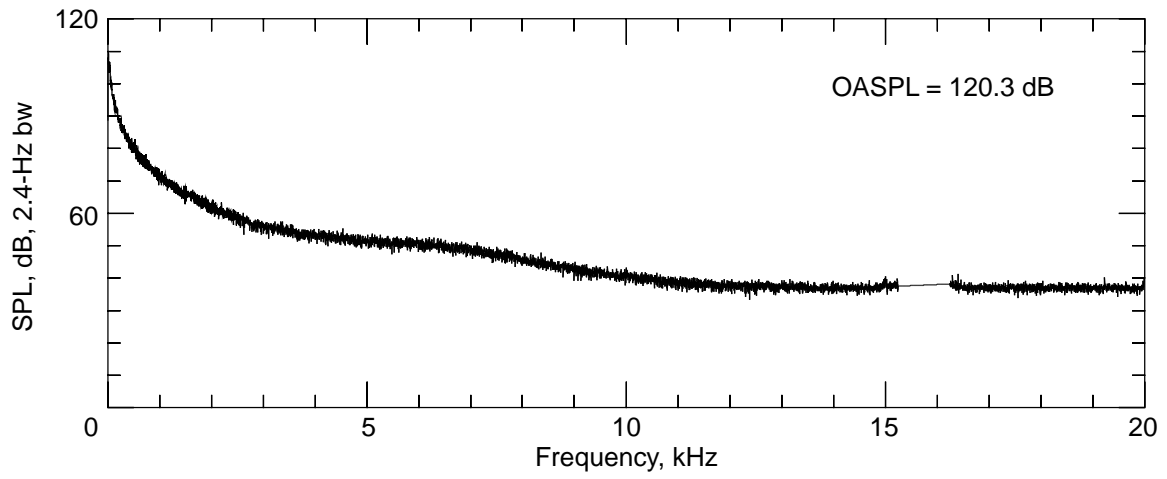
(d) Dynamic pressure = 70 lb/ft<sup>2</sup>.

Figure 18. Concluded.



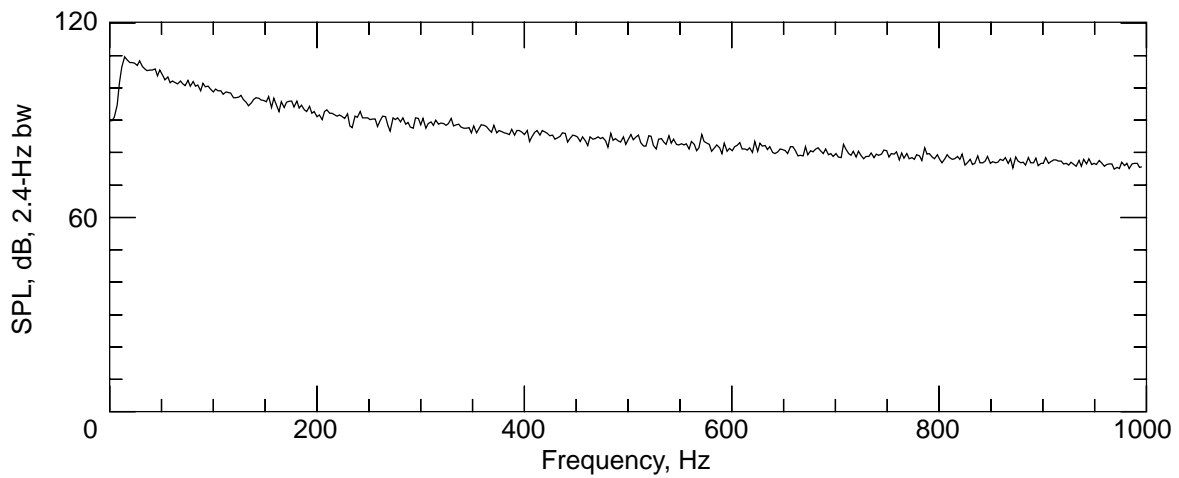
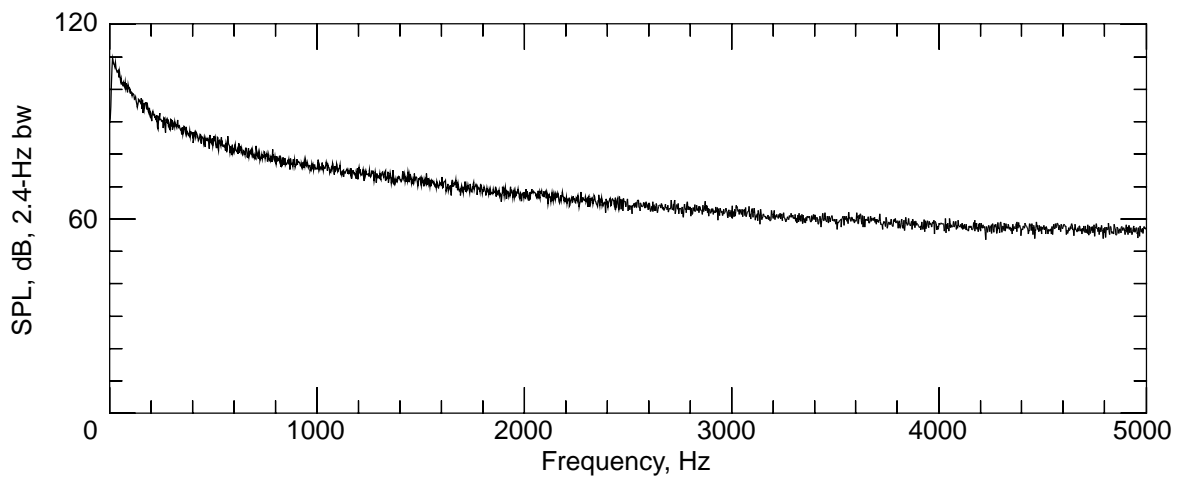
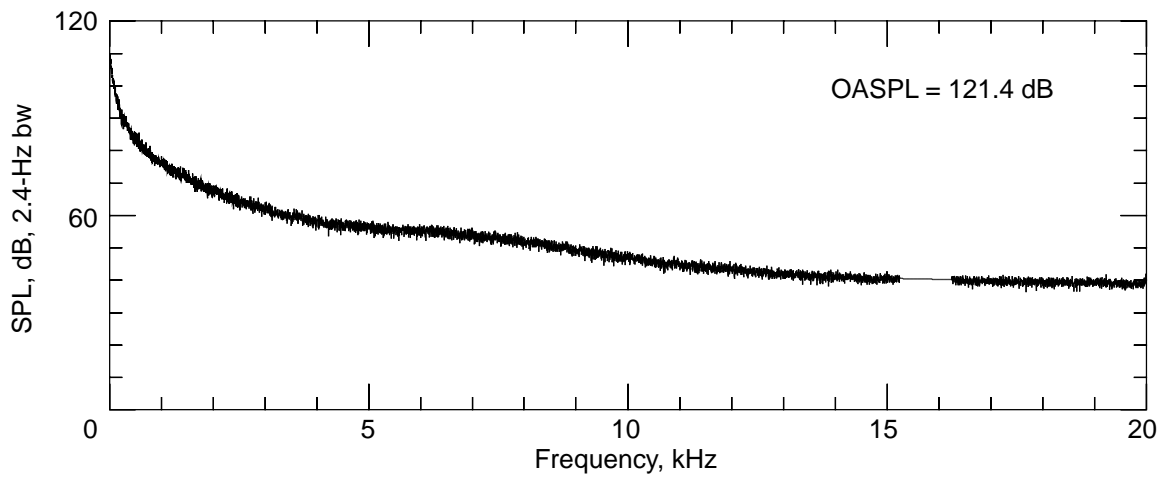
(a) Dynamic pressure = 20 lb/ft<sup>2</sup>.

Figure 19. Flow noise measurement in first diffuser with B.L.S. on.



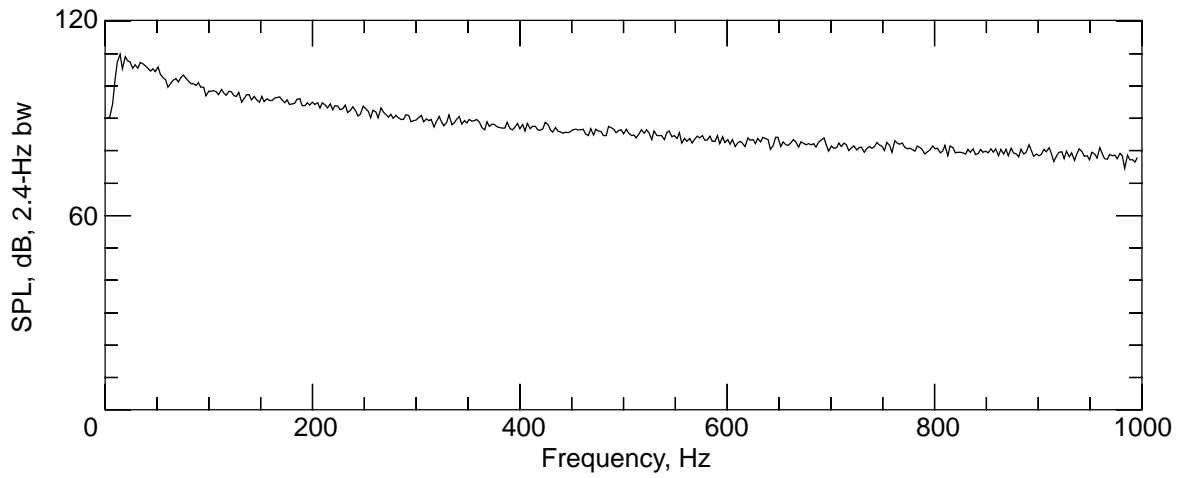
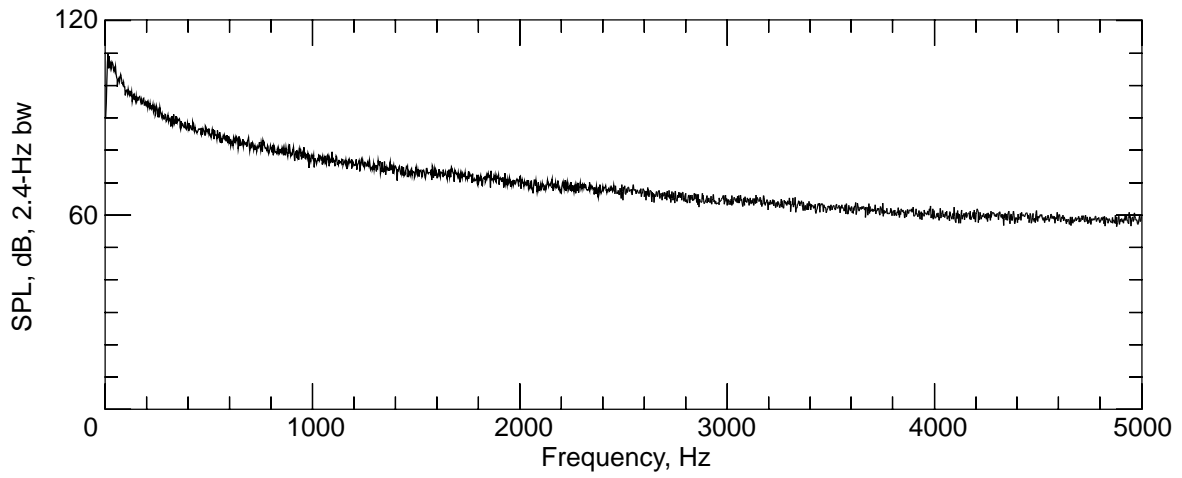
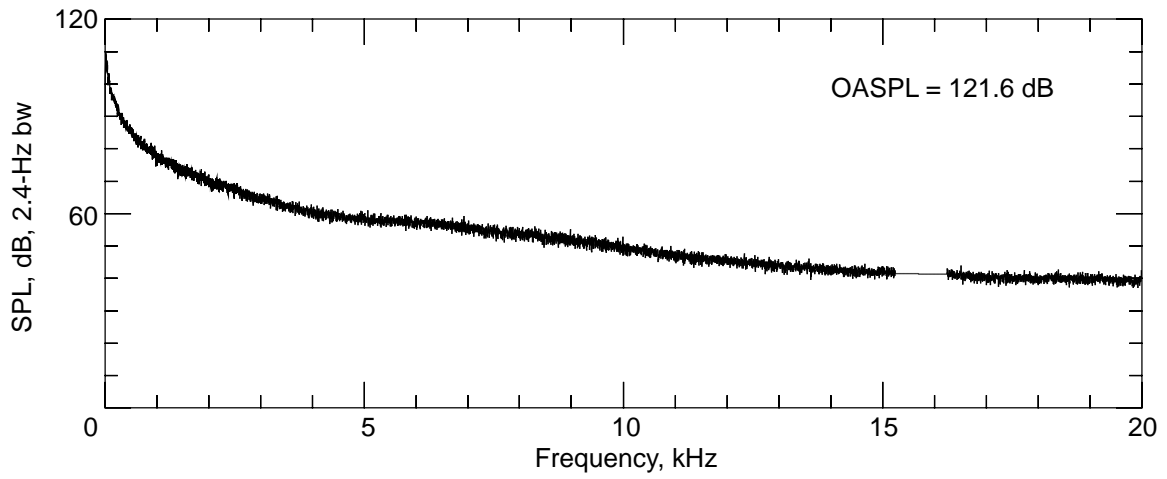
(b) Dynamic pressure = 40 lb/ft<sup>2</sup>.

Figure 19. Continued.



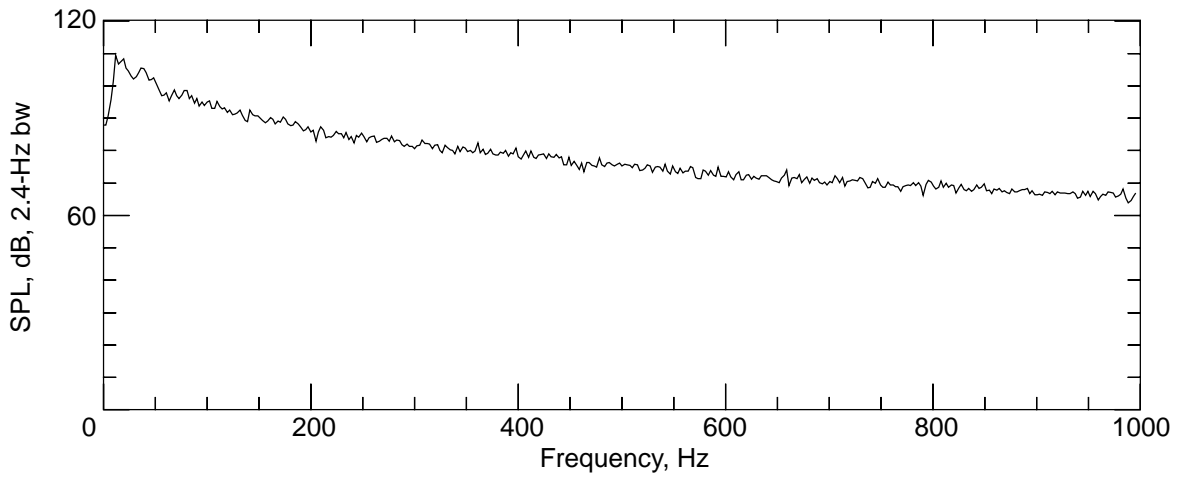
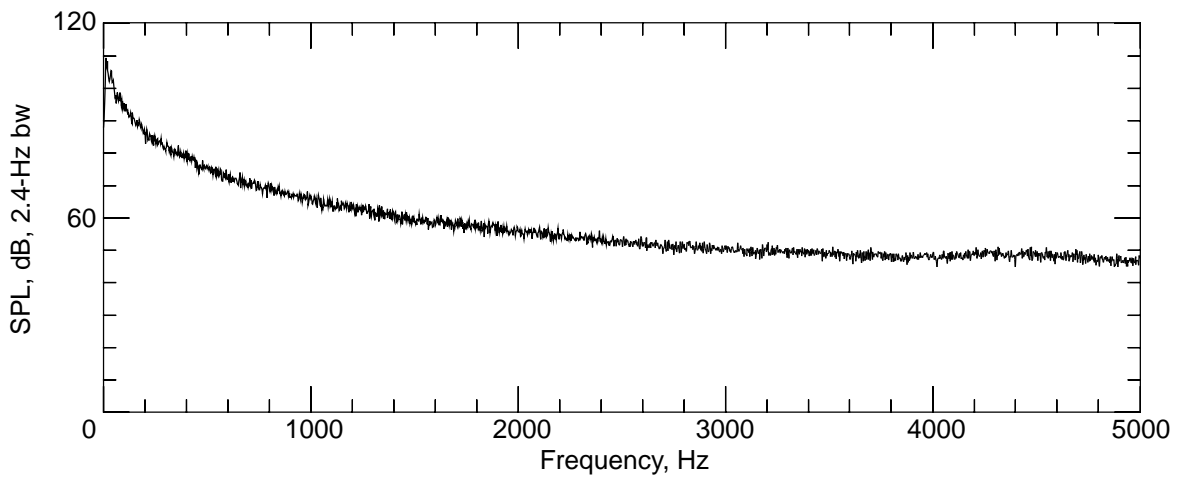
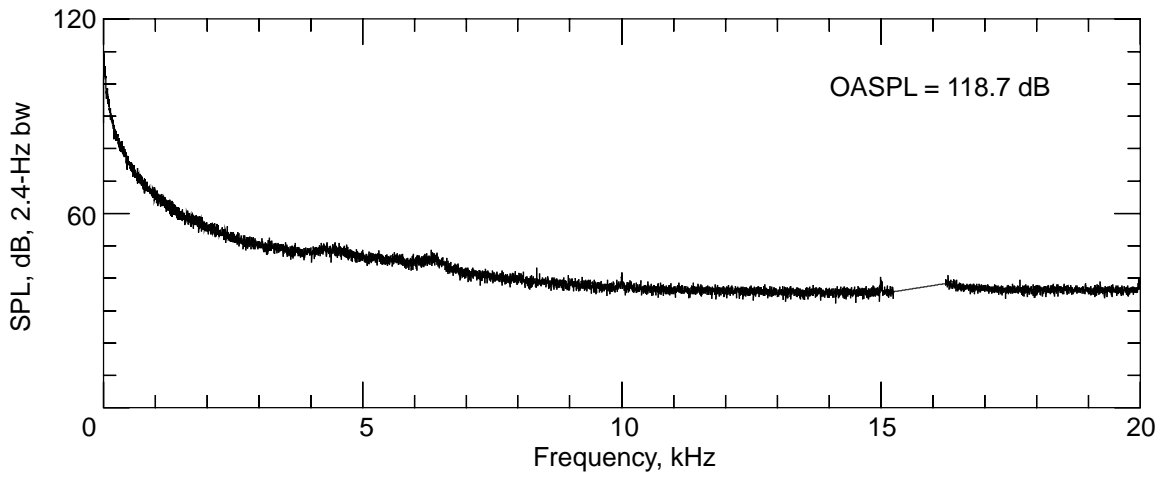
(c) Dynamic pressure = 60 lb/ft<sup>2</sup>.

Figure 19. Continued.



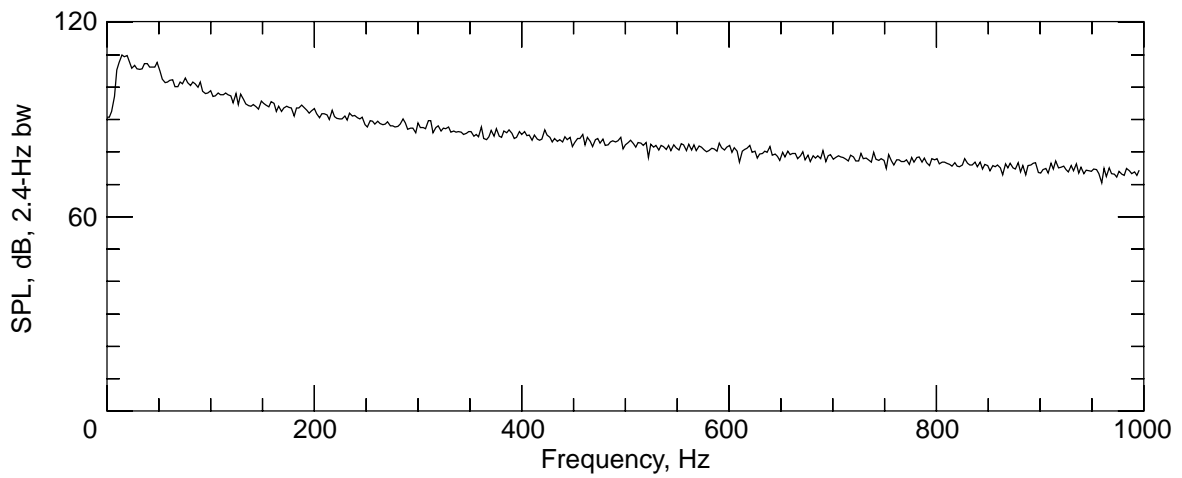
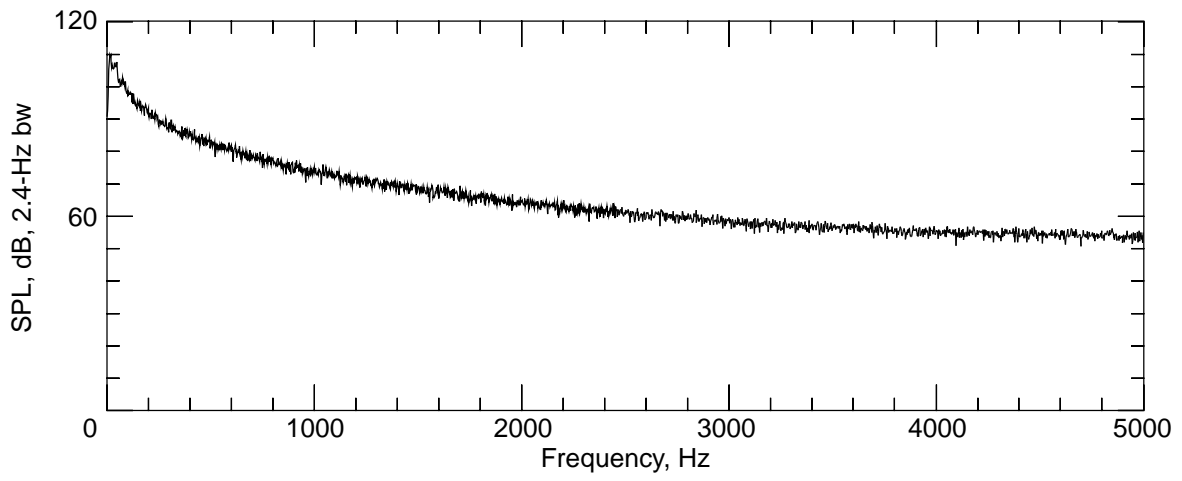
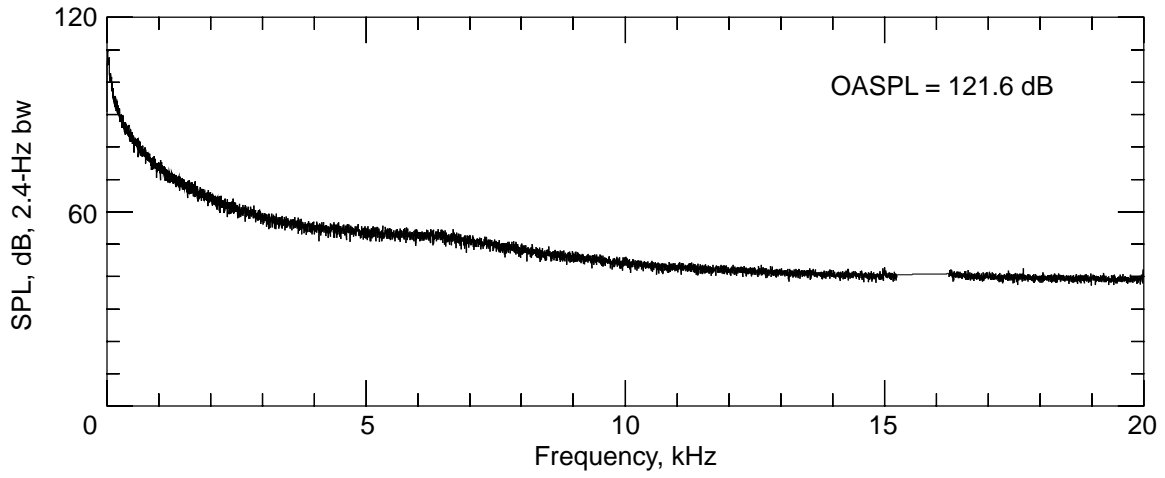
(d) Dynamic pressure = 70 lb/ft<sup>2</sup>.

Figure 19. Concluded.



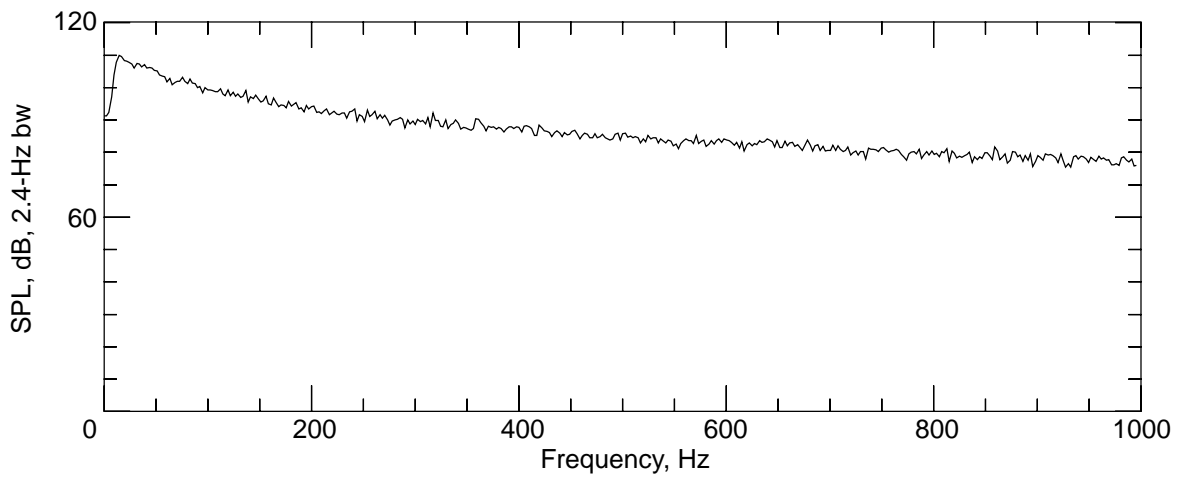
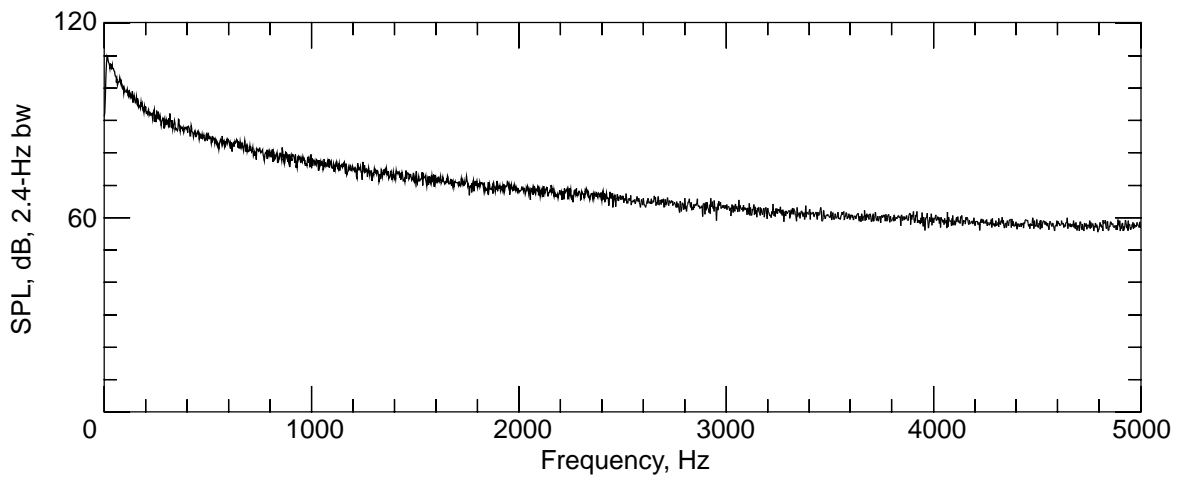
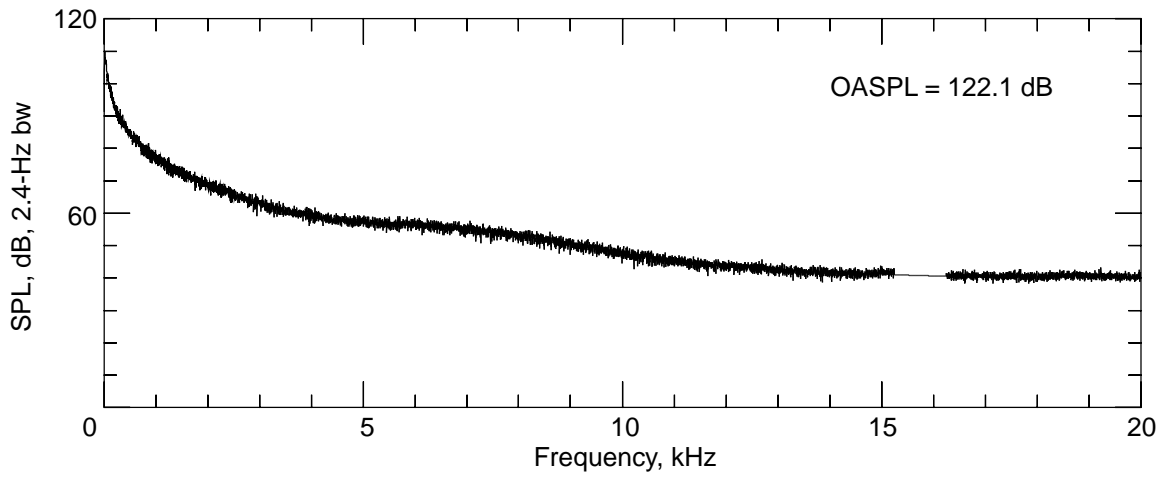
(a) Dynamic pressure = 20 lb/ft<sup>2</sup>.

Figure 20. Flow noise measurement in first diffuser with B.L.S. off.



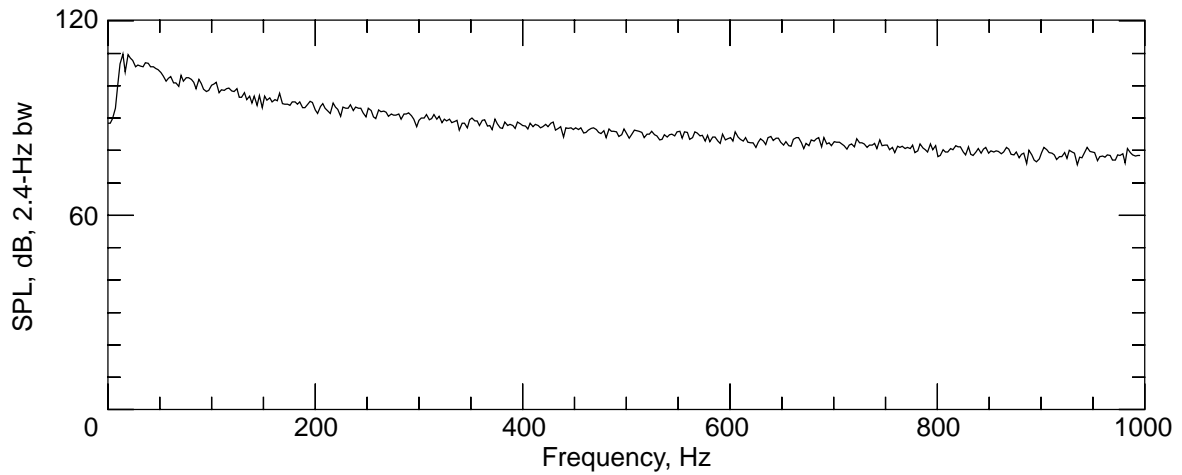
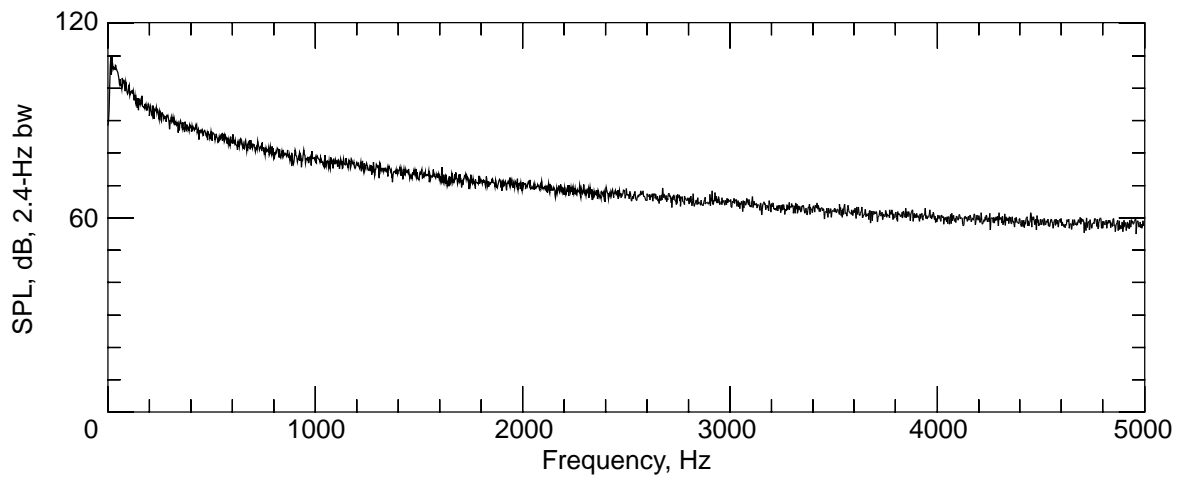
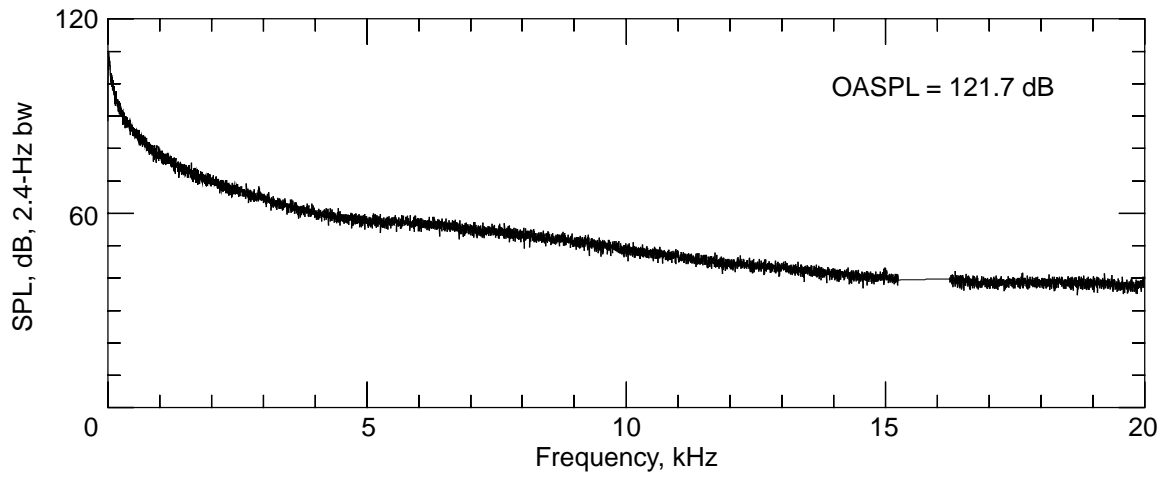
(b) Dynamic pressure = 40 lb/ft<sup>2</sup>.

Figure 20. Continued.



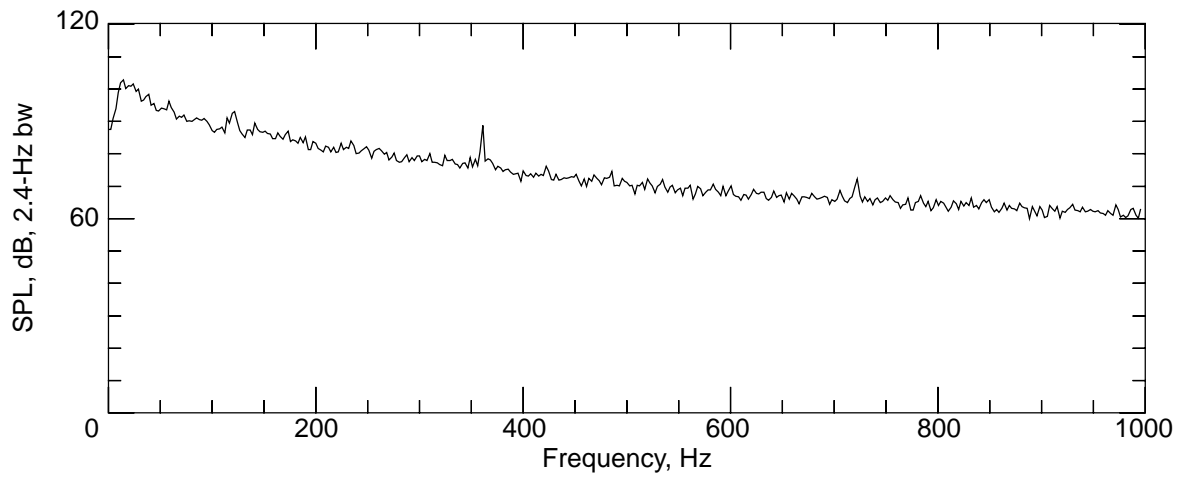
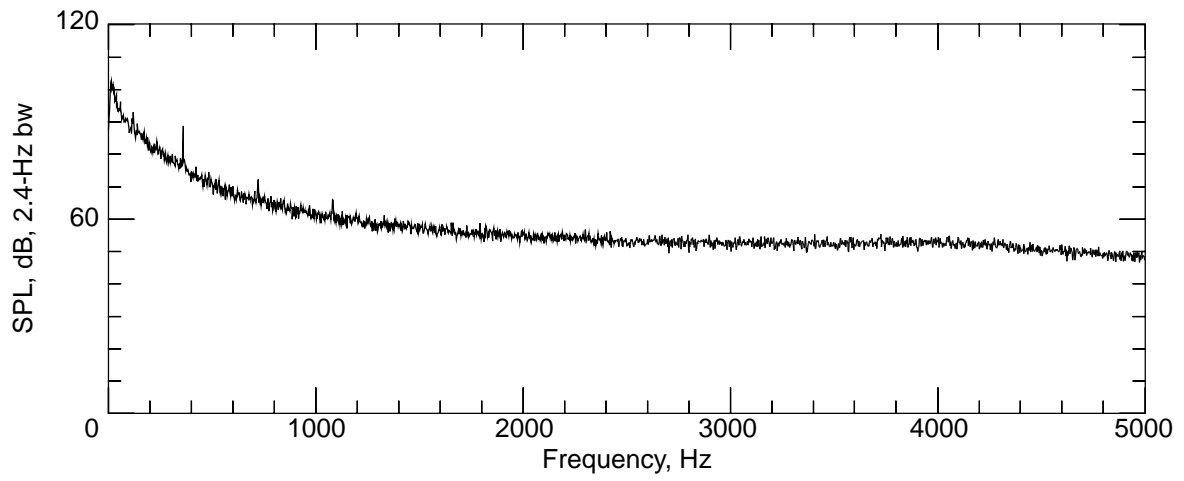
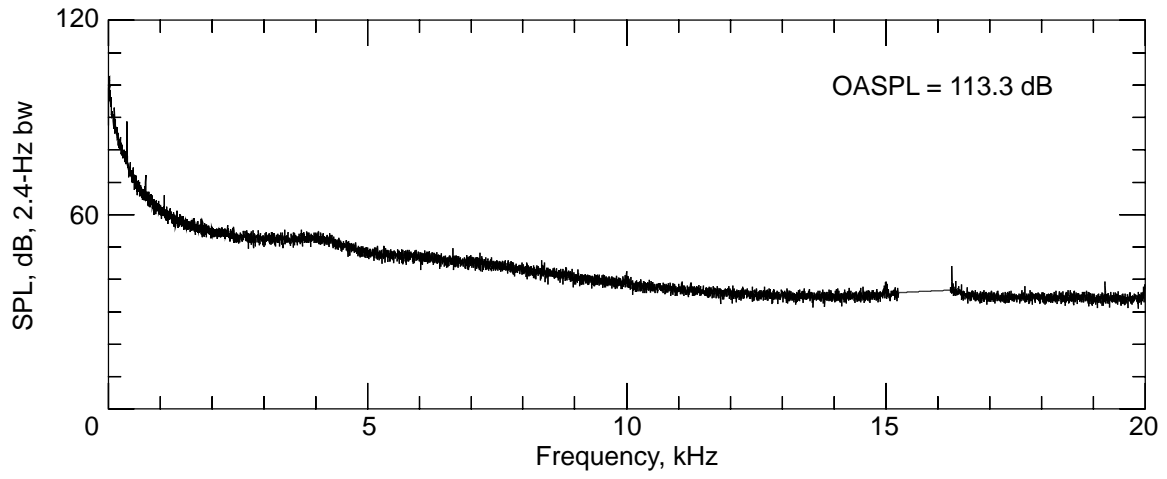
(c) Dynamic pressure = 60 lb/ft<sup>2</sup>.

Figure 20. Continued.



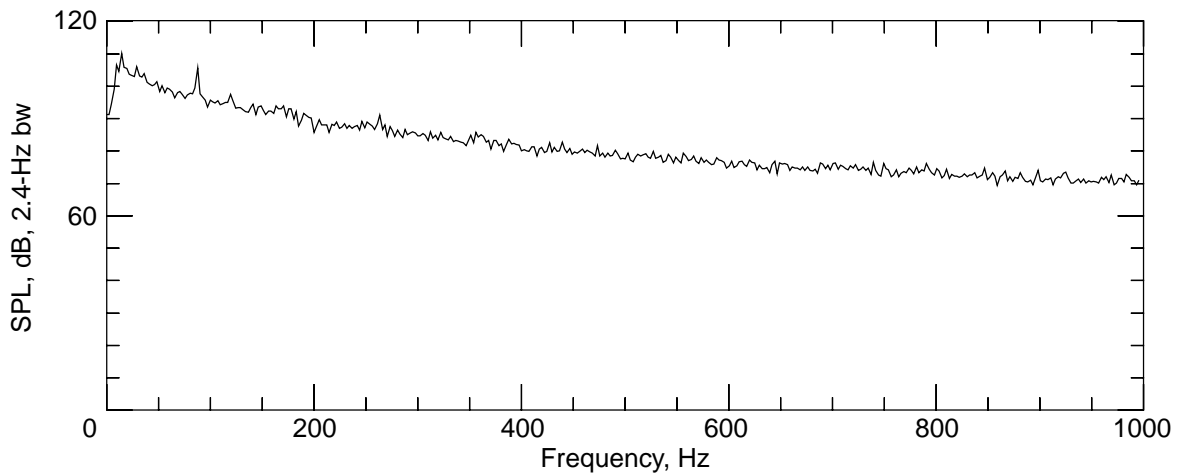
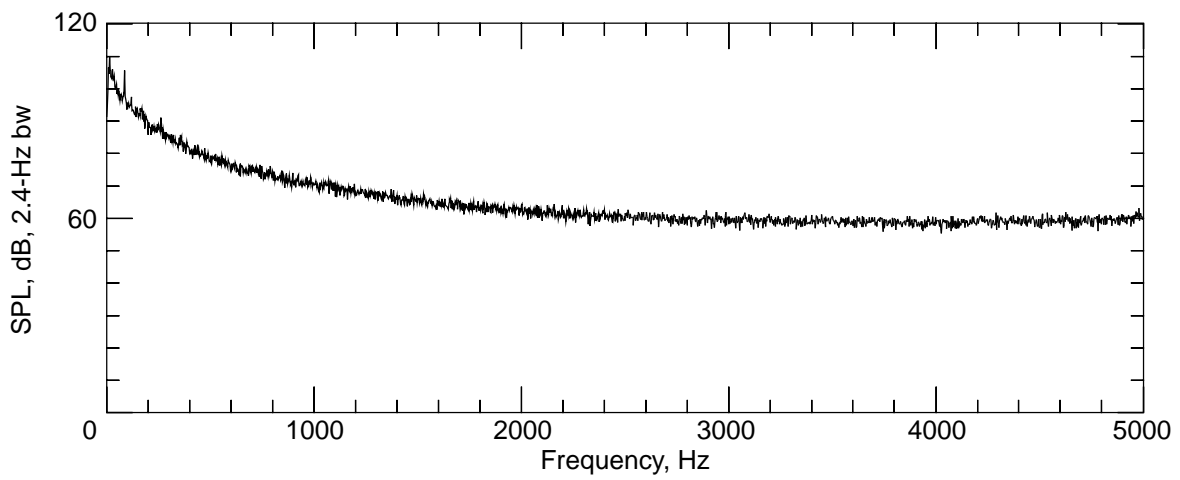
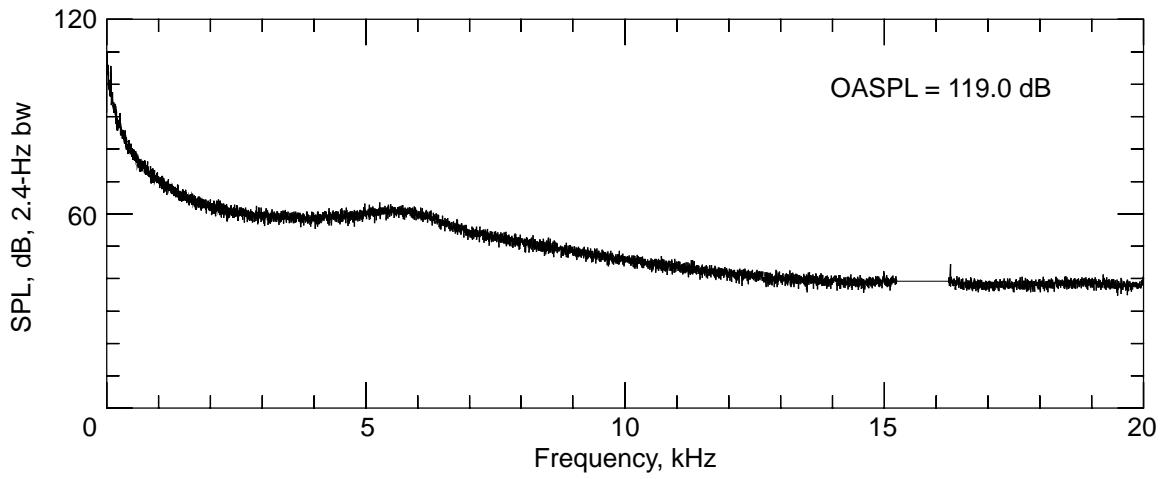
(d) Dynamic pressure = 70 lb/ft<sup>2</sup>.

Figure 20. Concluded.



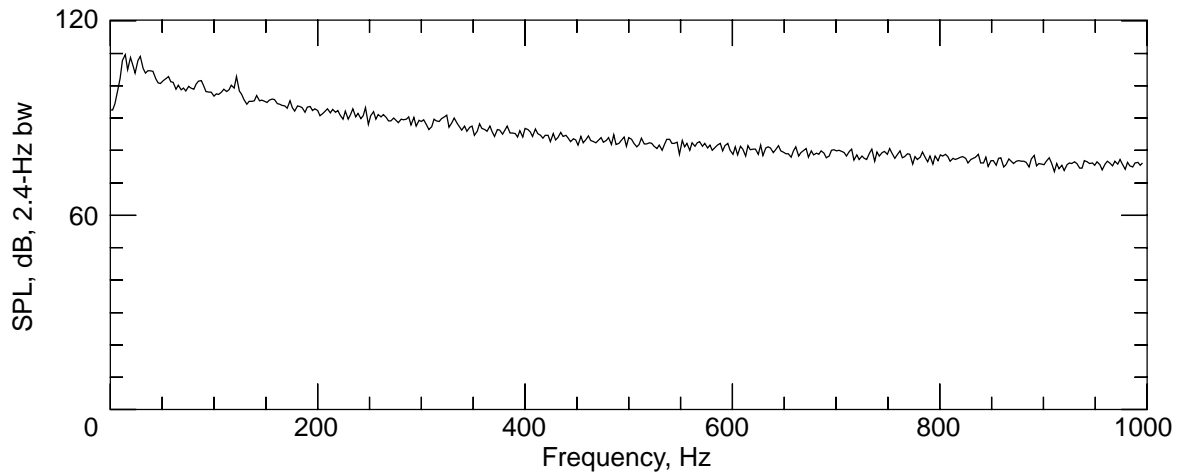
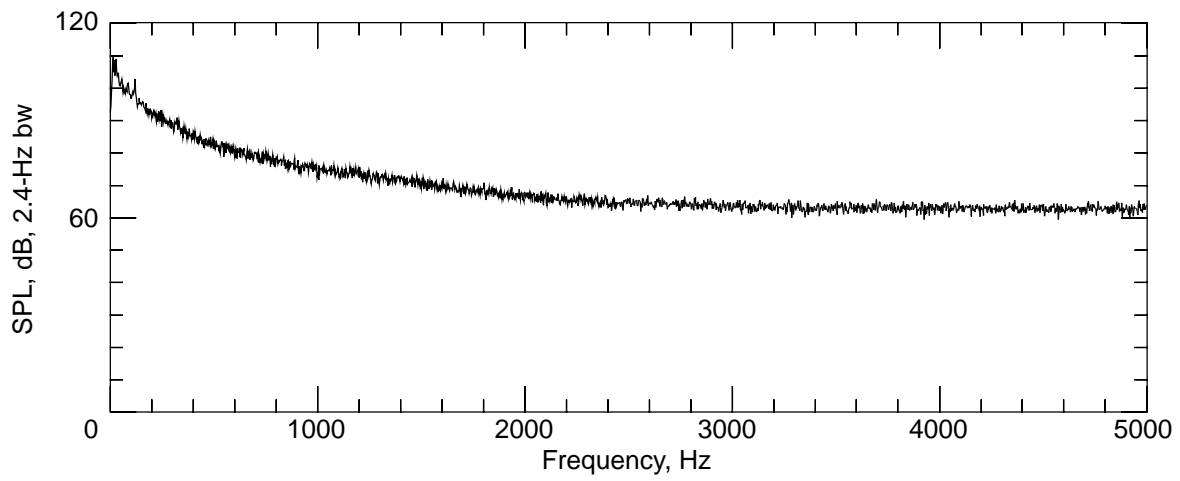
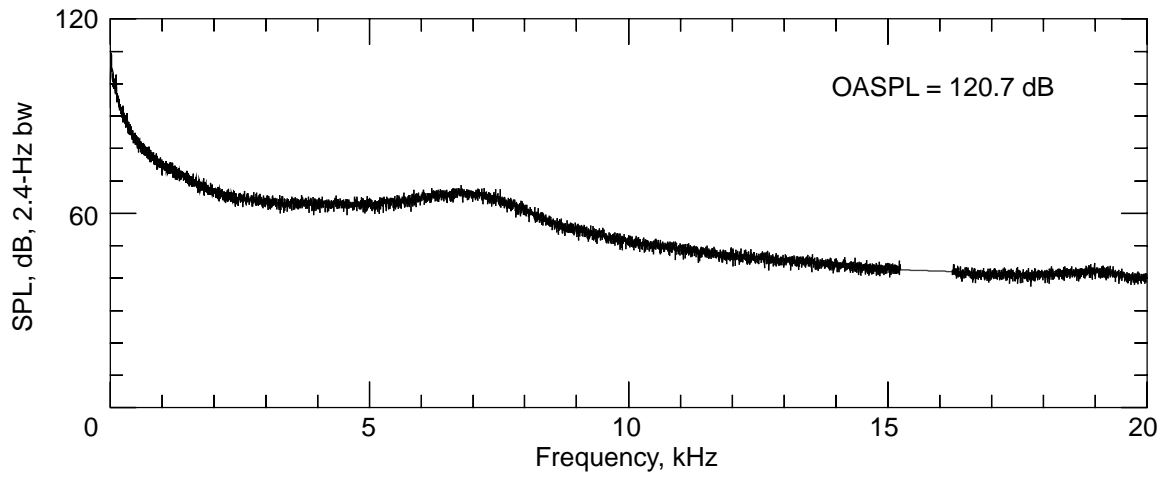
(a) Dynamic pressure = 20 lb/ft<sup>2</sup>.

Figure 21. Flow noise measurement upstream of turn 2 with B.L.S. on.



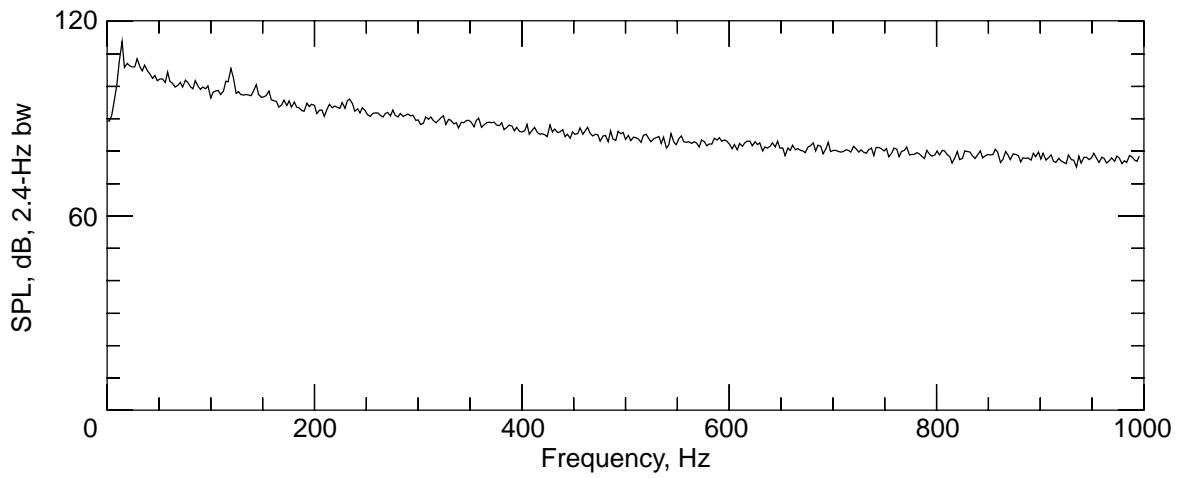
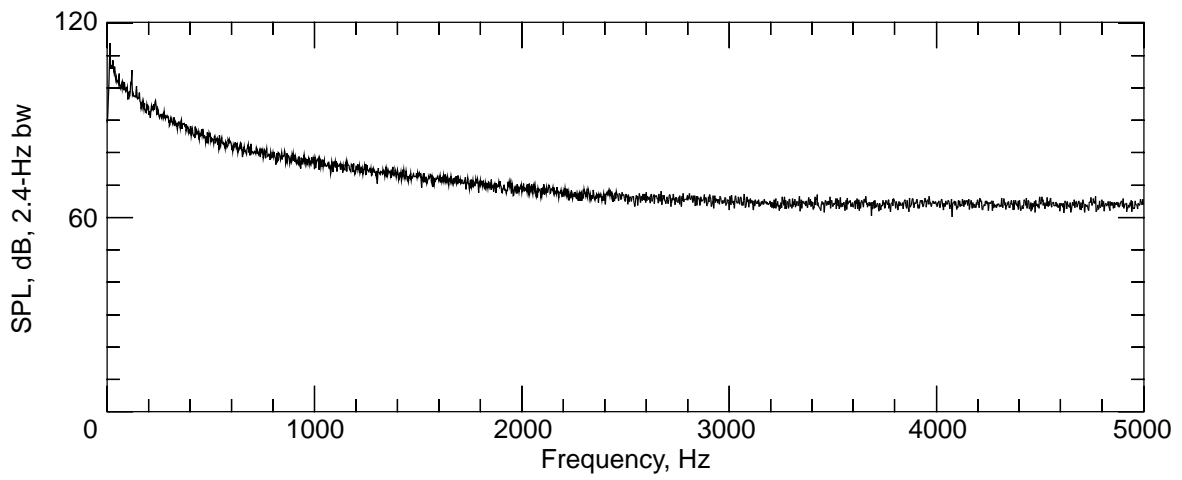
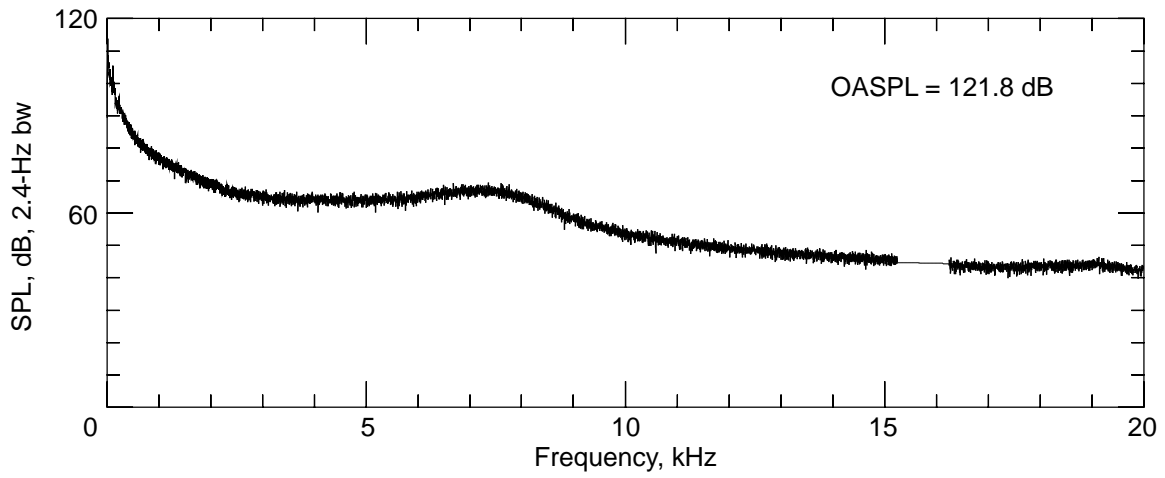
(b) Dynamic pressure = 40 lb/ft<sup>2</sup>.

Figure 21. Continued.



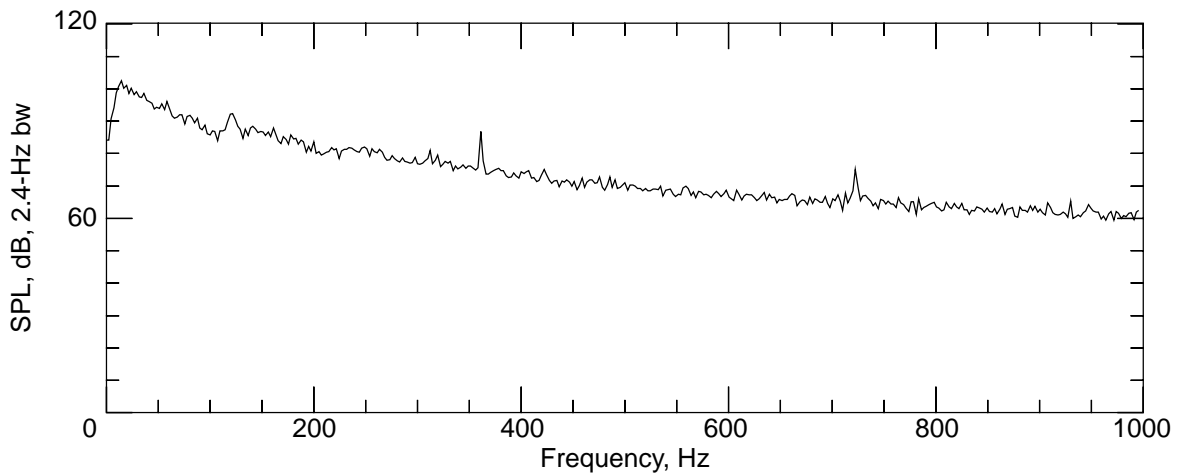
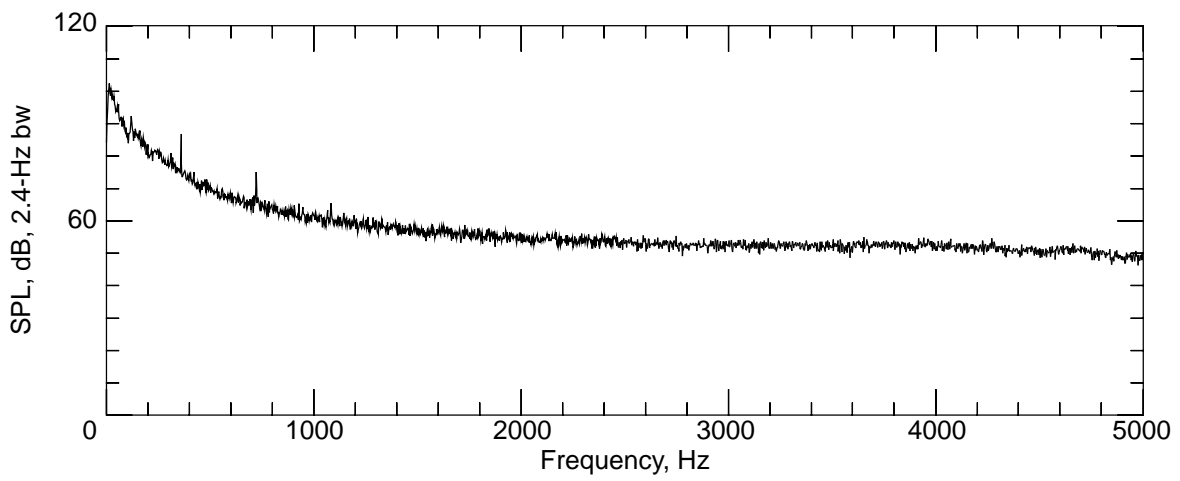
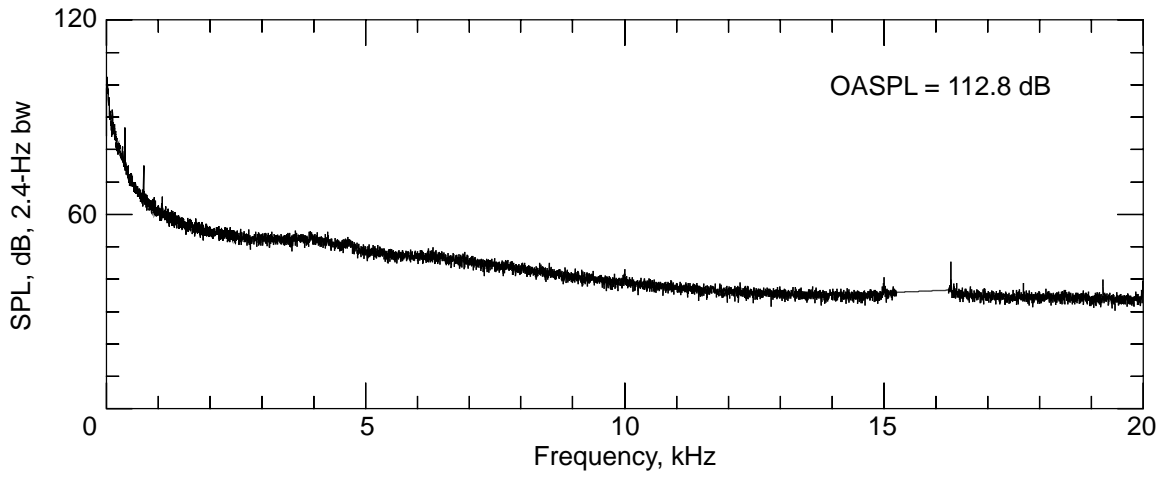
(c) Dynamic pressure = 60 lb/ft<sup>2</sup>.

Figure 21. Continued.



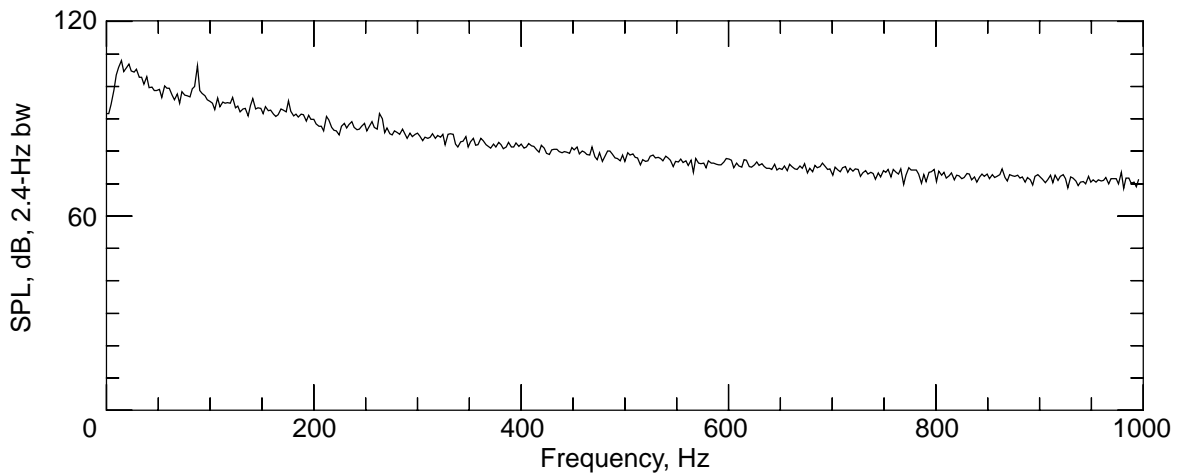
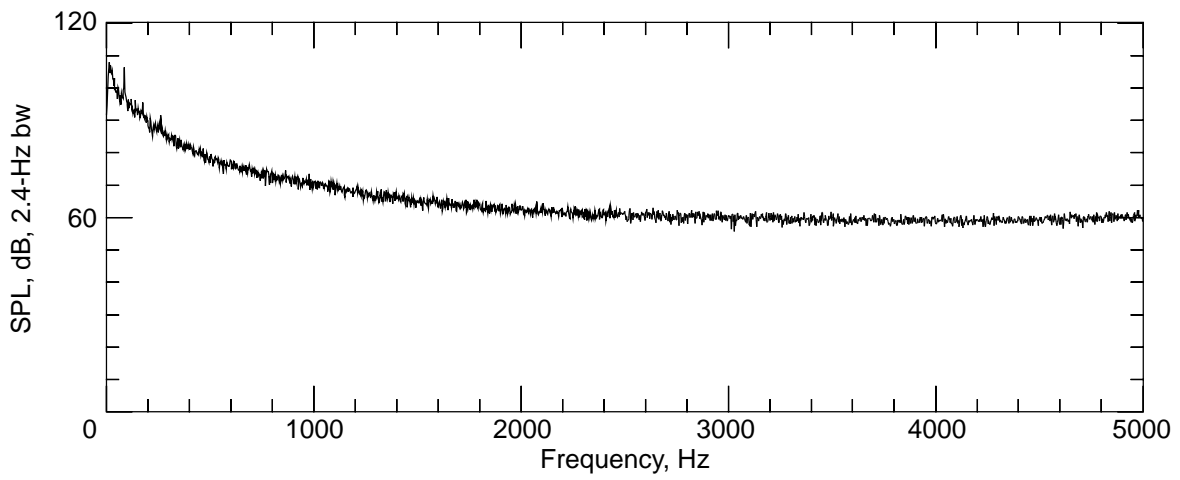
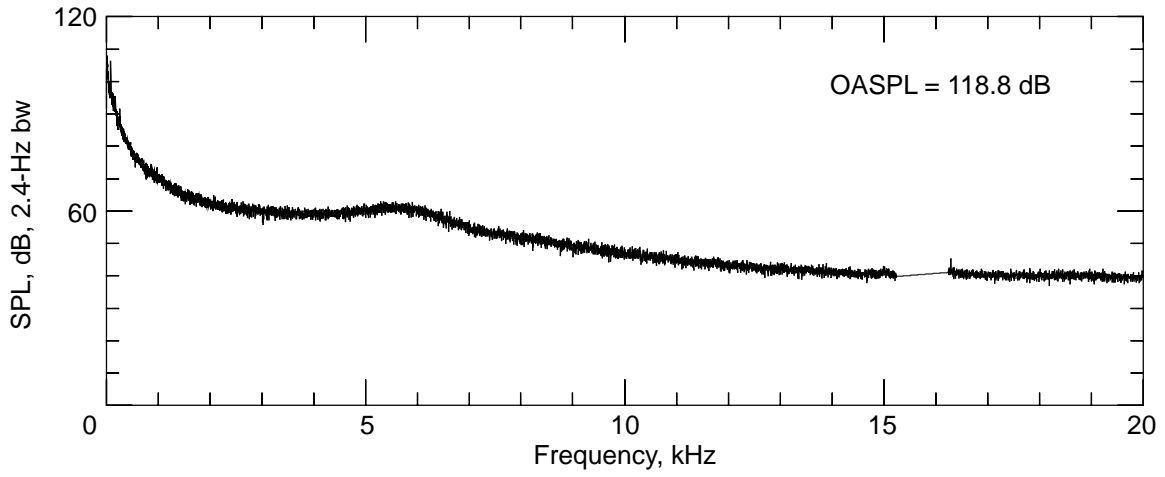
(d) Dynamic pressure = 70 lb/ft<sup>2</sup>.

Figure 21. Concluded.



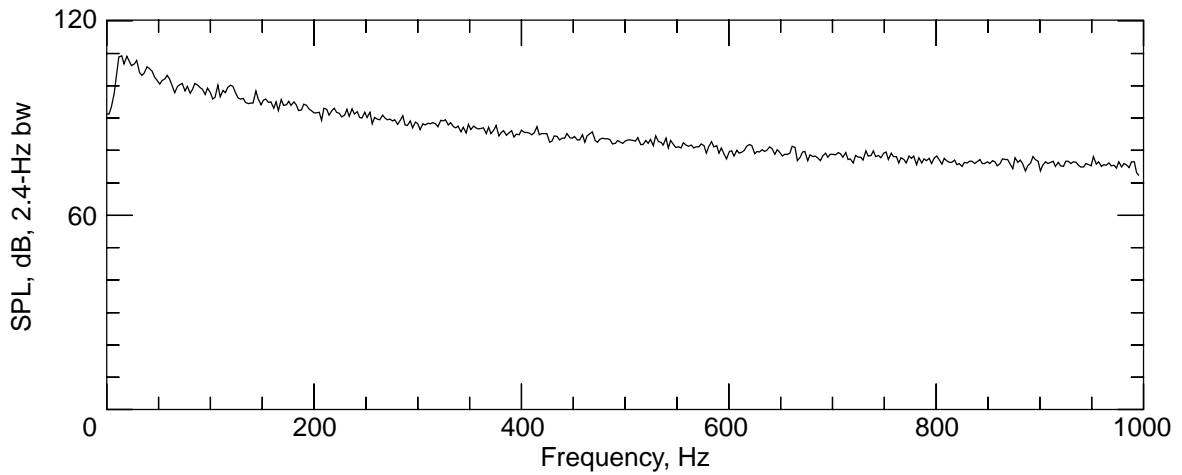
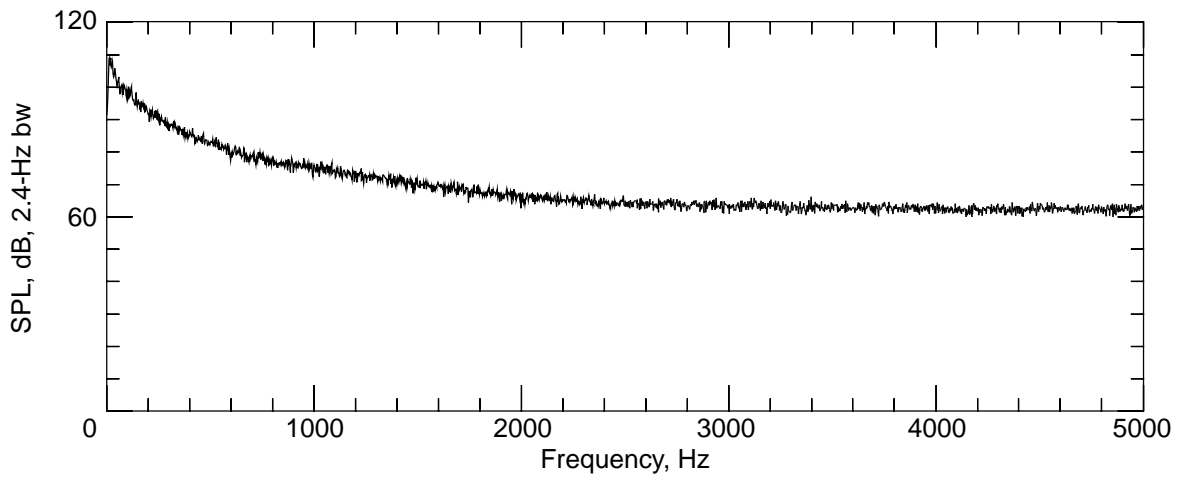
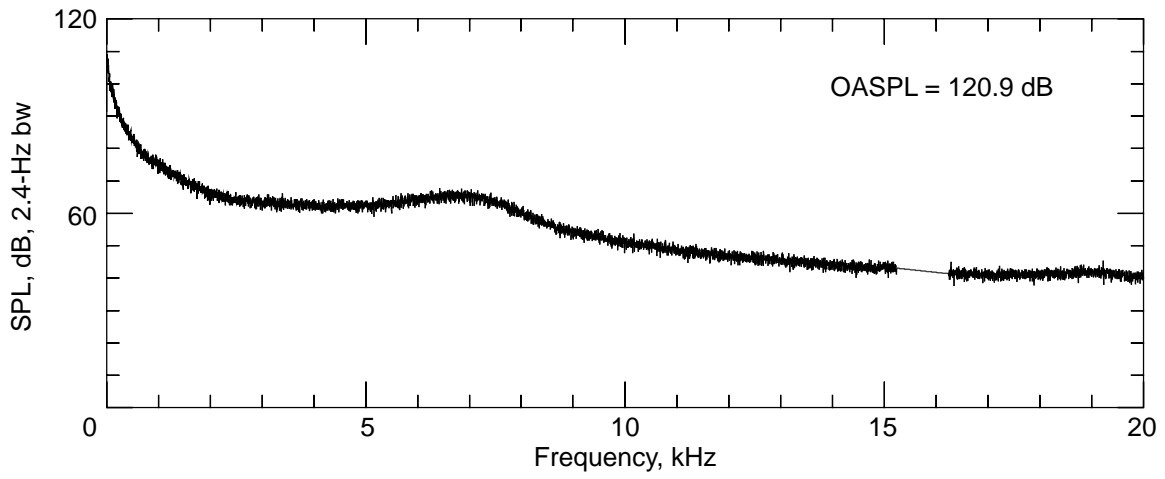
(a) Dynamic pressure = 20 lb/ft<sup>2</sup>.

Figure 22. Flow noise measurement upstream of turn 2 with B.L.S. off.



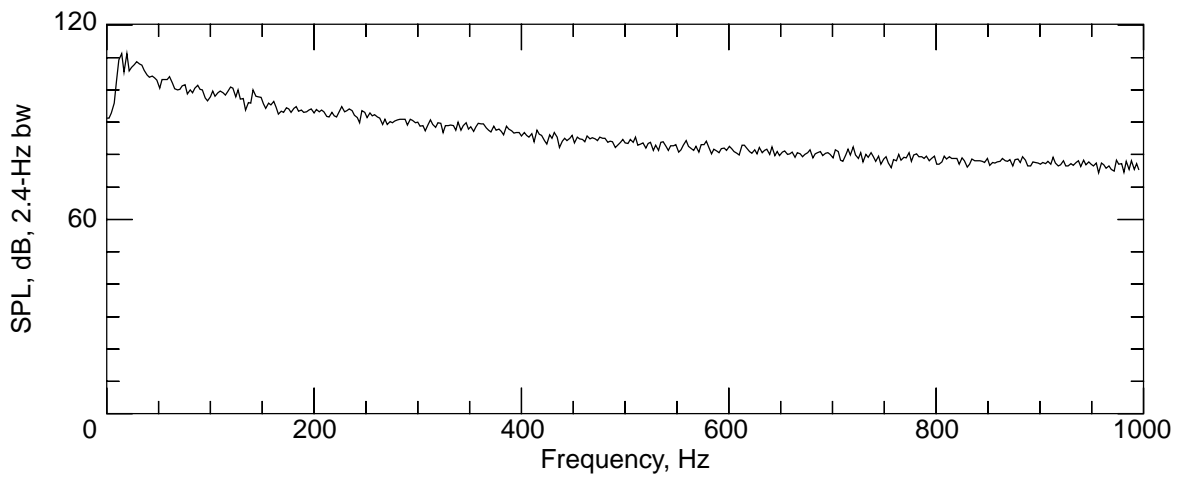
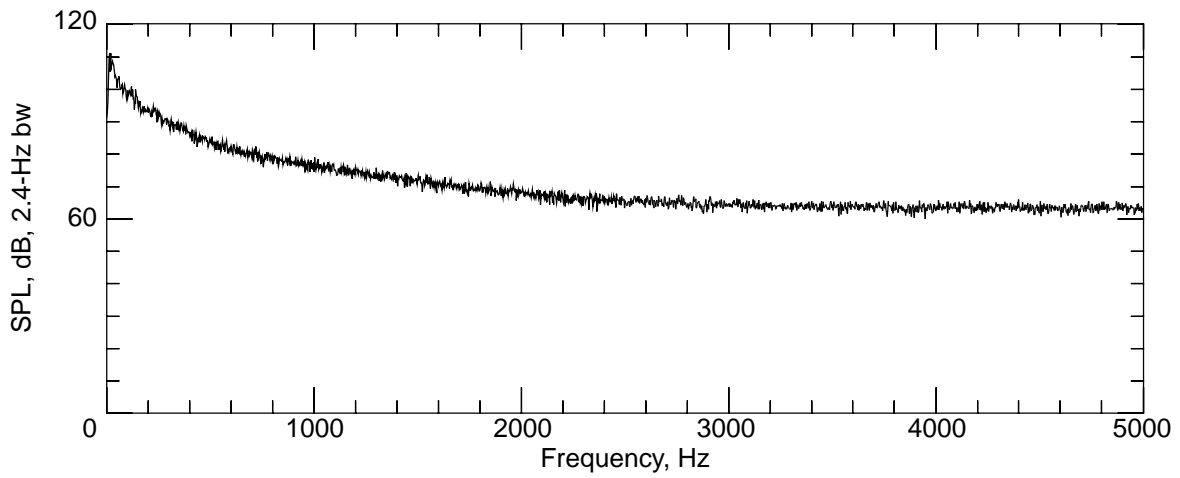
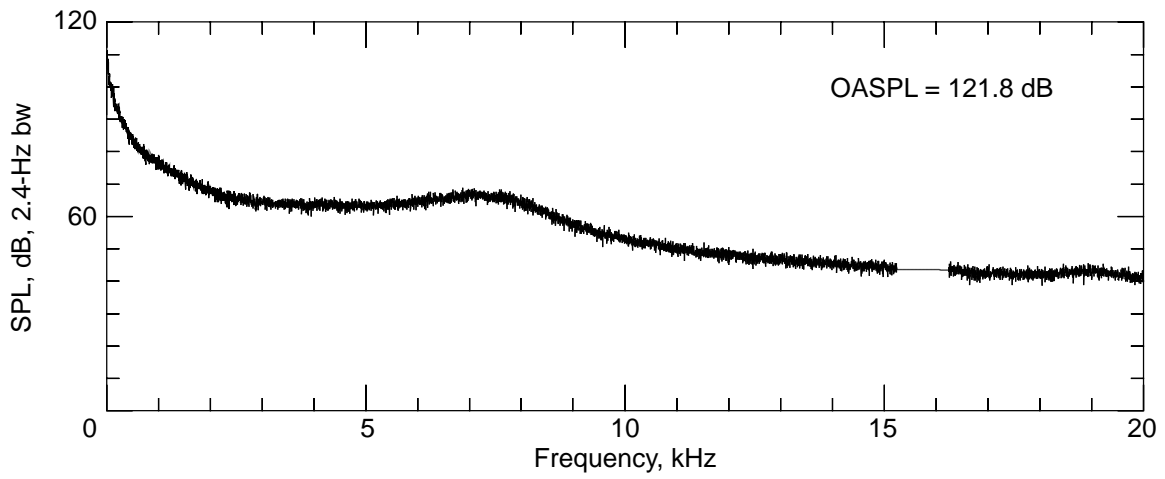
(b) Dynamic pressure = 40 lb/ft<sup>2</sup>.

Figure 22. Continued.



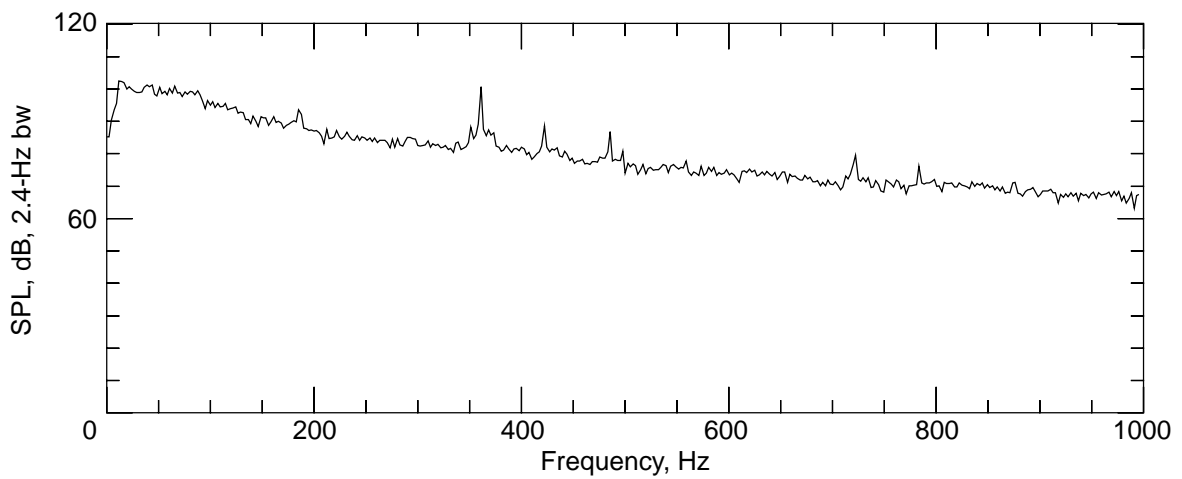
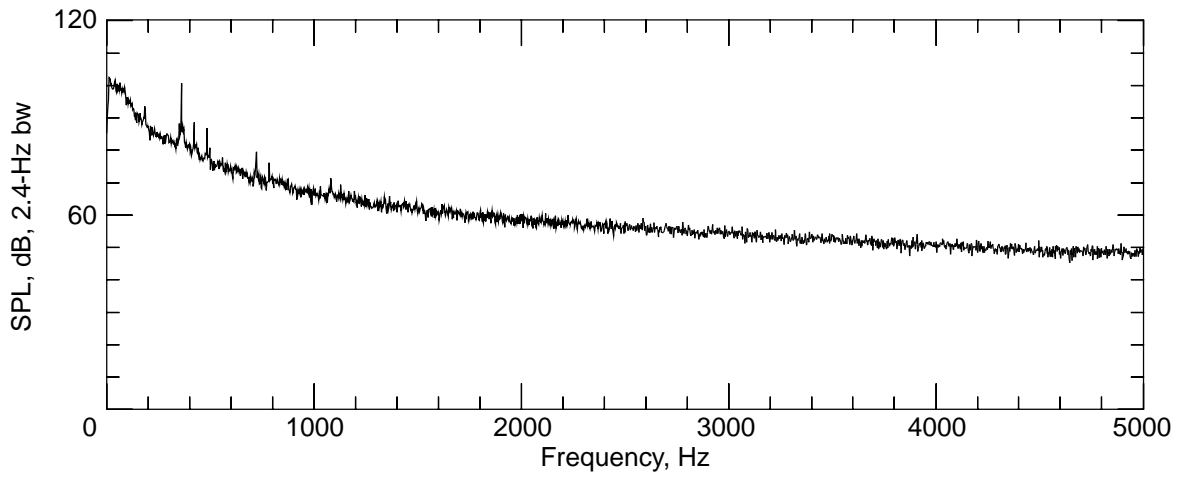
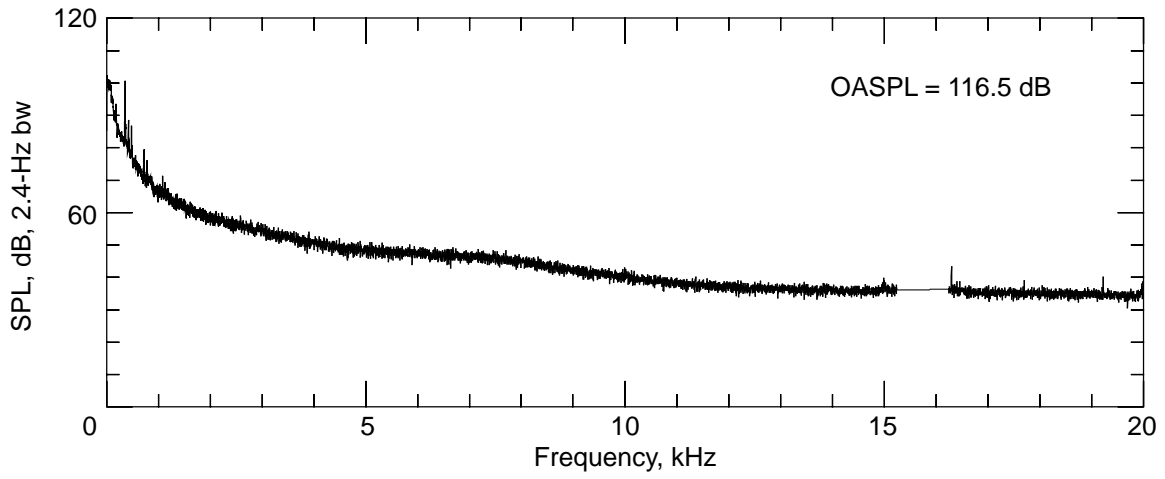
(c) Dynamic pressure = 60 lb/ft<sup>2</sup>.

Figure 22. Continued.



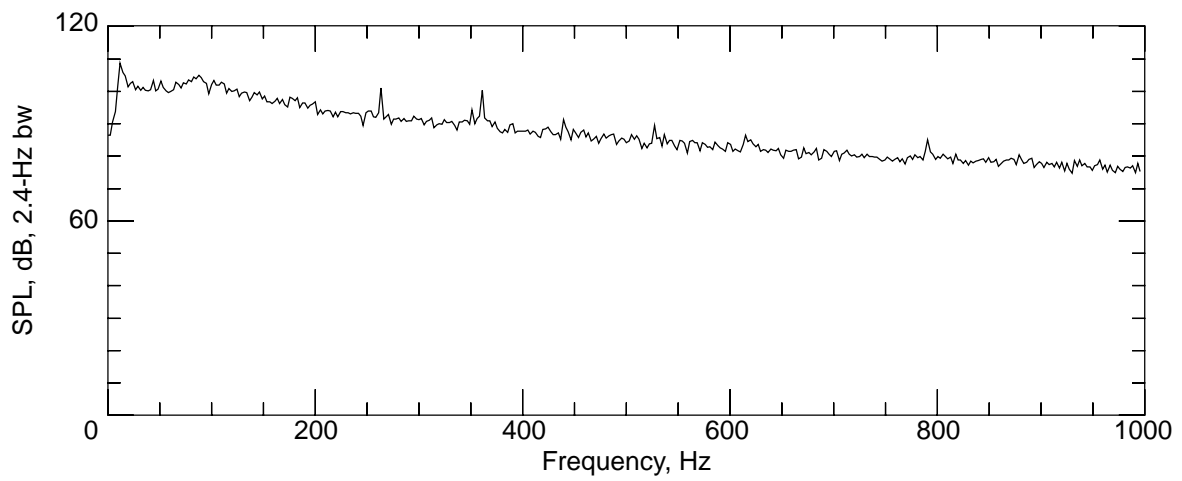
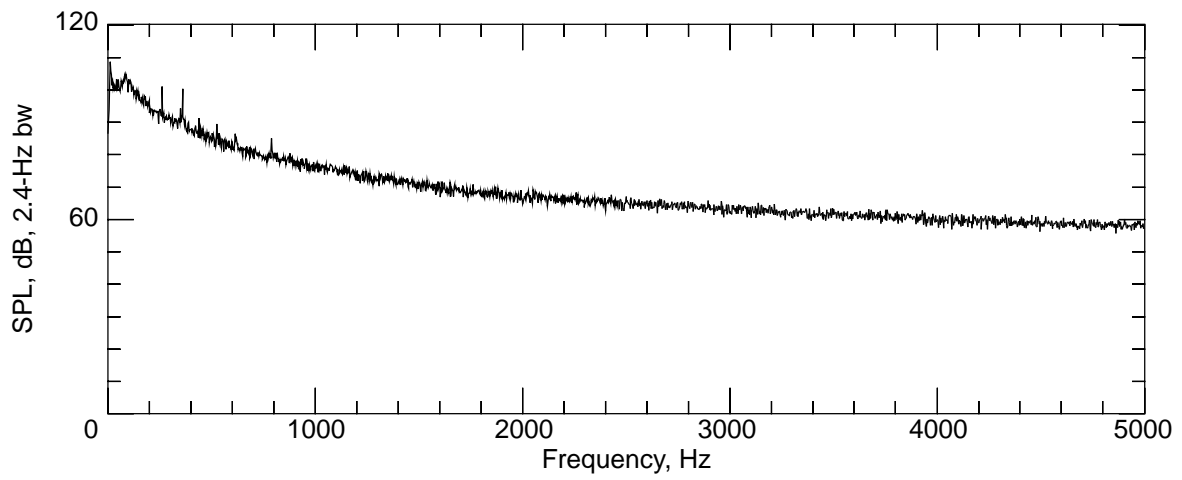
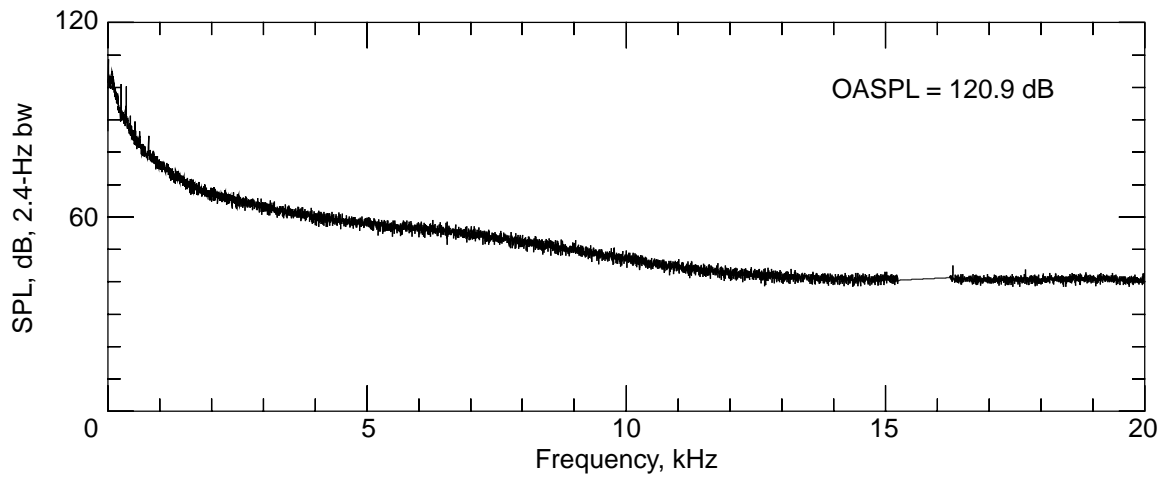
(d) Dynamic pressure = 70 lb/ft<sup>2</sup>.

Figure 22. Concluded.



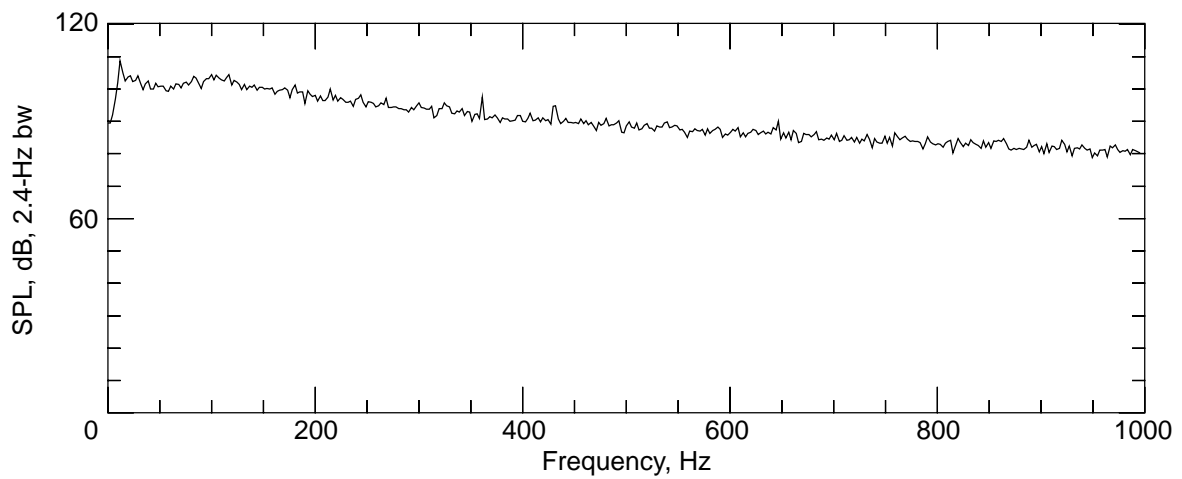
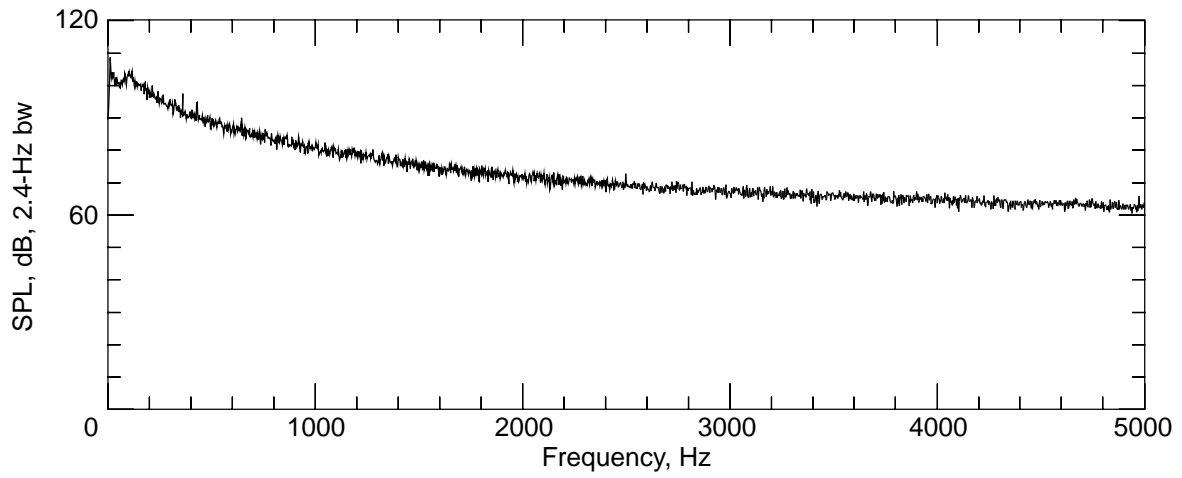
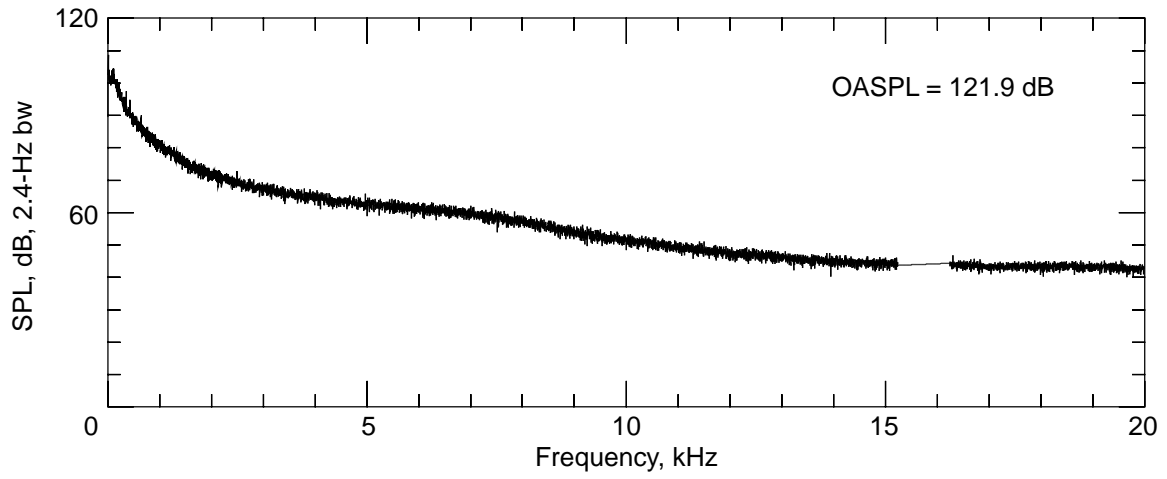
(a) Dynamic pressure = 20 lb/ft<sup>2</sup>.

Figure 23. Flow noise measurement upstream of drive fan.



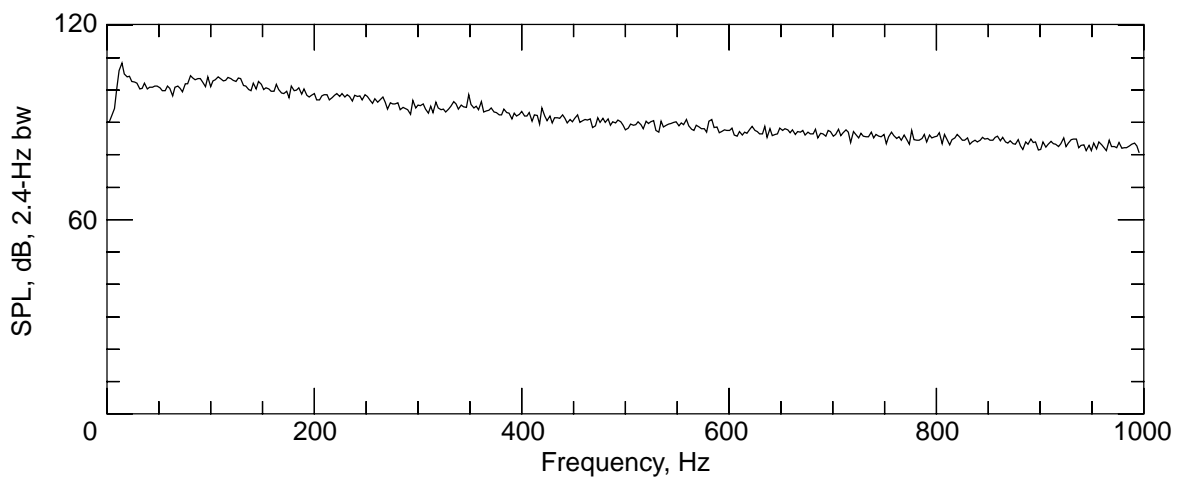
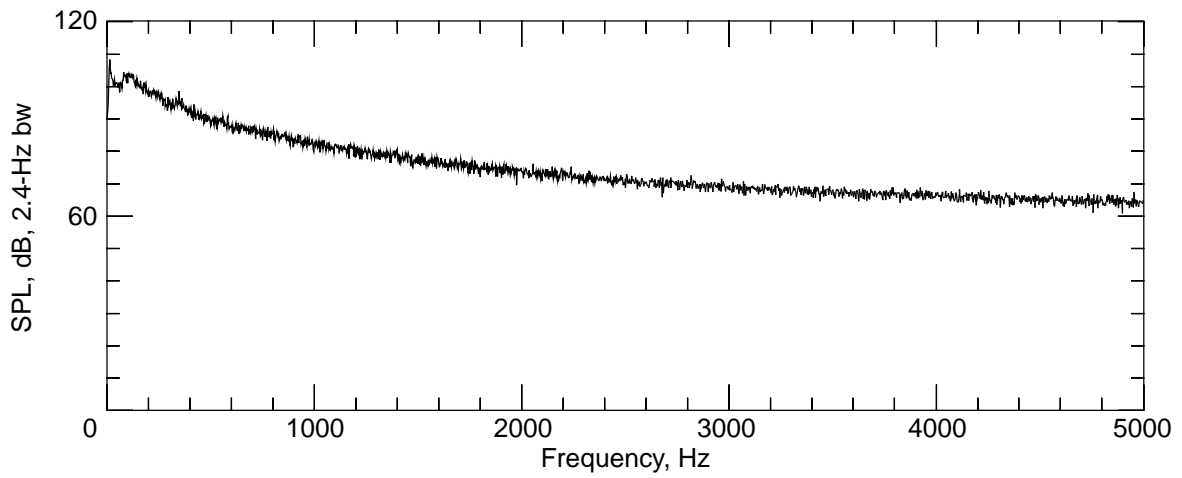
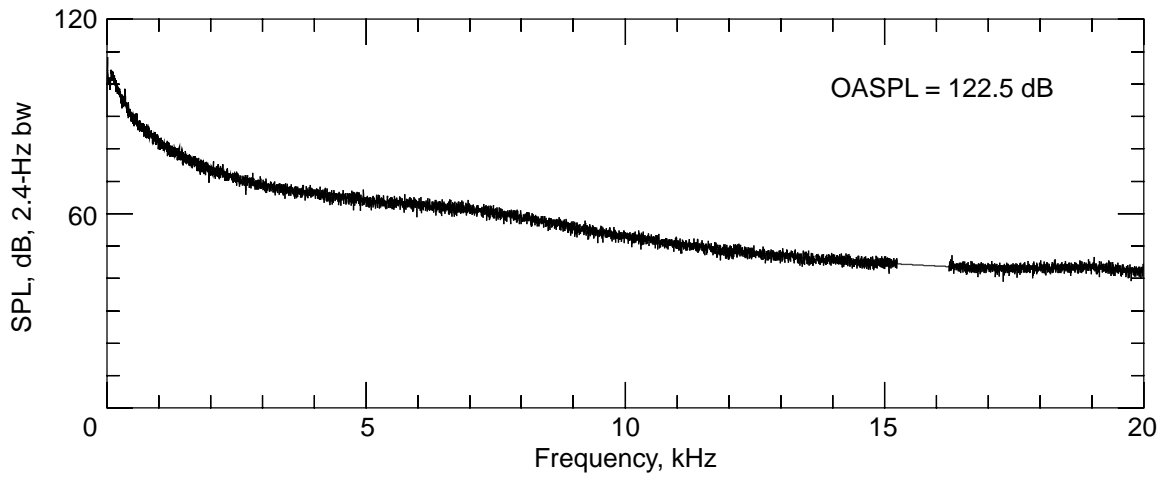
(b) Dynamic pressure = 40 lb/ft<sup>2</sup>.

Figure 23. Continued.



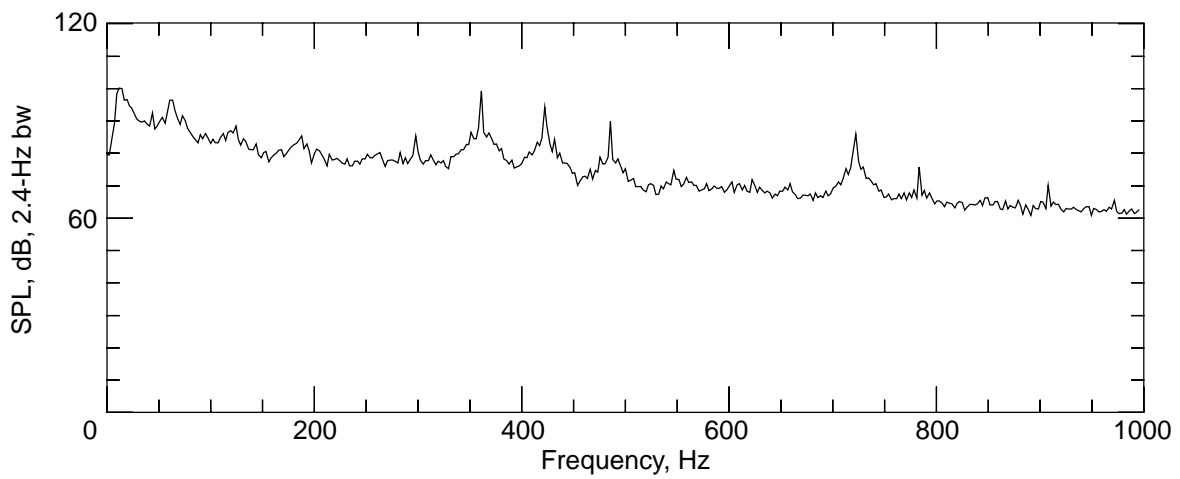
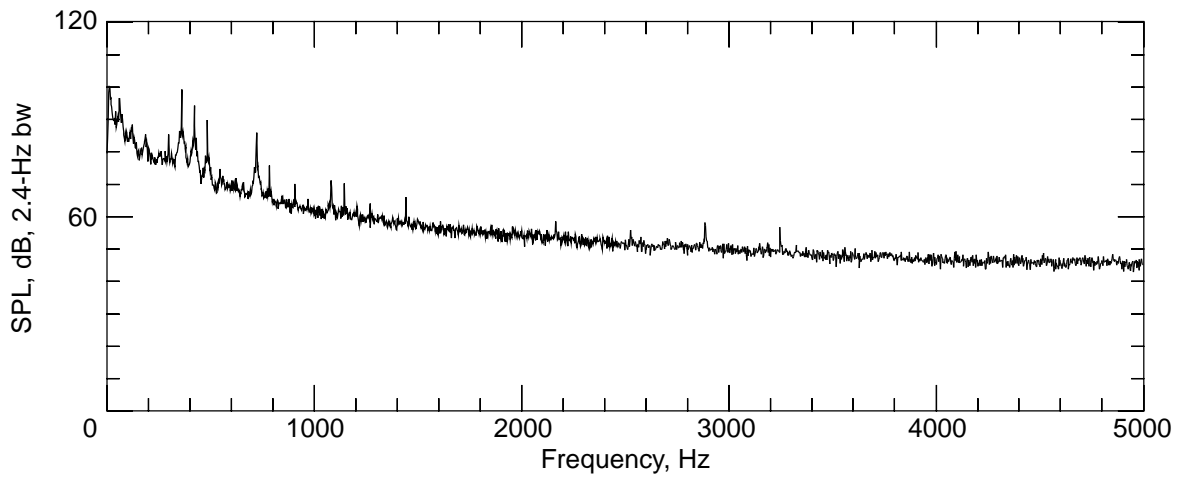
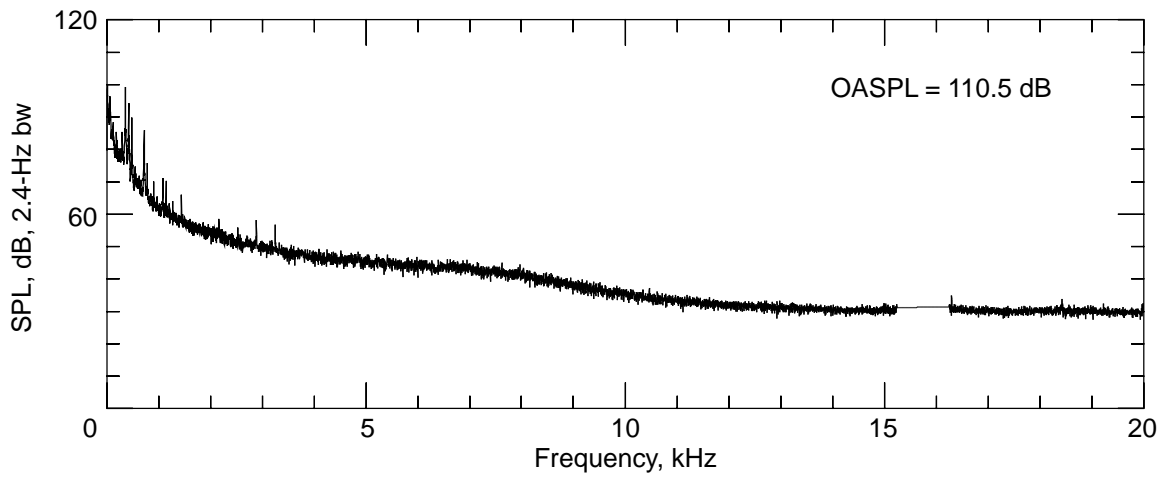
(c) Dynamic pressure = 60 lb/ft<sup>2</sup>.

Figure 23. Continued.



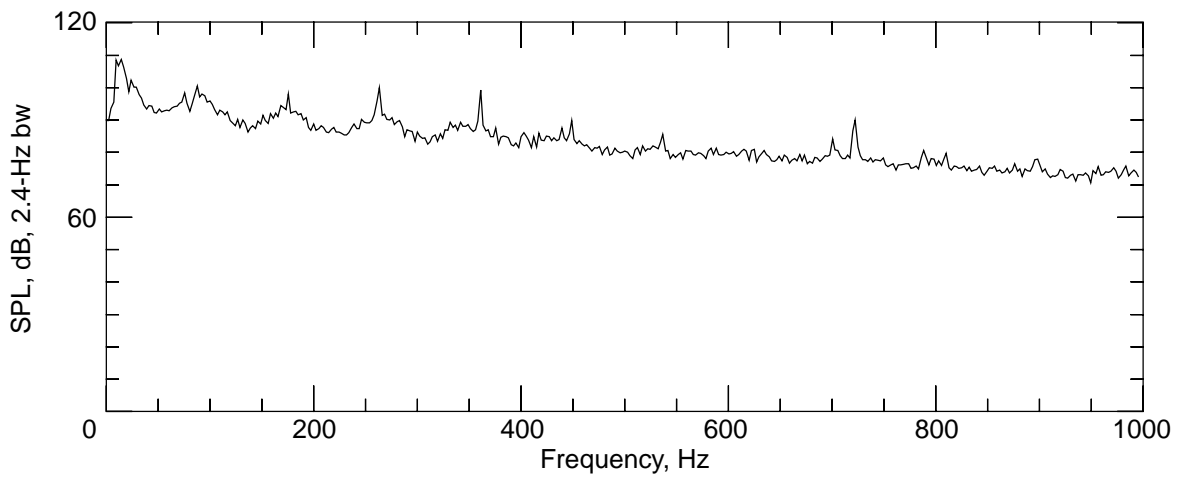
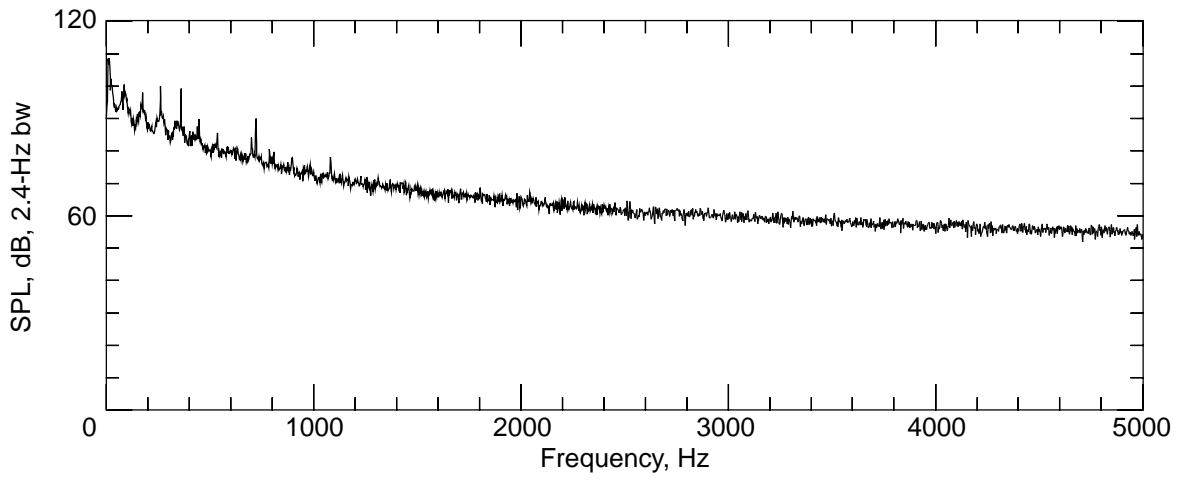
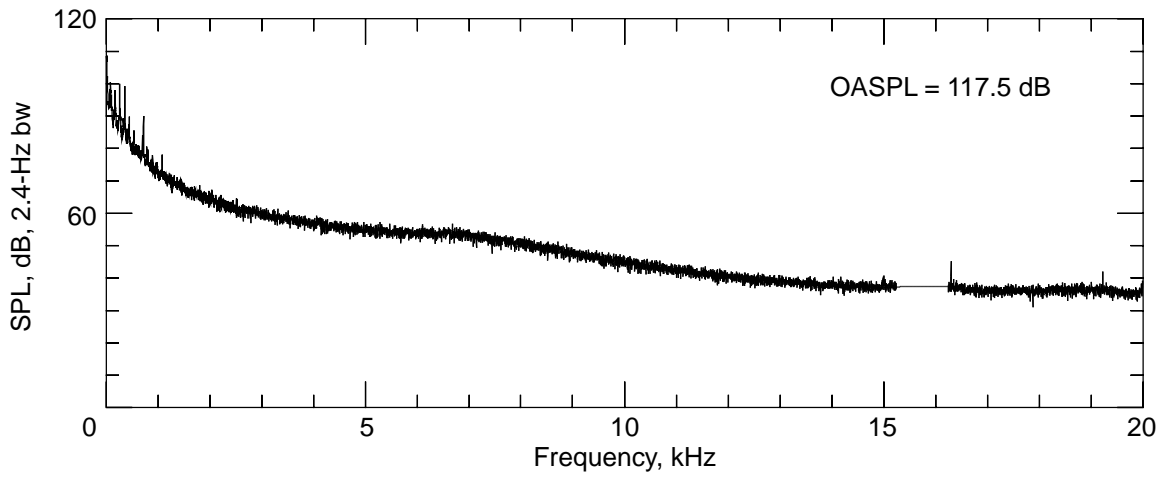
(d) Dynamic pressure = 70 lb/ft<sup>2</sup>.

Figure 23. Concluded.



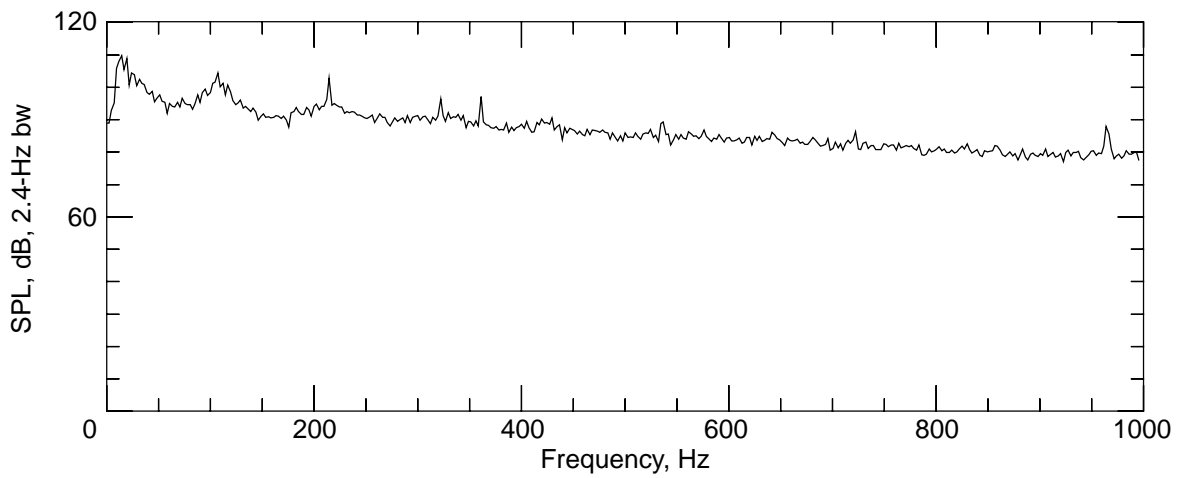
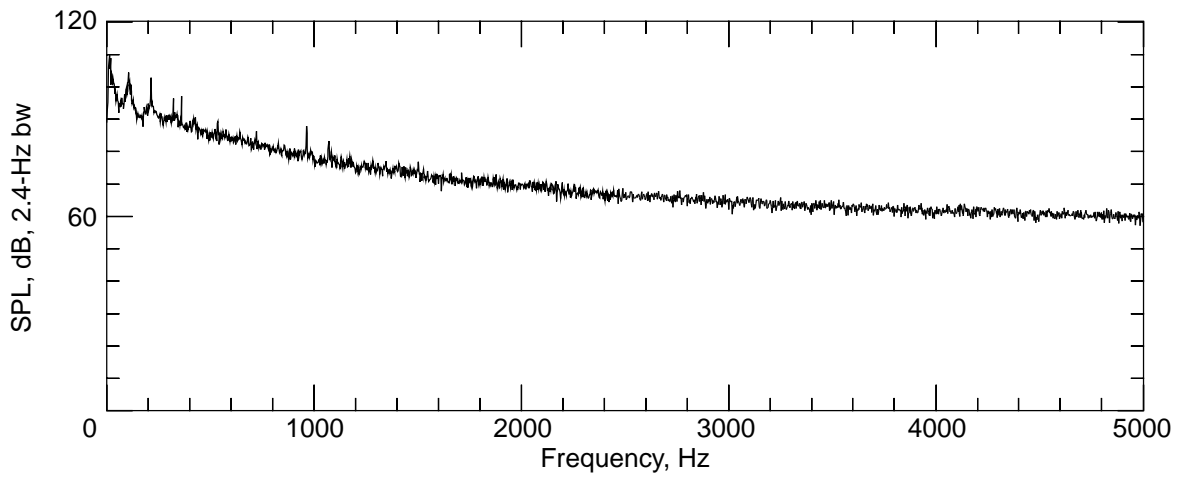
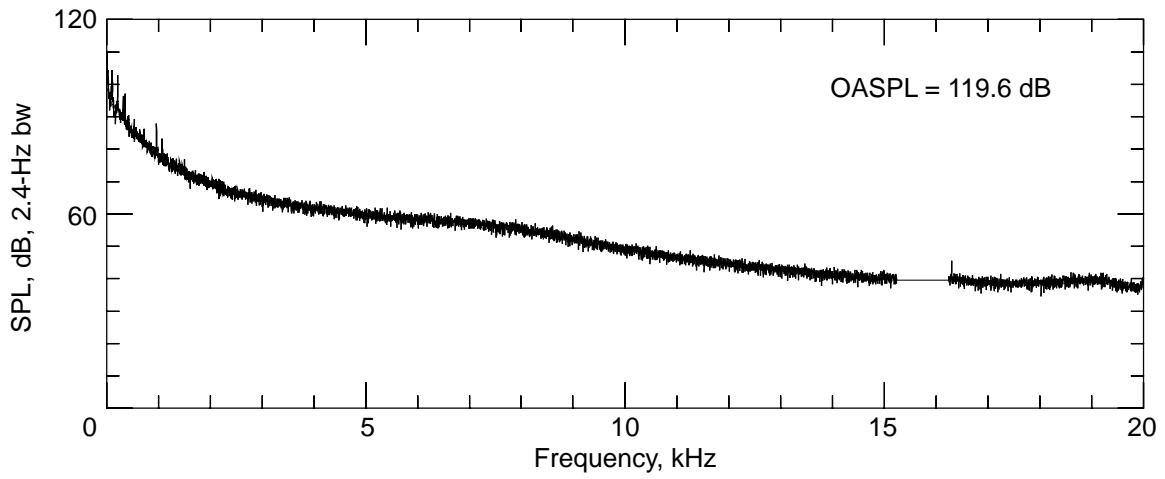
(a) Dynamic pressure = 20 lb/ft<sup>2</sup>.

Figure 24. Flow noise measurement downstream of drive fan.



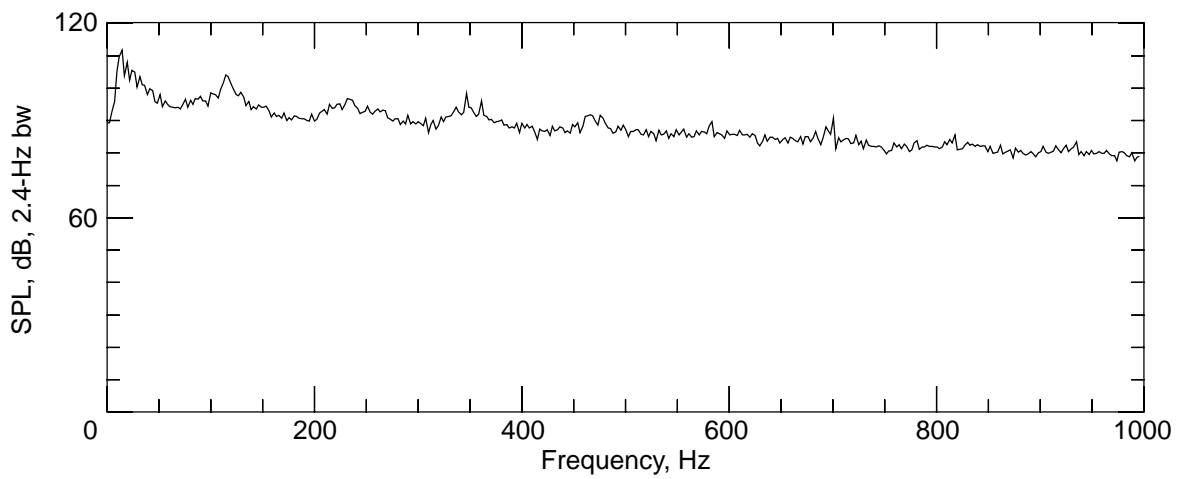
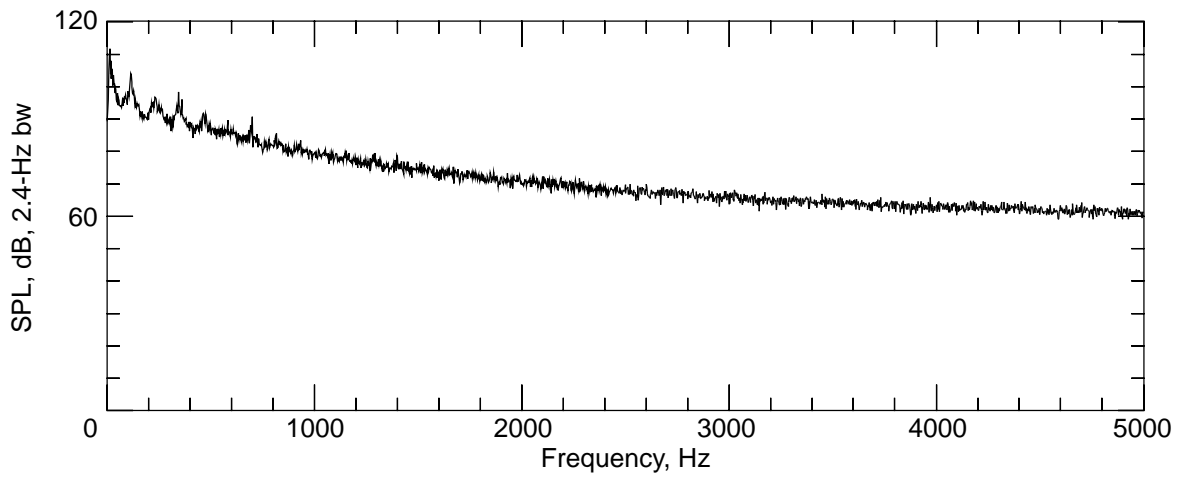
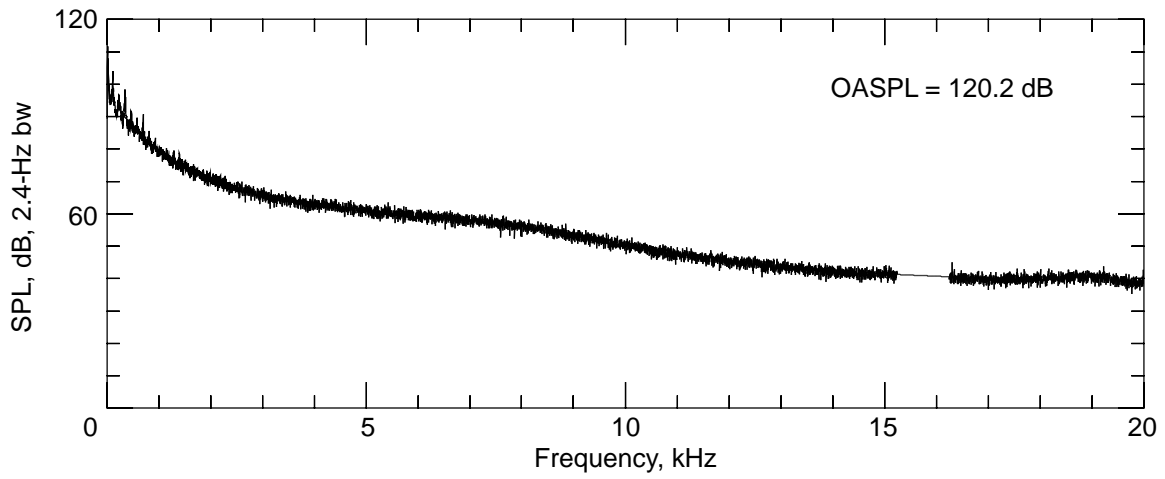
(b) Dynamic pressure = 40 lb/ft<sup>2</sup>.

Figure 24. Continued.



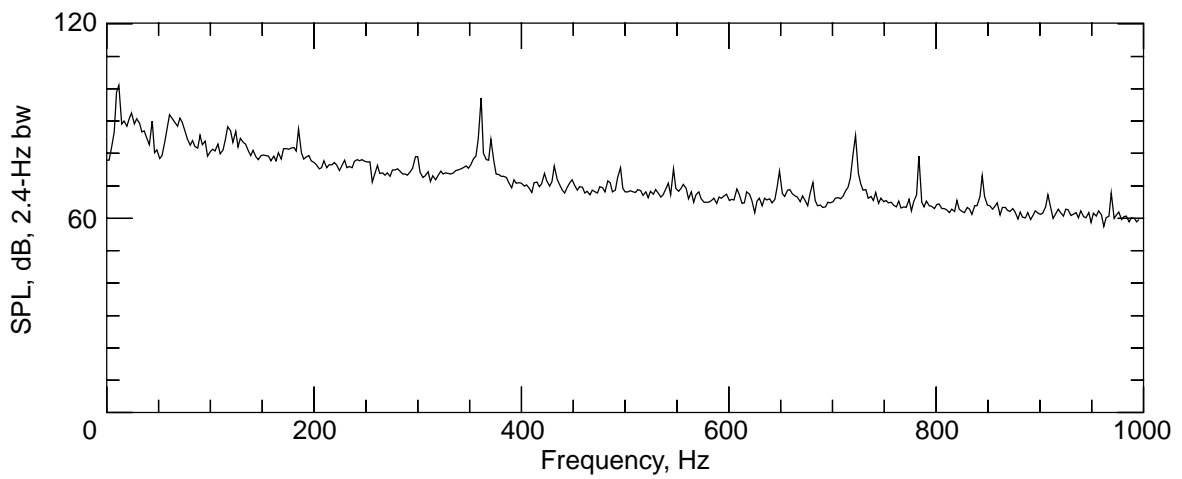
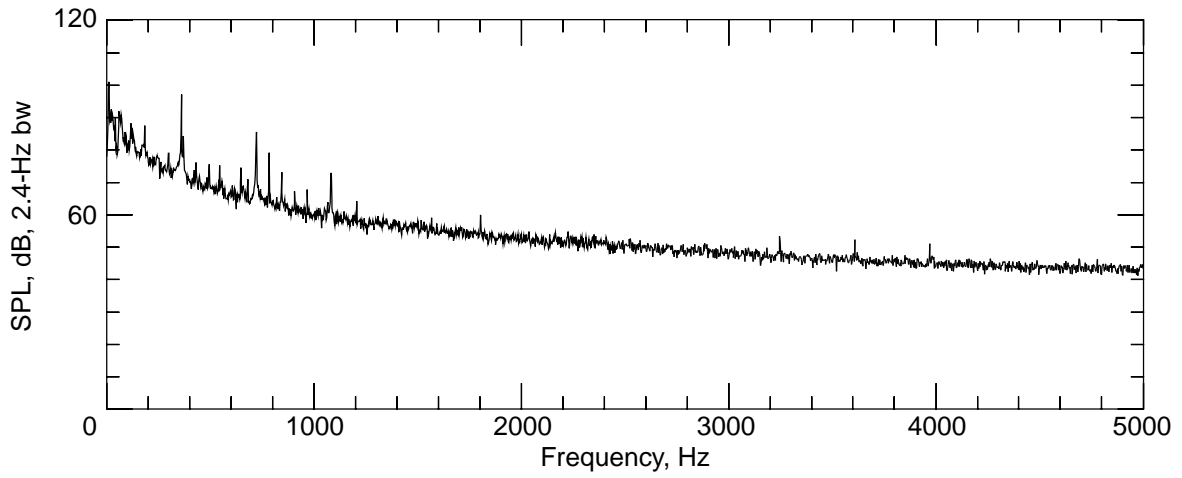
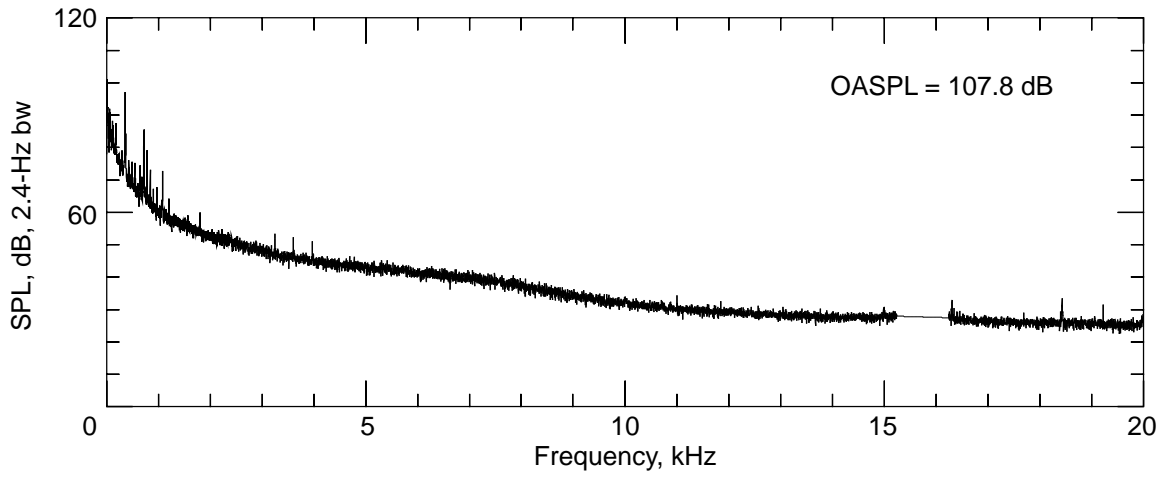
(c) Dynamic pressure = 60 lb/ft<sup>2</sup>.

Figure 24. Continued.



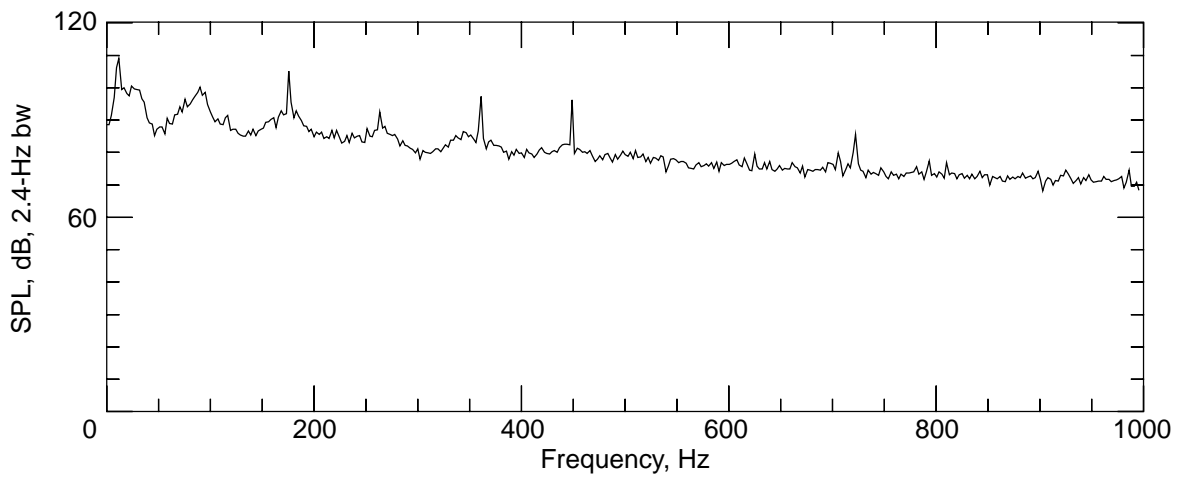
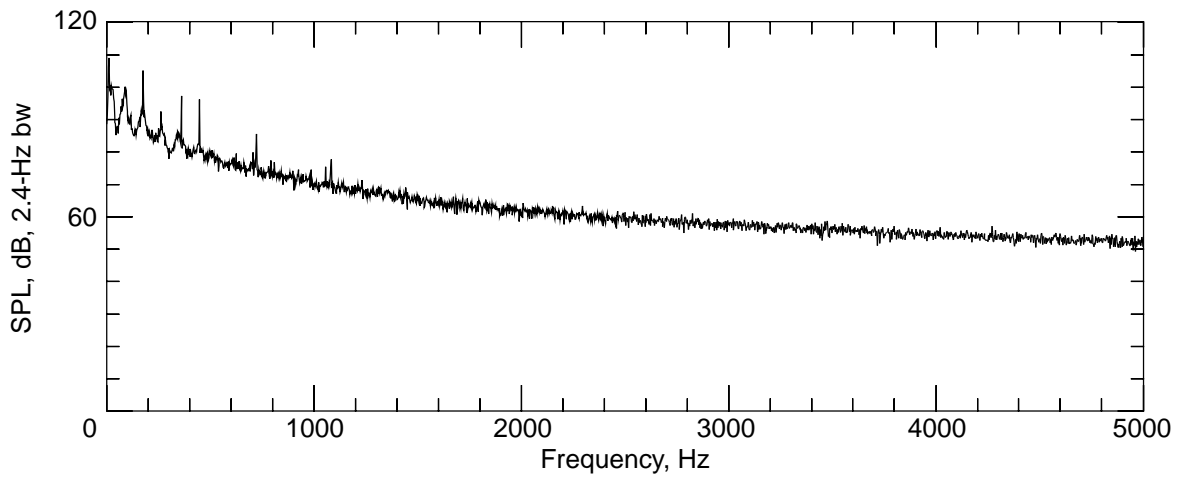
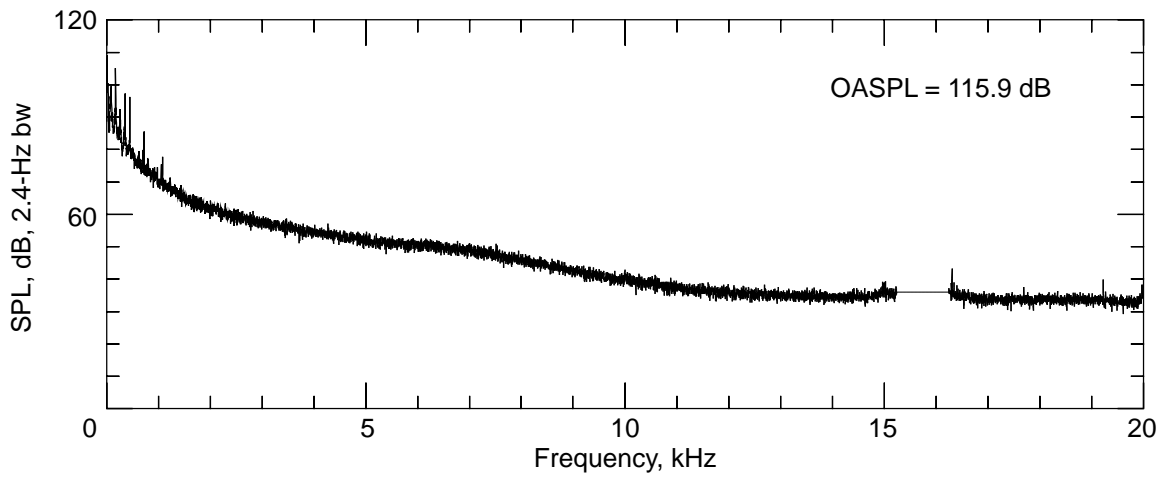
(d) Dynamic pressure = 70 lb/ft<sup>2</sup>.

Figure 24. Concluded.



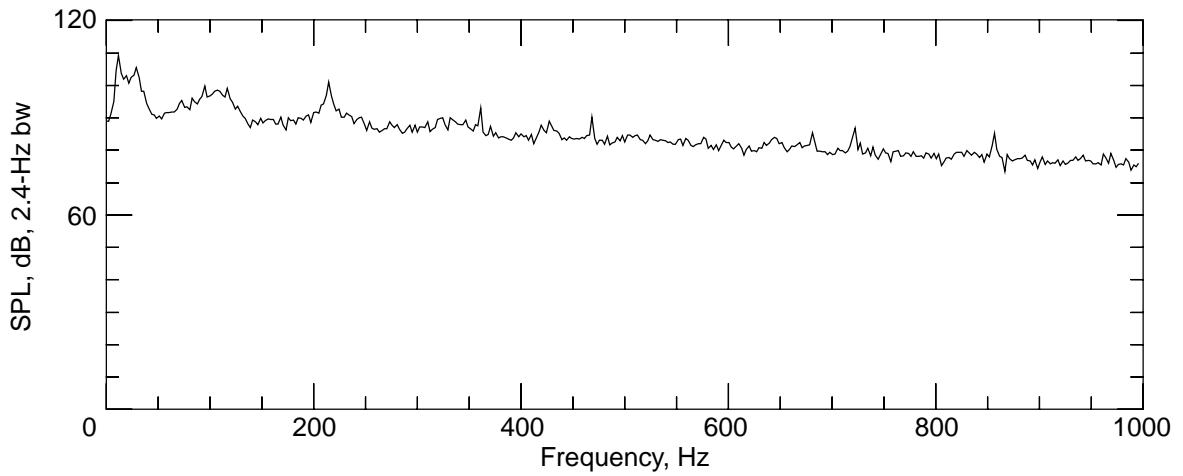
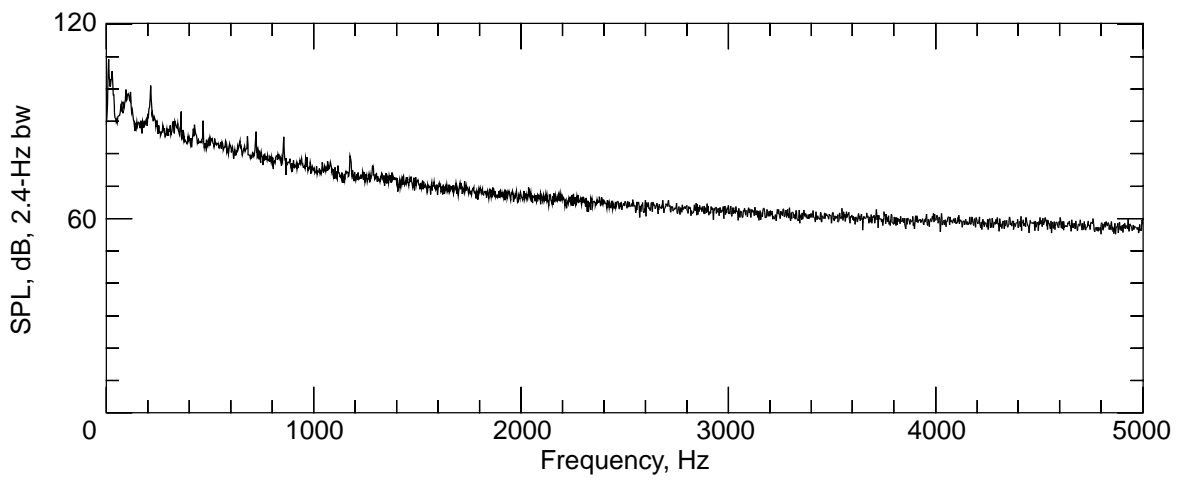
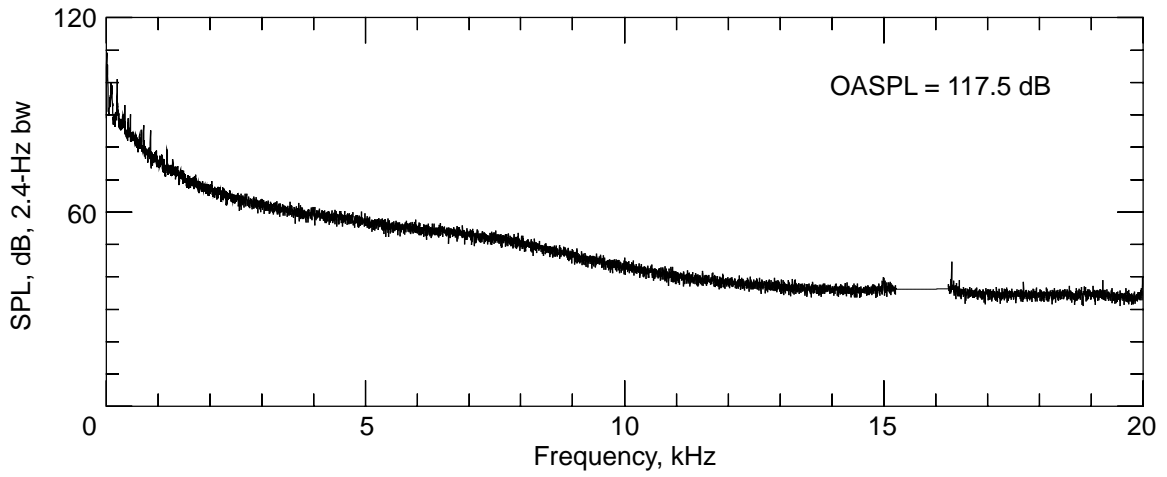
(a) Dynamic pressure = 20 lb/ft<sup>2</sup>.

Figure 25. Flow noise measurement upstream of turn 3.



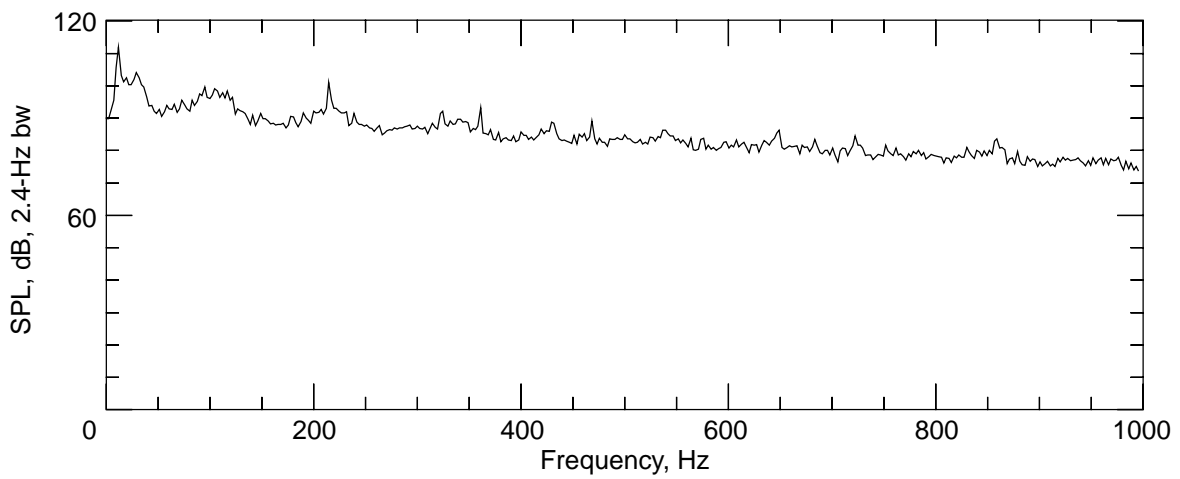
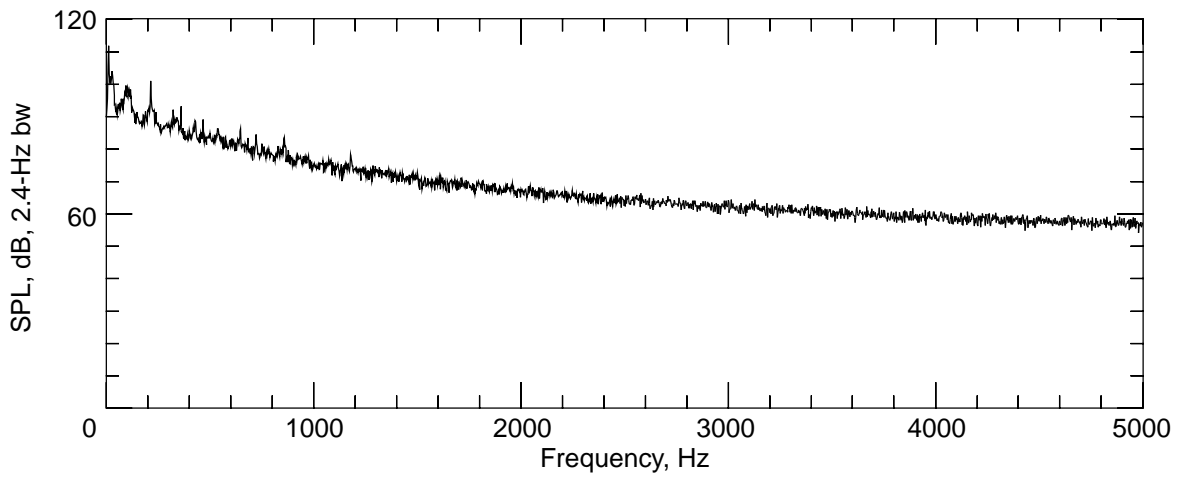
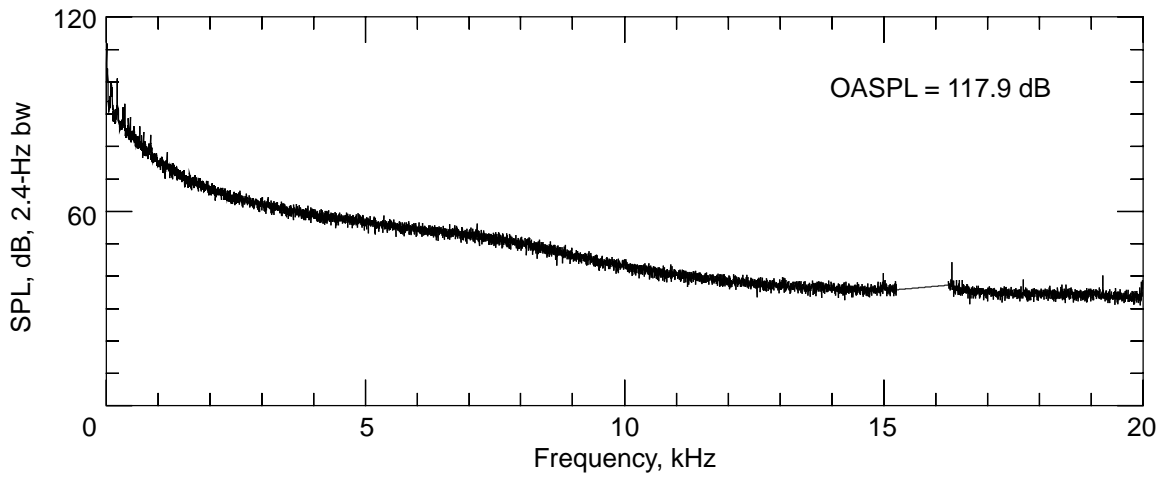
(b) Dynamic pressure = 40 lb/ft<sup>2</sup>.

Figure 25. Continued.



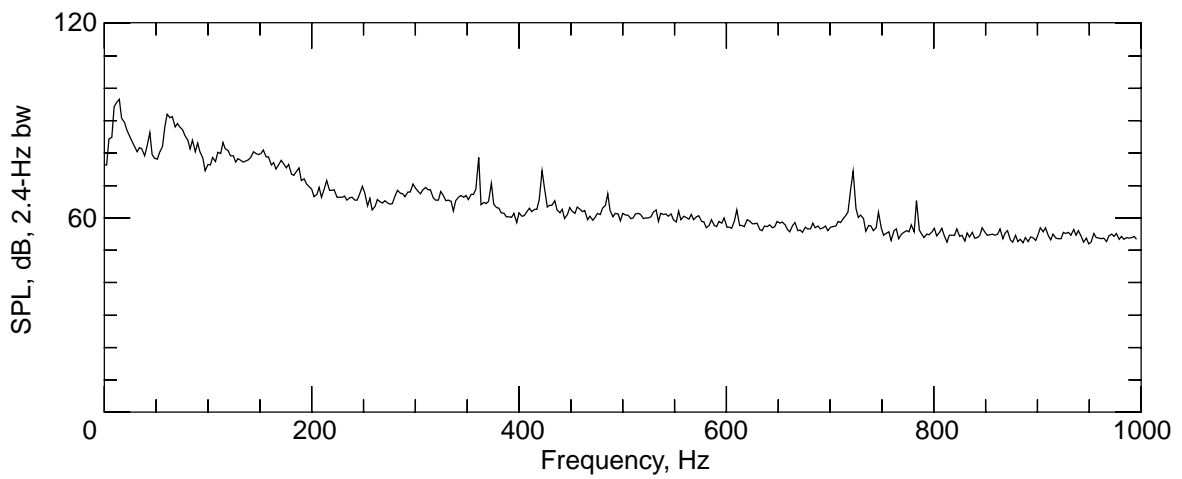
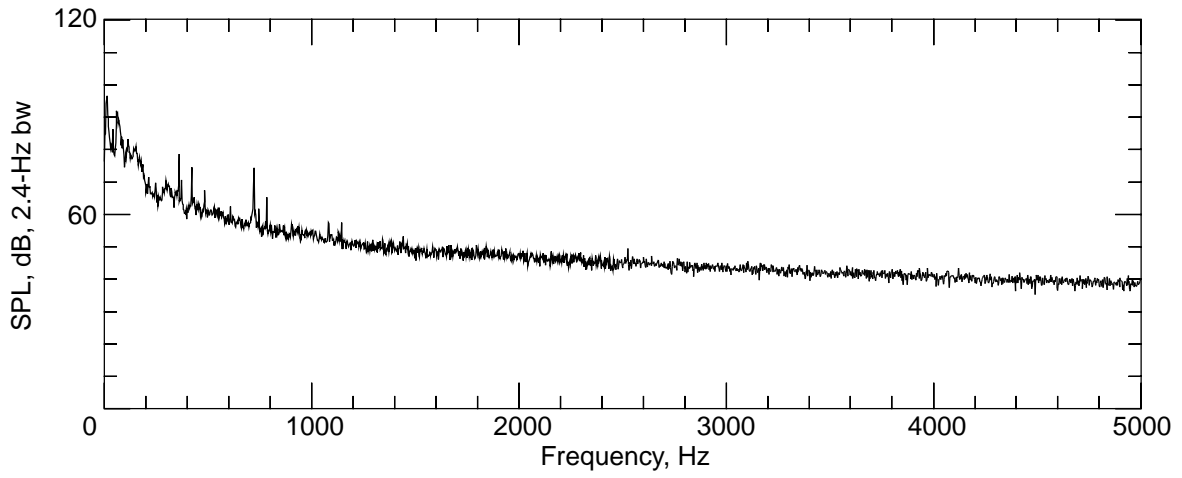
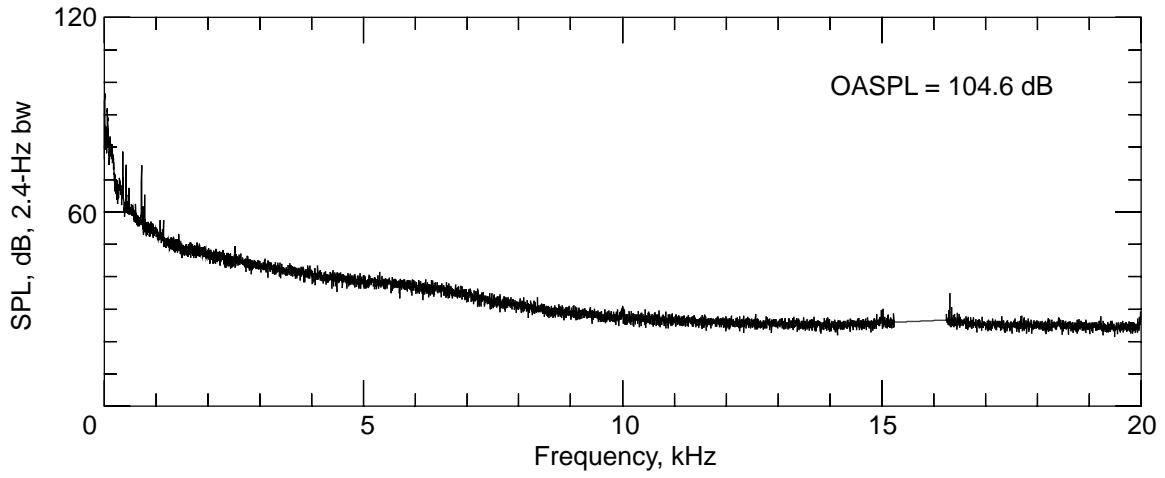
(c) Dynamic pressure = 60 lb/ft<sup>2</sup>.

Figure 25. Continued.



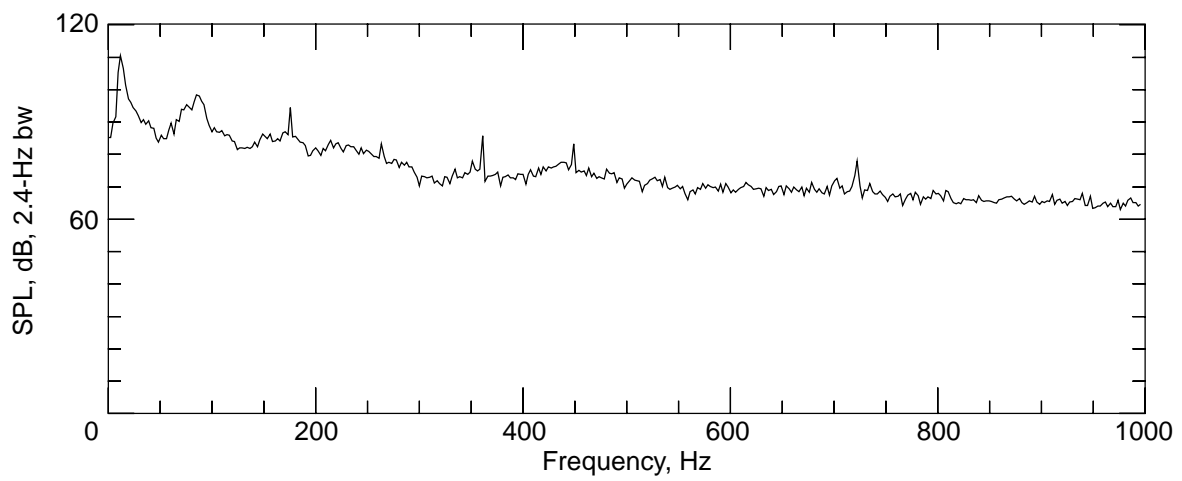
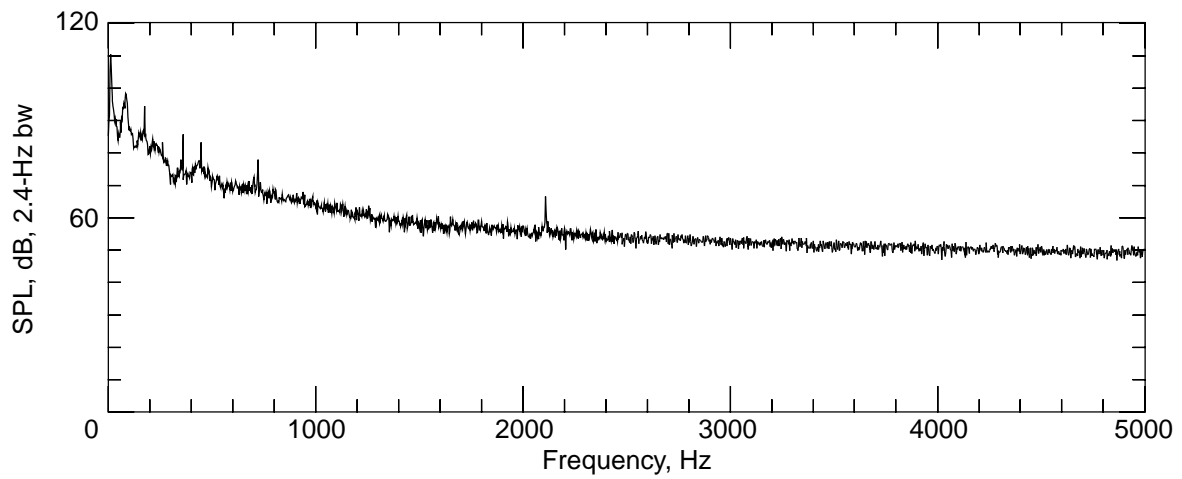
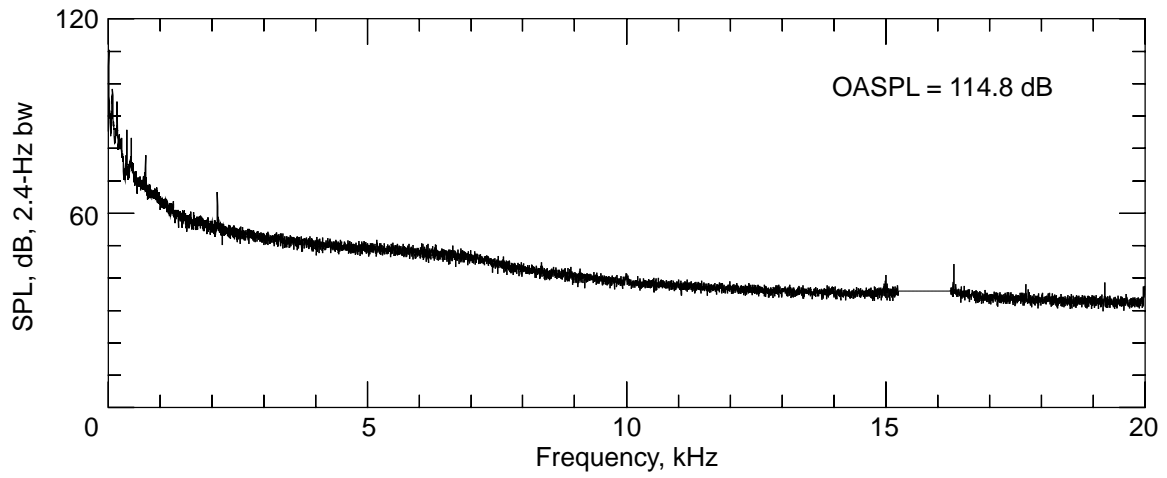
(d) Dynamic pressure = 70 lb/ft<sup>2</sup>.

Figure 25. Concluded.



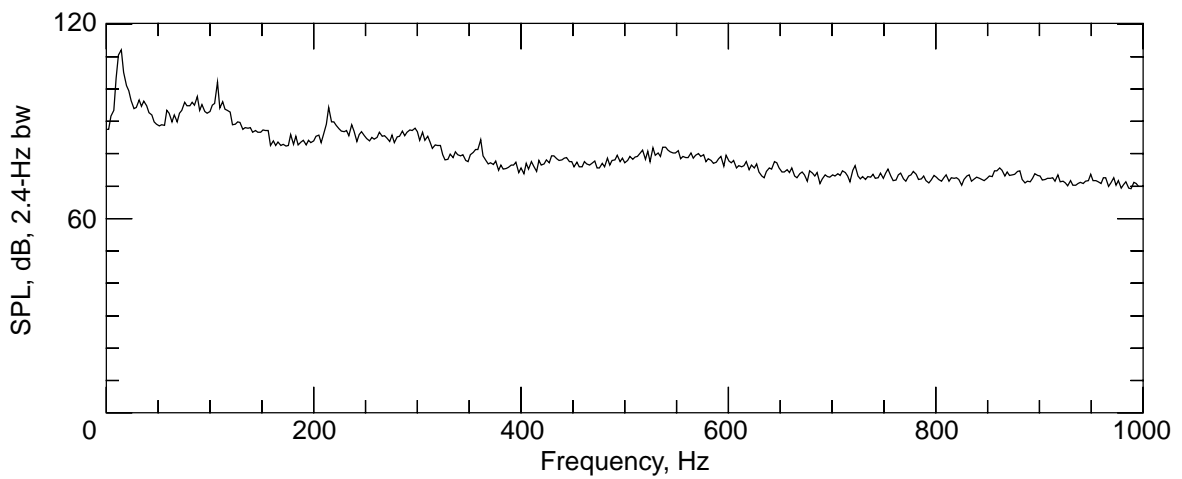
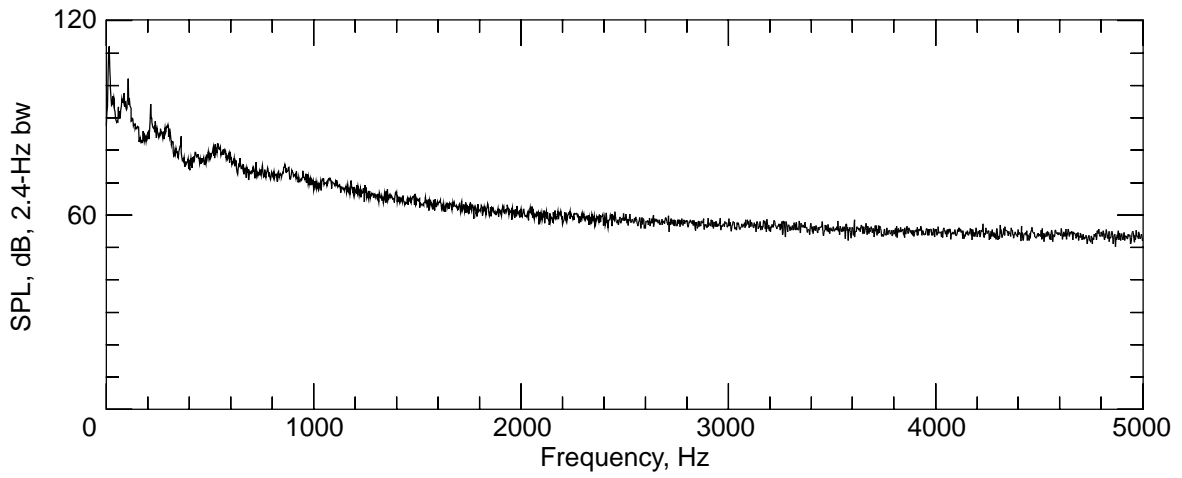
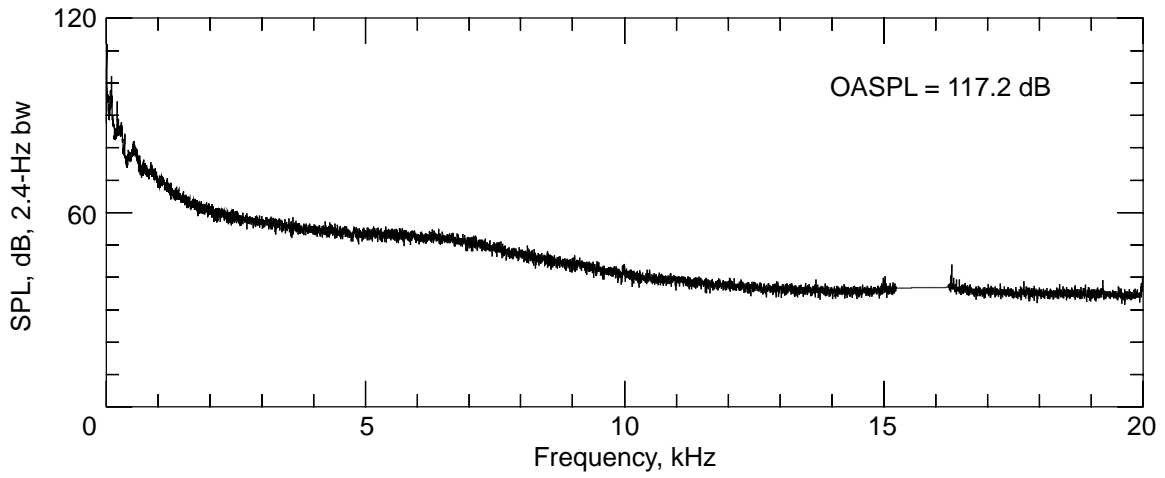
(a) Dynamic pressure = 20 lb/ft<sup>2</sup>.

Figure 26. Flow noise measurement downstream of turn 3.



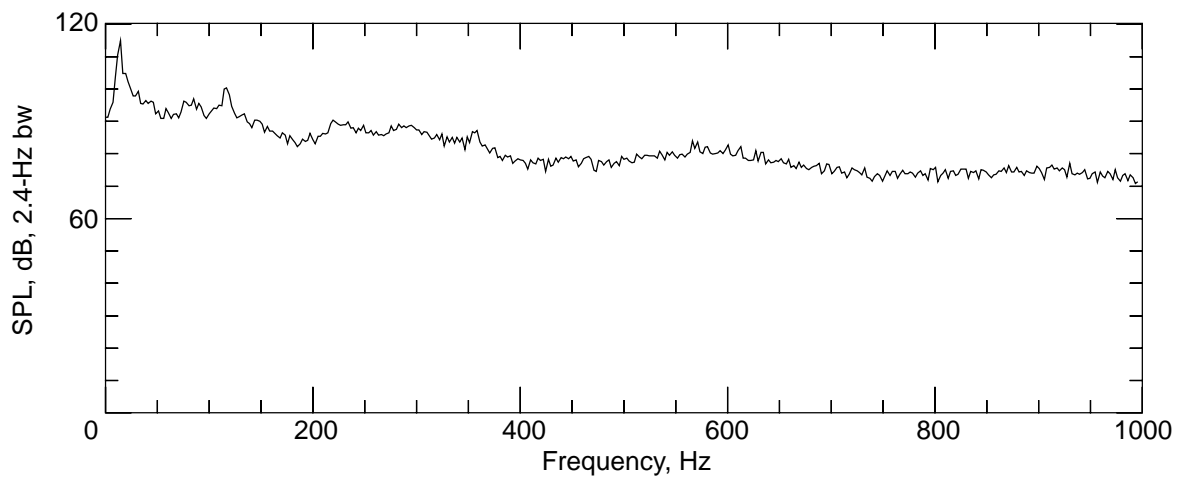
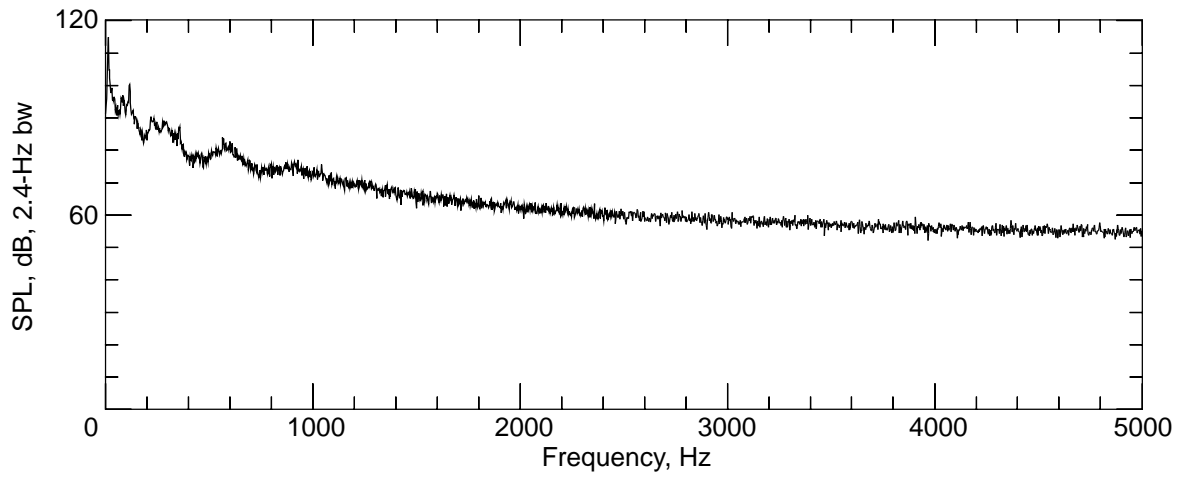
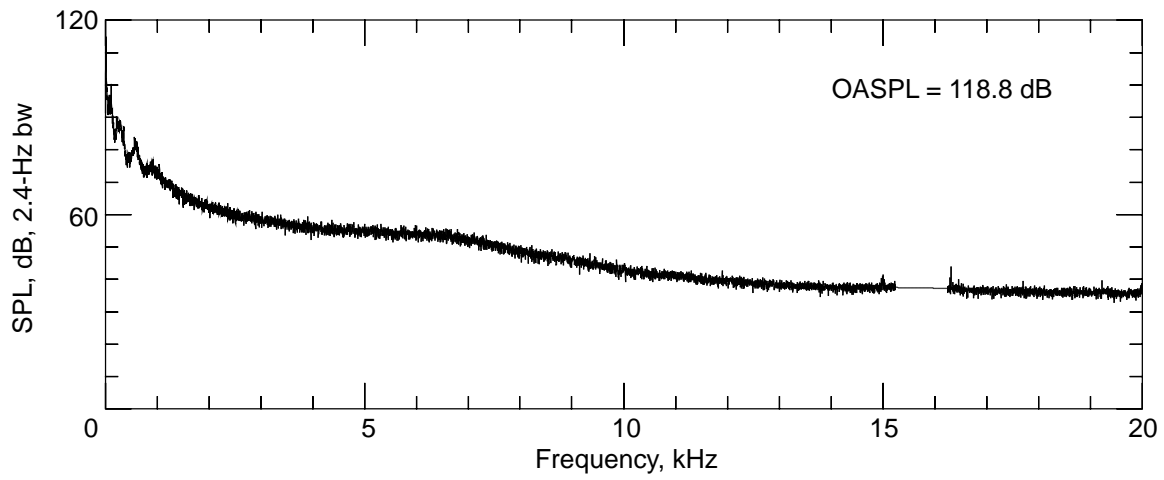
(b) Dynamic pressure = 40 lb/ft<sup>2</sup>.

Figure 26. Continued.



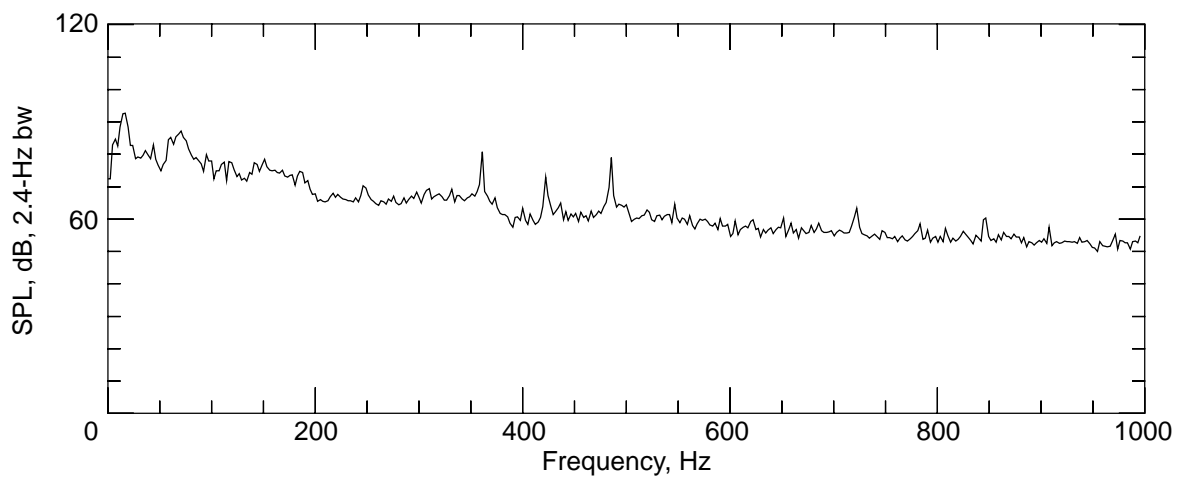
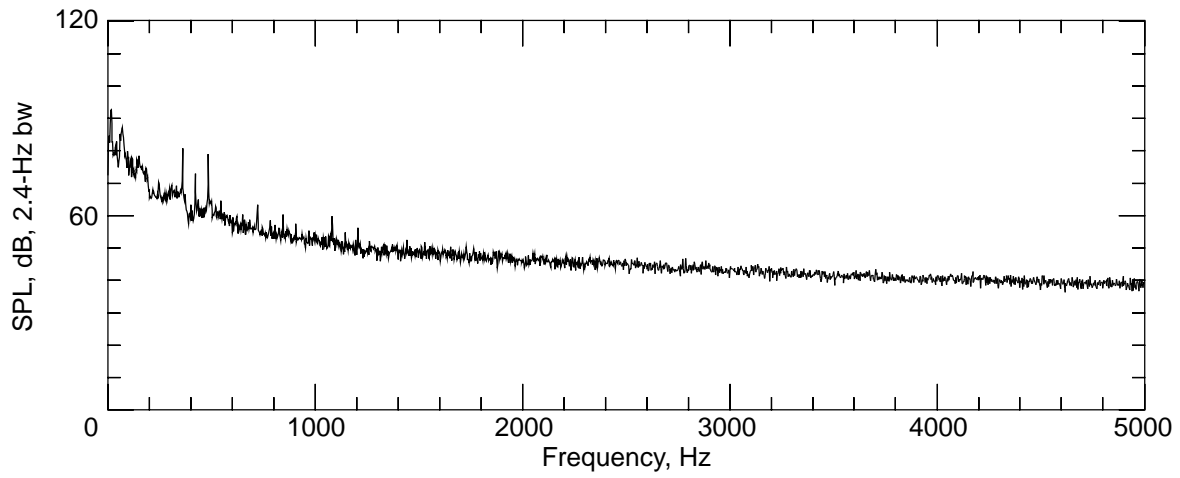
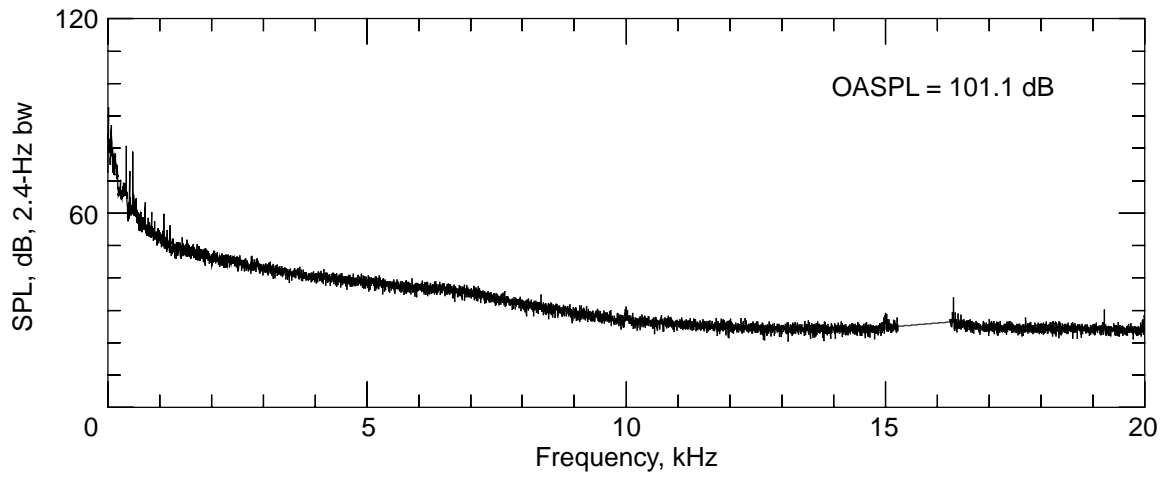
(c) Dynamic pressure = 60 lb/ft<sup>2</sup>.

Figure 26. Continued.



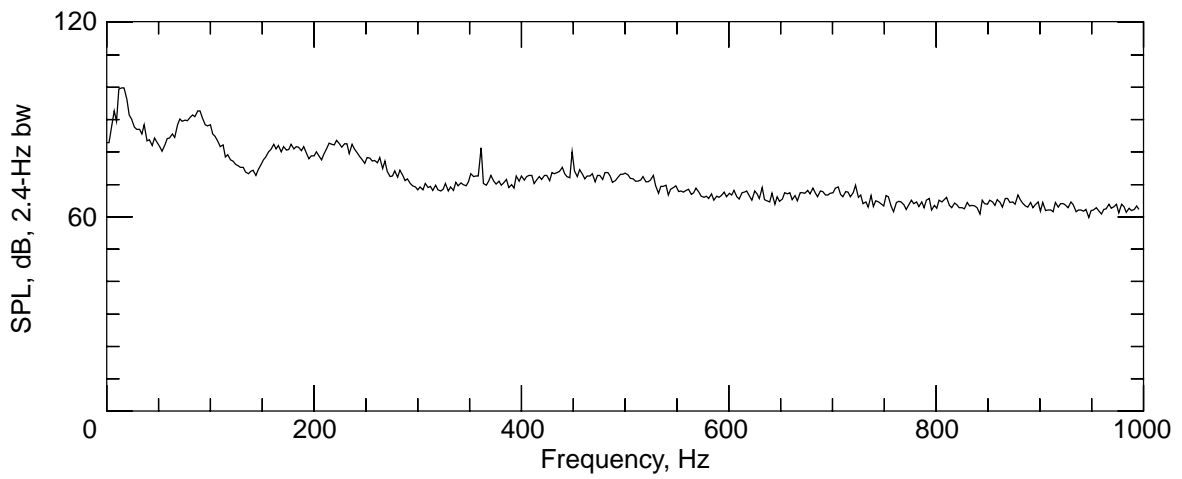
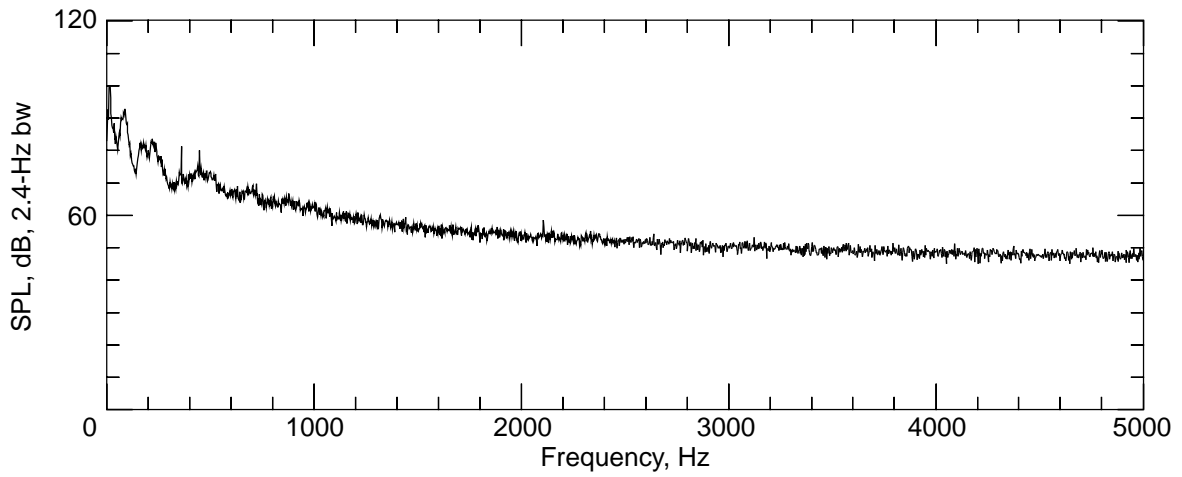
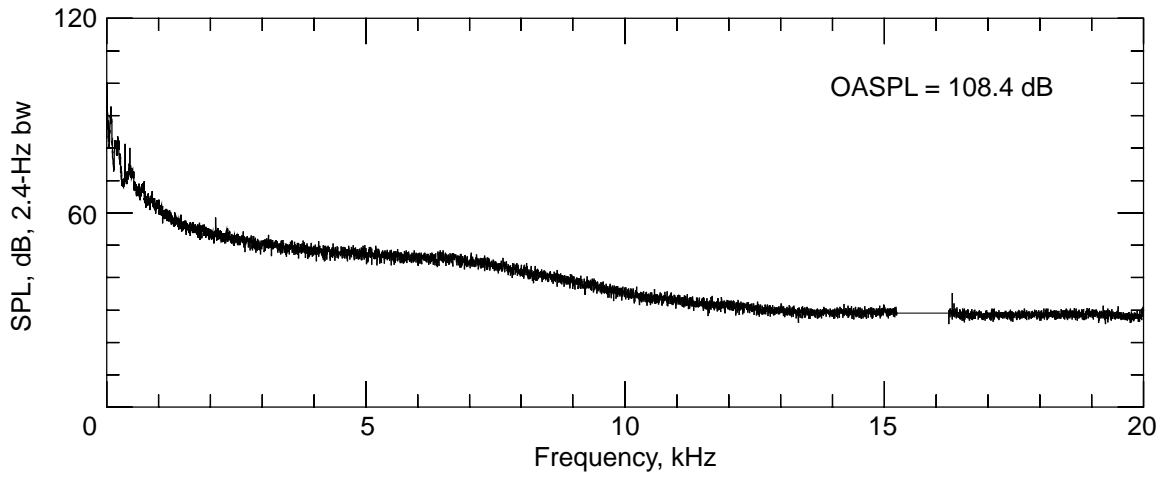
(d) Dynamic pressure = 70 lb/ft<sup>2</sup>.

Figure 26. Concluded.



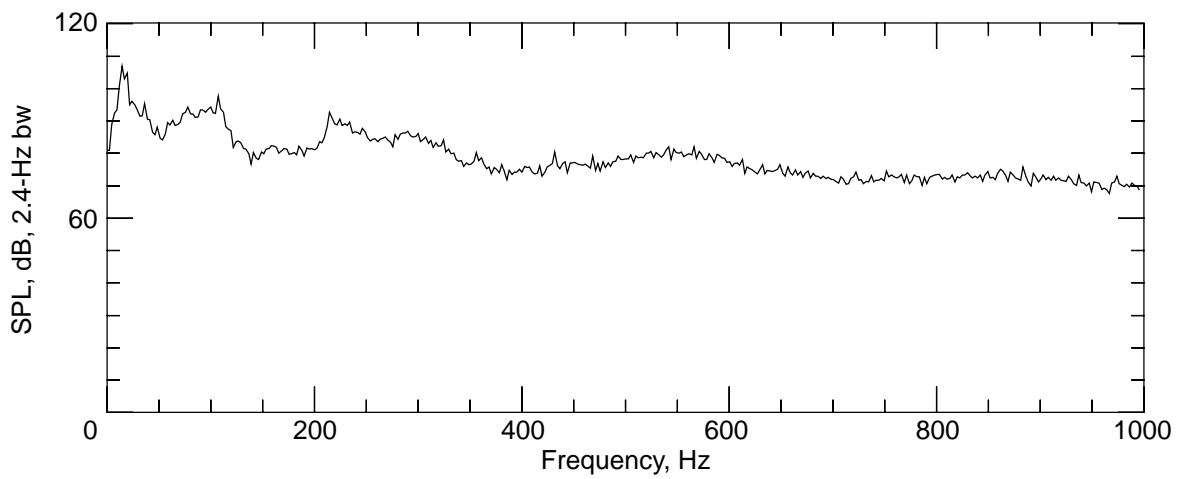
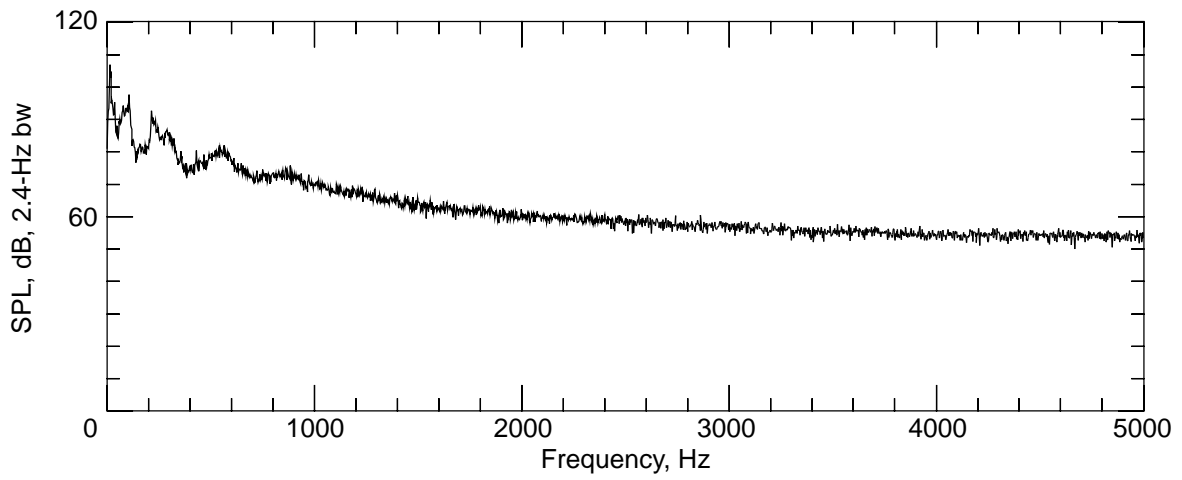
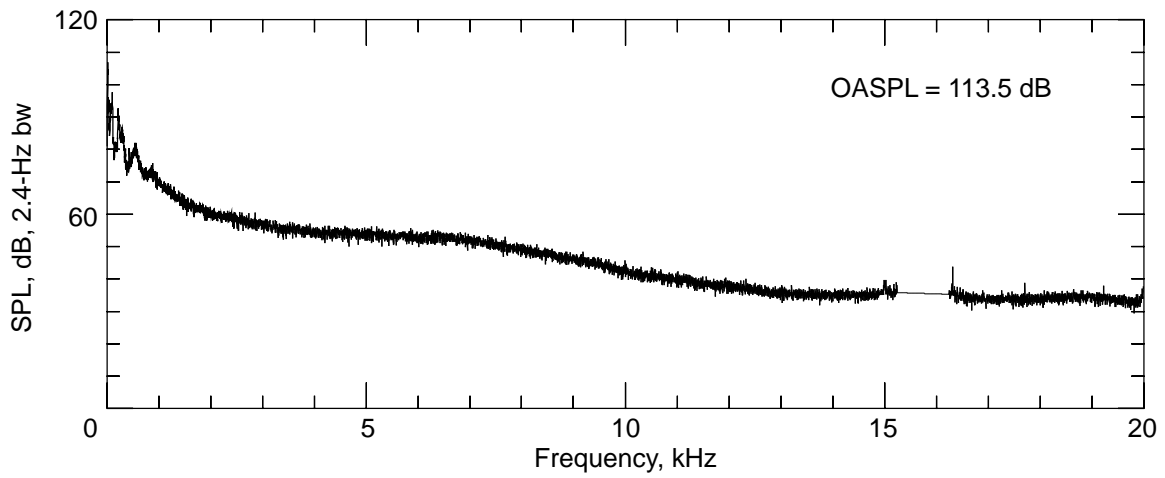
(a) Dynamic pressure = 20 lb/ft<sup>2</sup>.

Figure 27. Flow noise measurement upstream of turn 4.



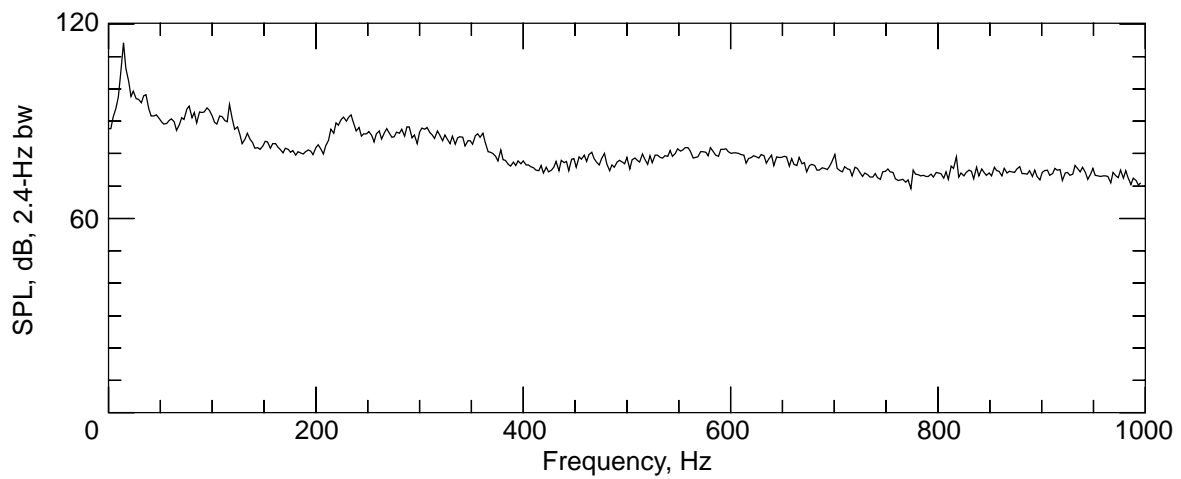
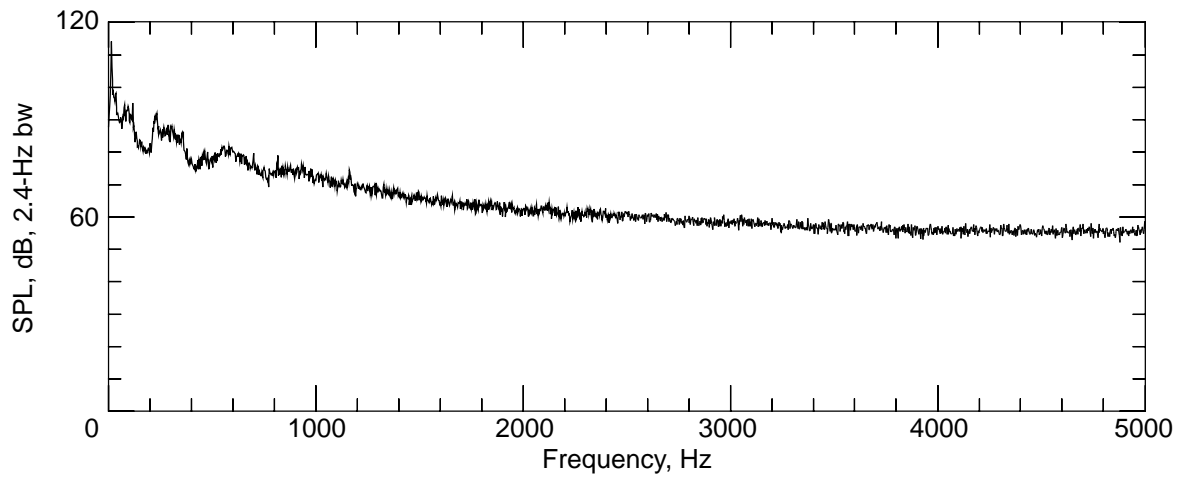
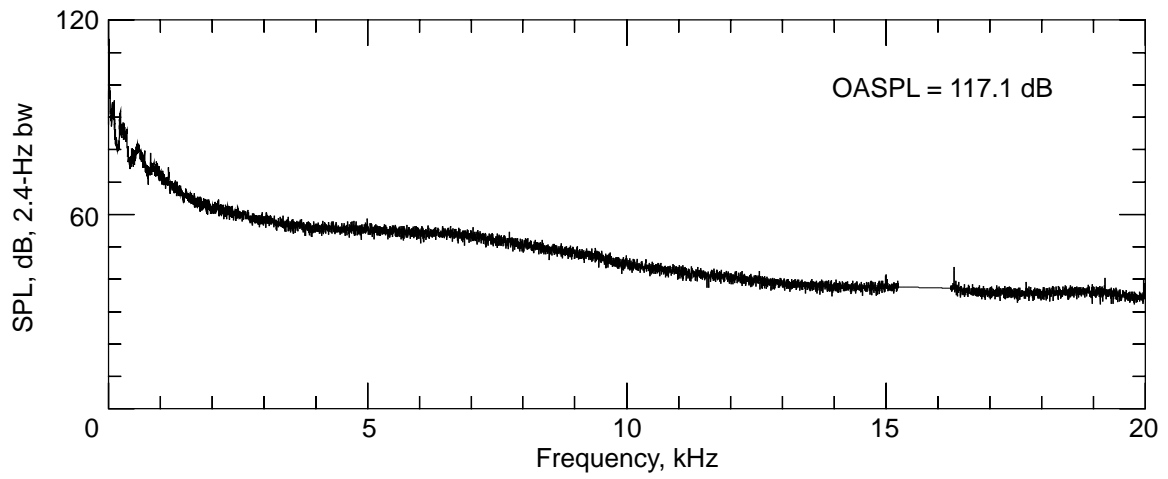
(b) Dynamic pressure = 40 lb/ft<sup>2</sup>.

Figure 27. Continued.



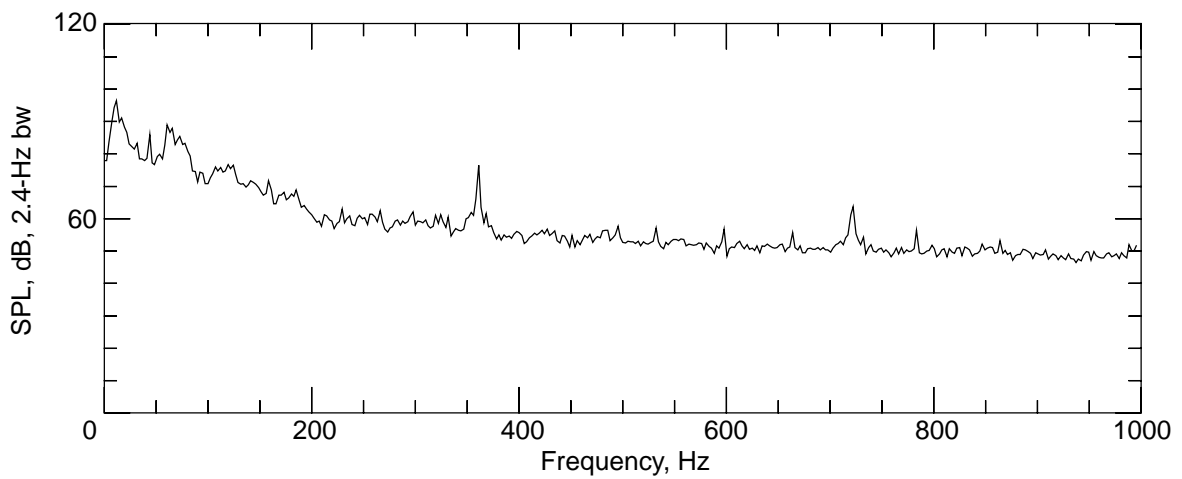
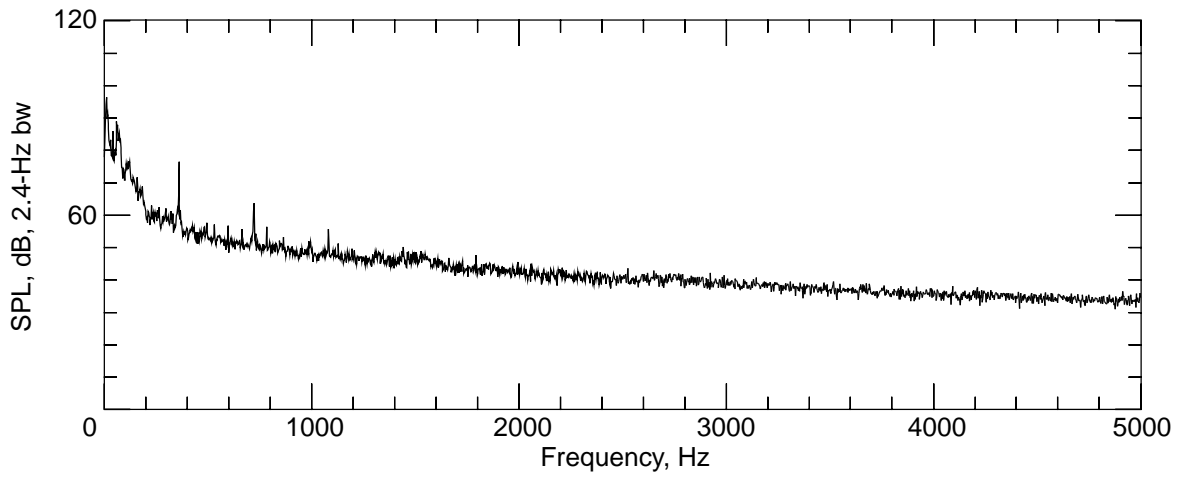
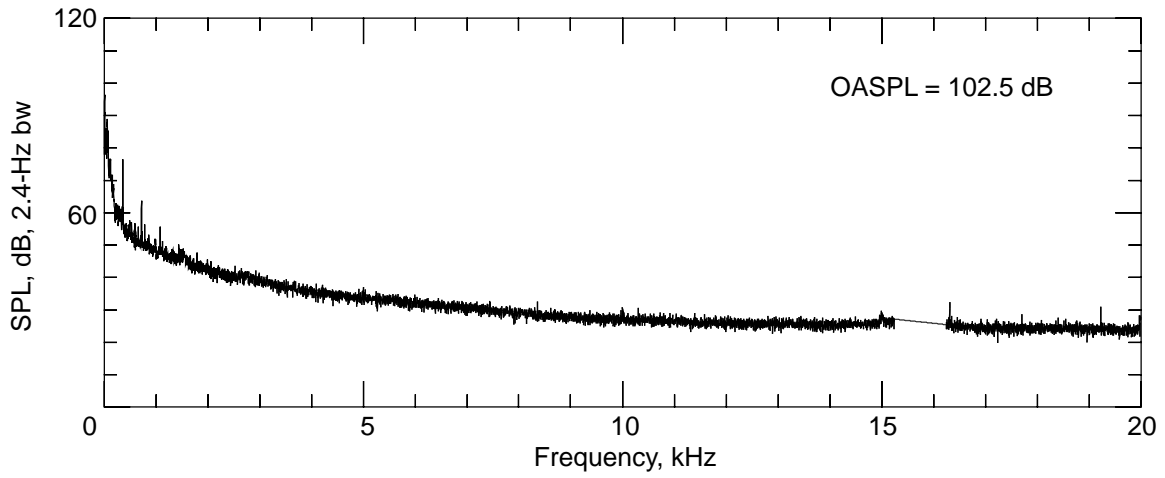
(c) Dynamic pressure = 60 lb/ft<sup>2</sup>.

Figure 27. Continued.



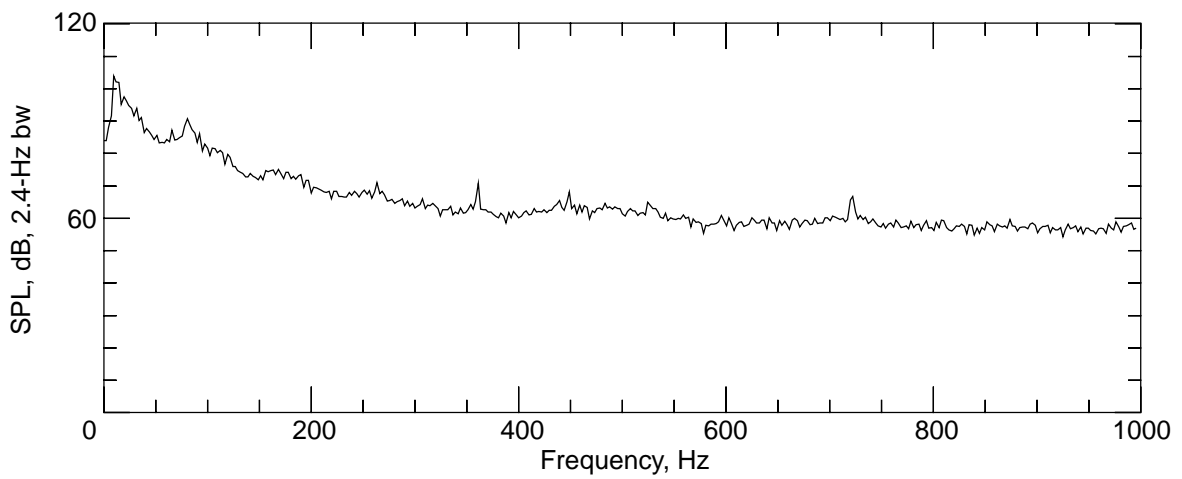
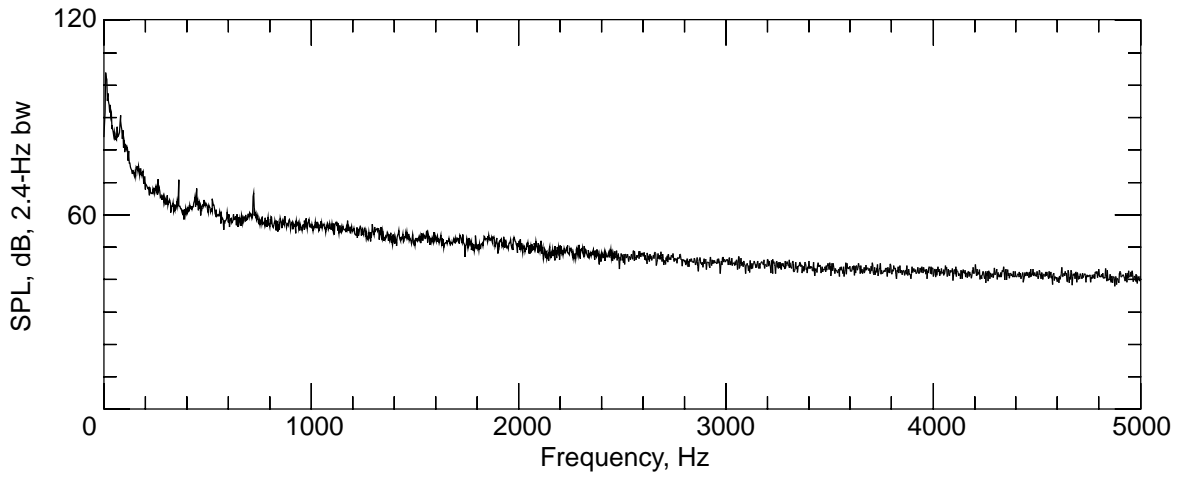
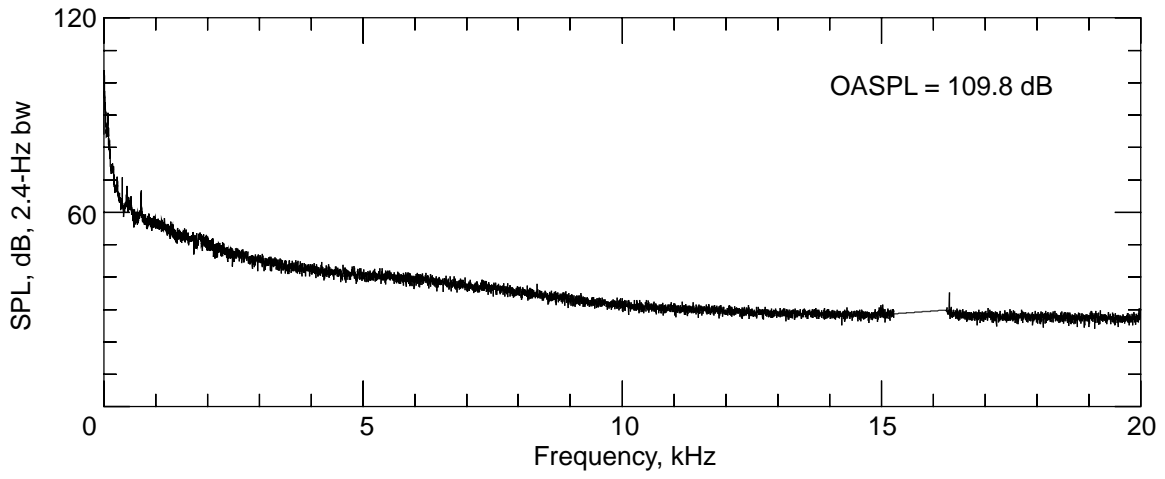
(d) Dynamic pressure = 70 lb/ft<sup>2</sup>.

Figure 27. Concluded.



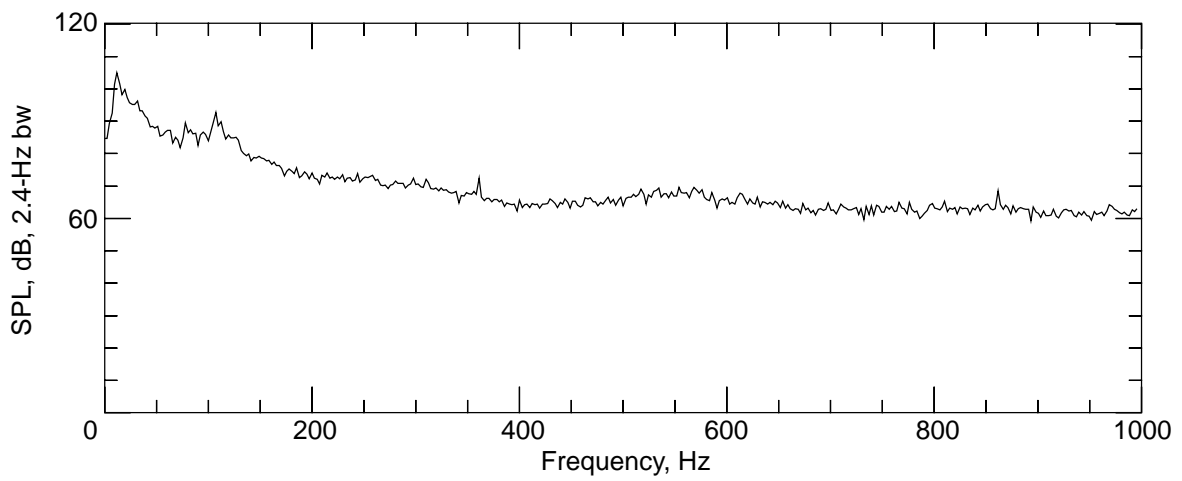
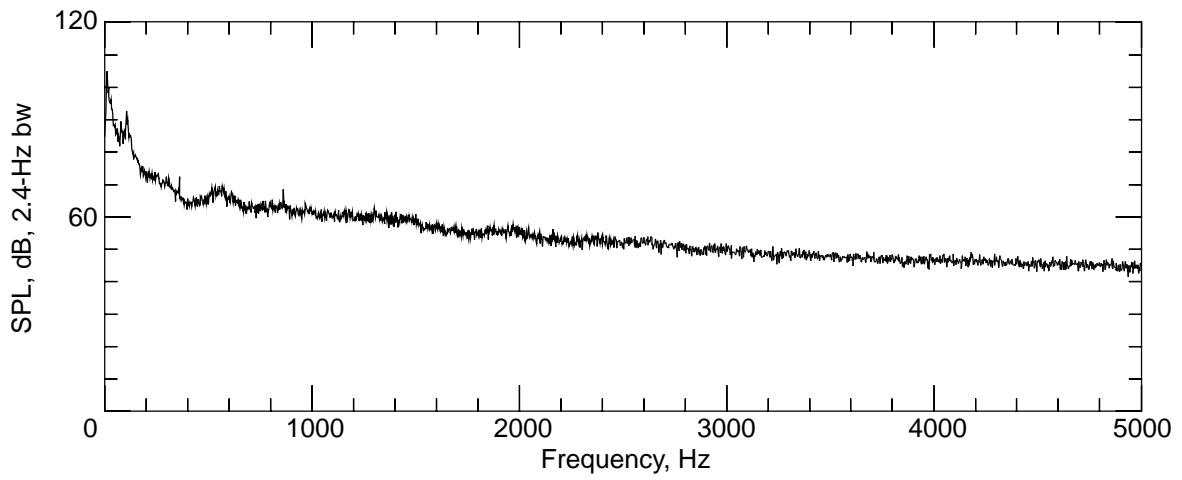
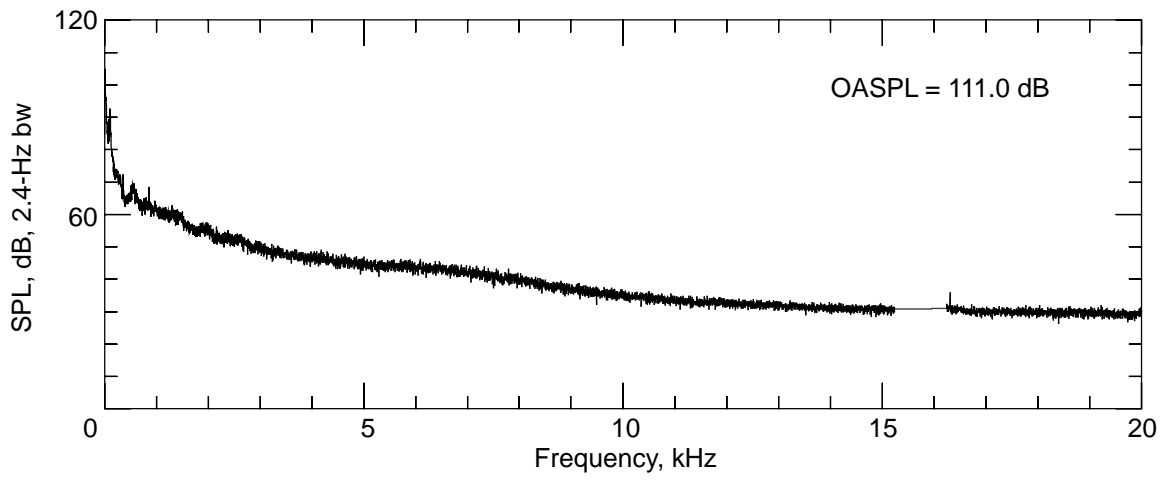
(a) Dynamic pressure = 20 lb/ft<sup>2</sup>.

Figure 28. Flow noise measurement in settling chamber.



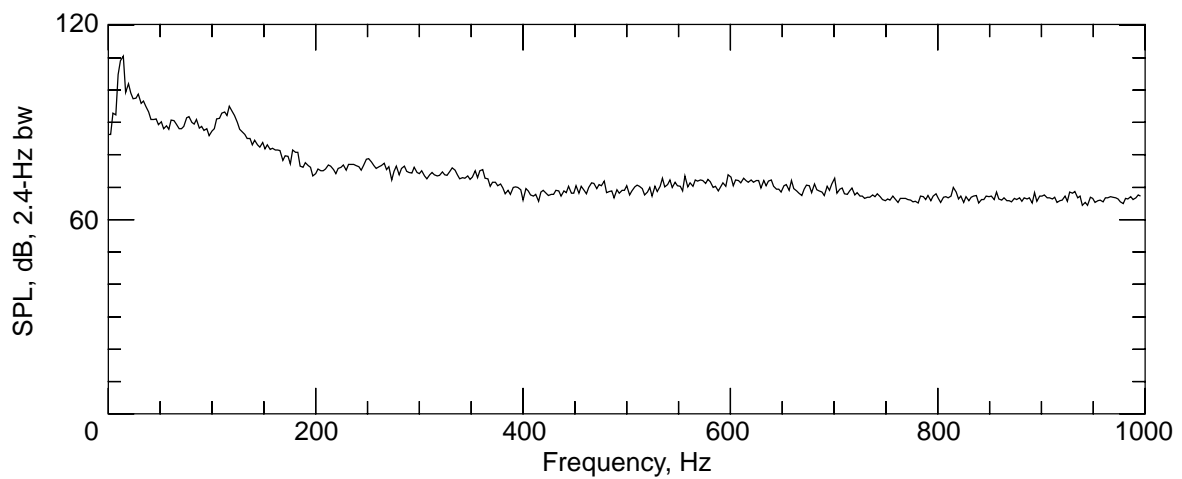
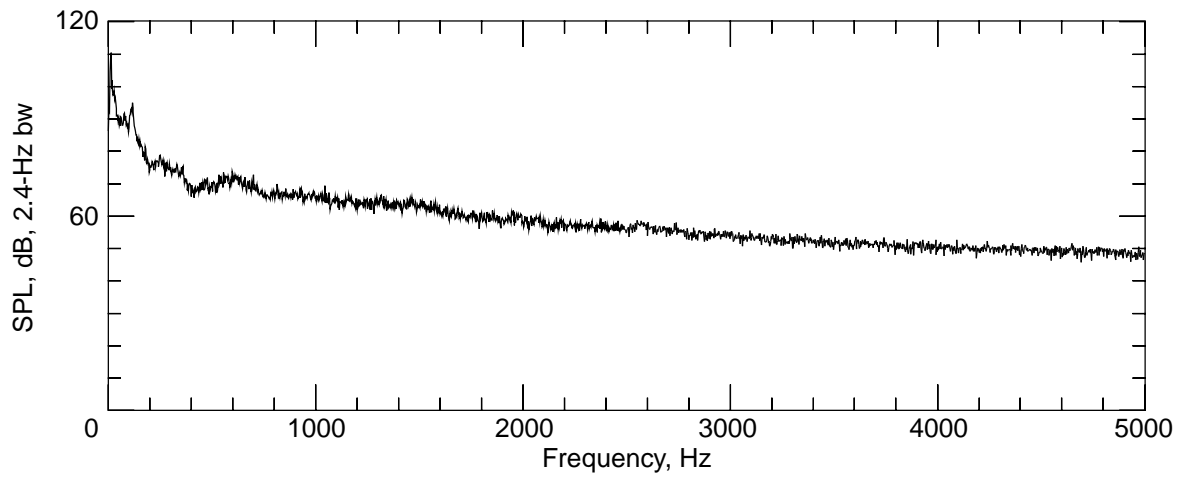
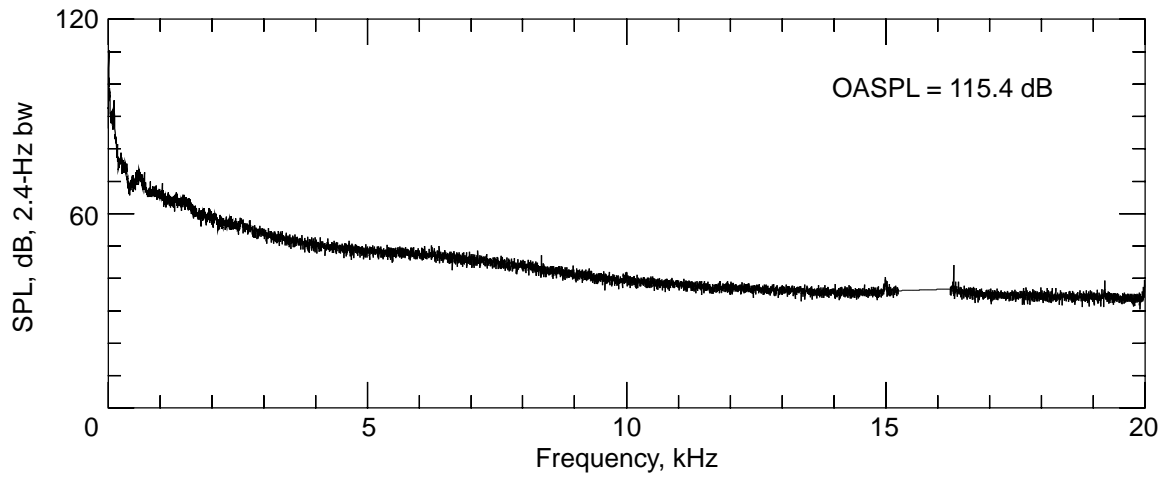
(b) Dynamic pressure = 40 lb/ft<sup>2</sup>.

Figure 28. Continued.



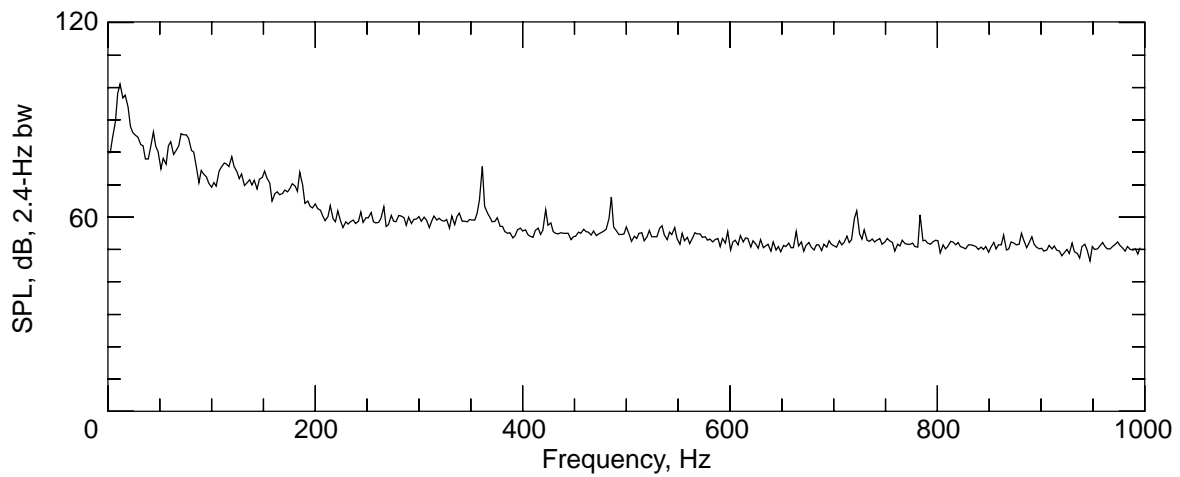
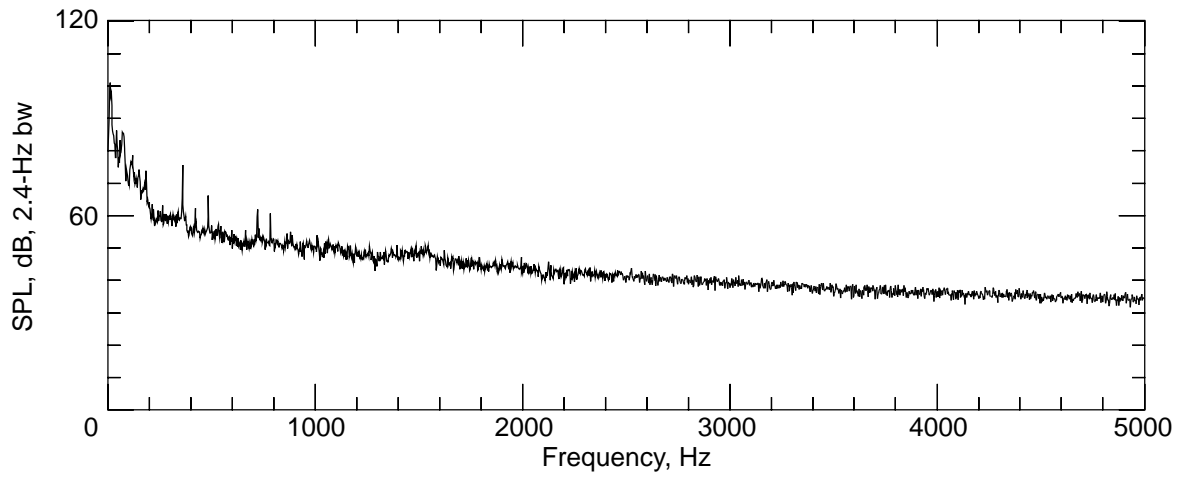
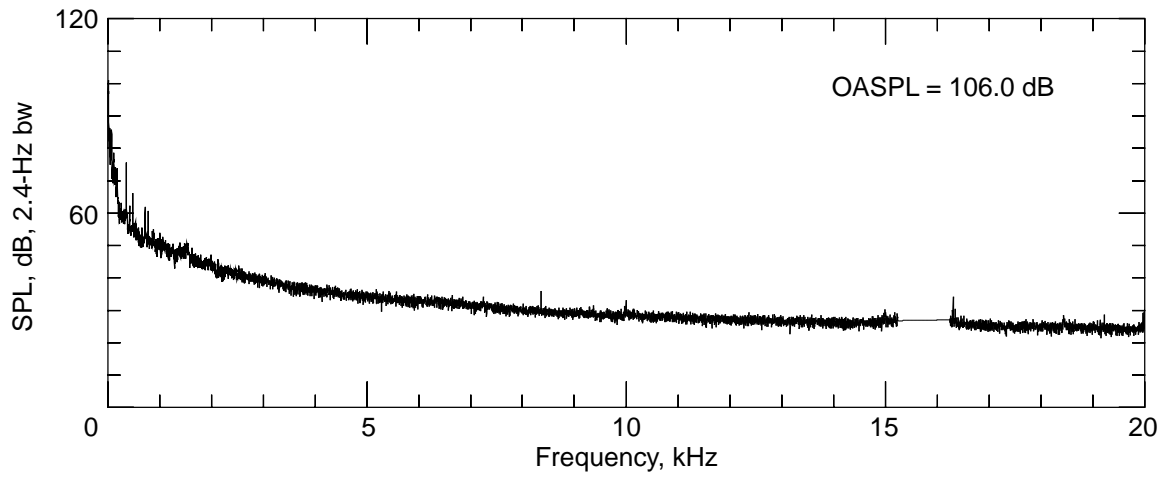
(c) Dynamic pressure = 60 lb/ft<sup>2</sup>.

Figure 28. Continued.



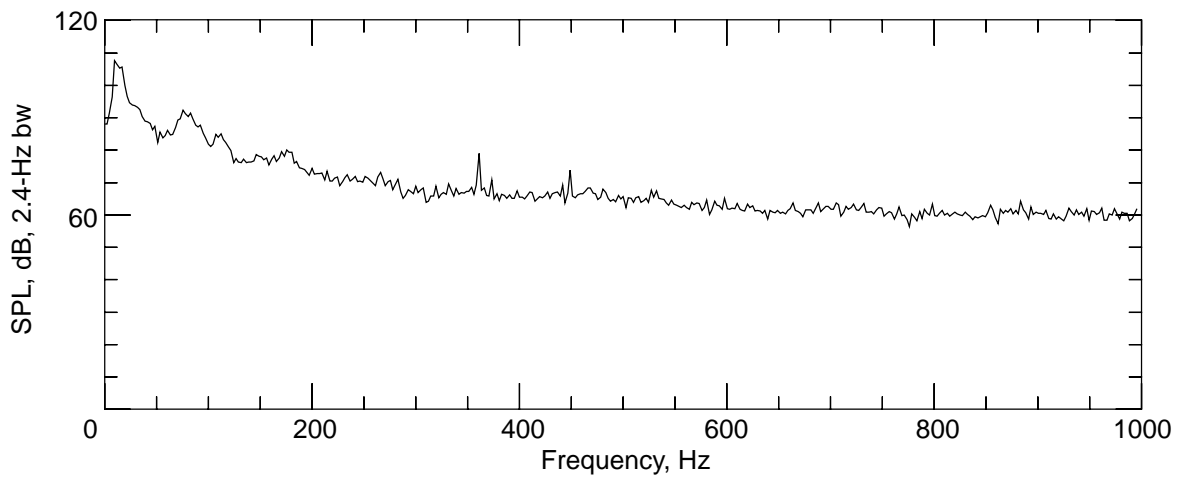
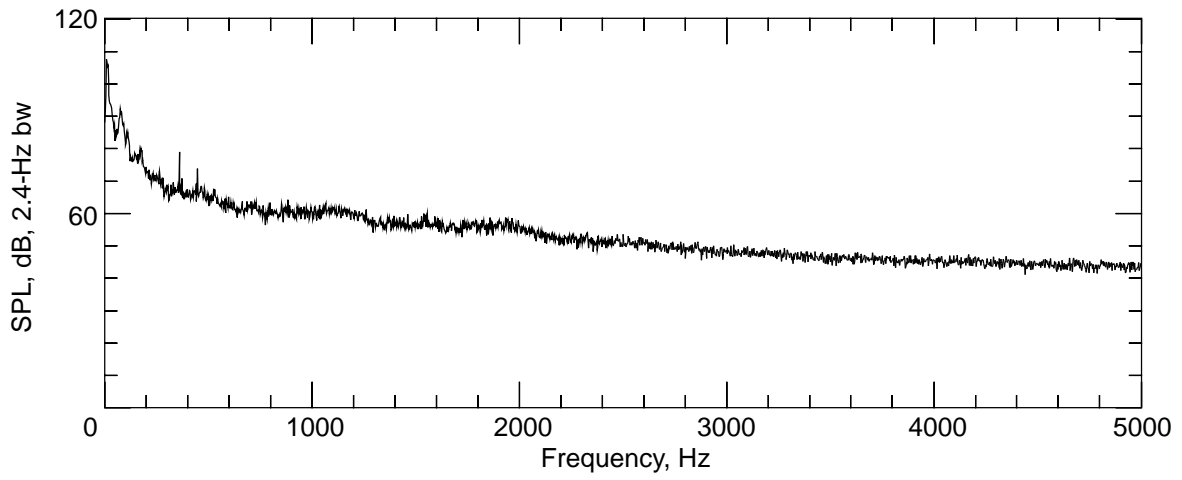
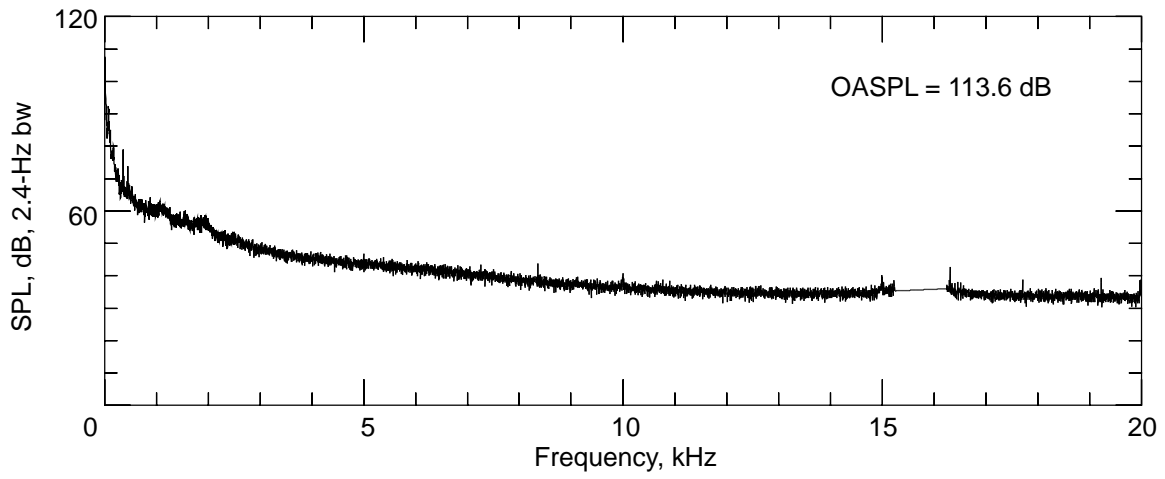
(d) Dynamic pressure = 70 lb/ft<sup>2</sup>.

Figure 28. Concluded.



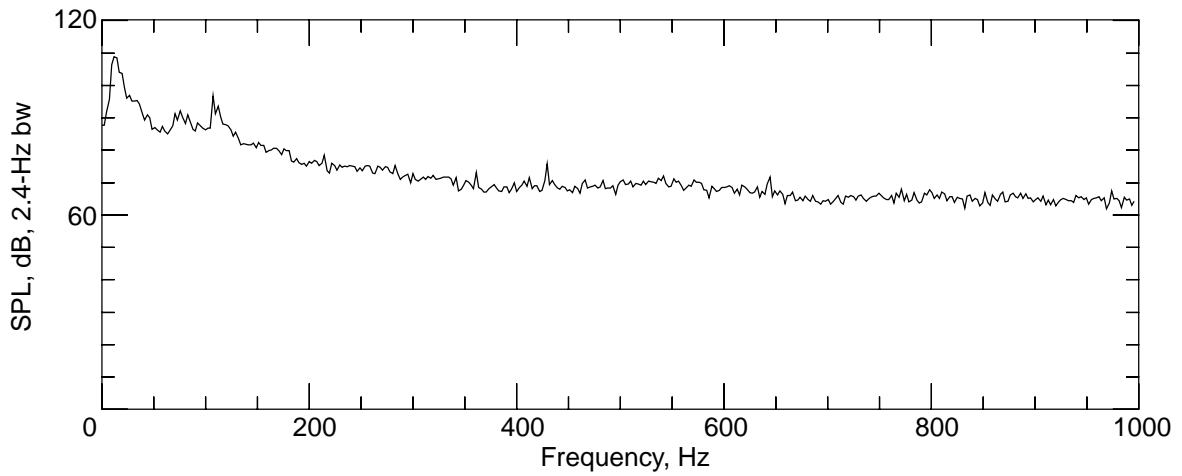
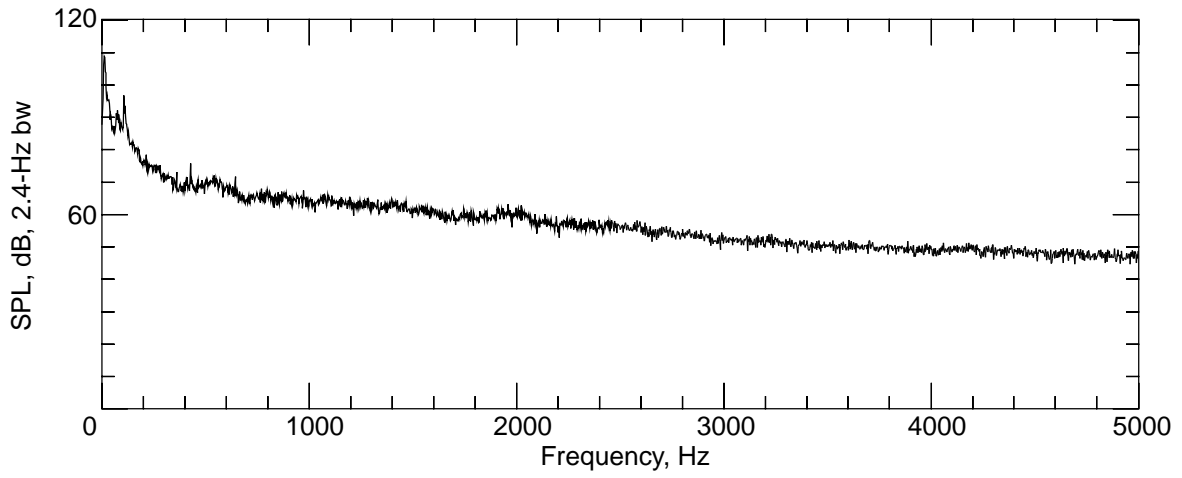
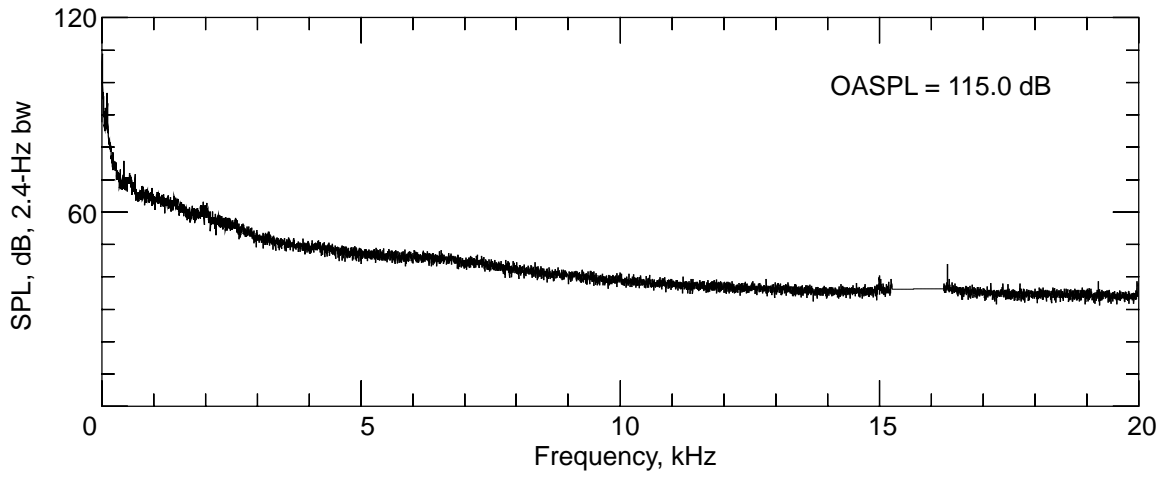
(a) Dynamic pressure = 20 lb/ft<sup>2</sup>.

Figure 29. Flow noise measurement in contraction.



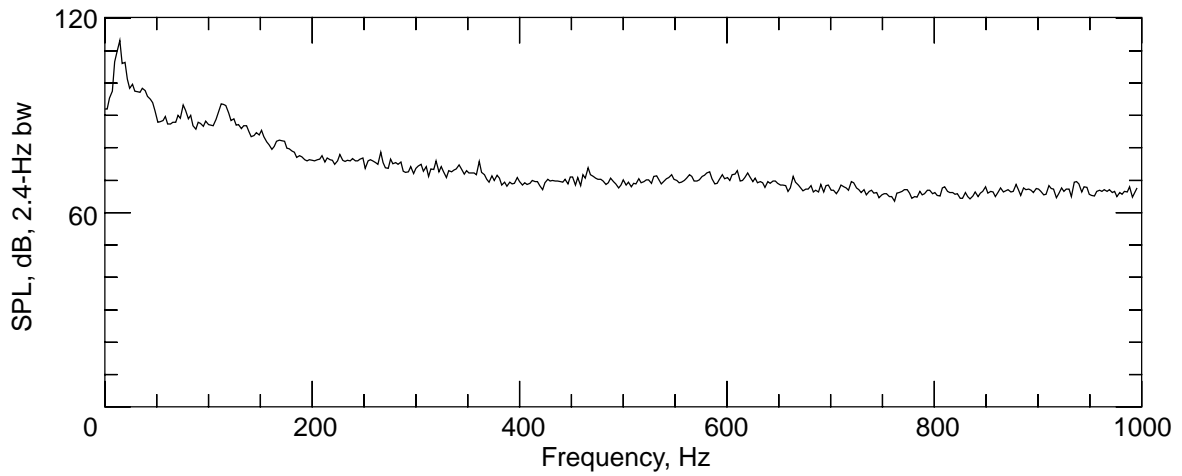
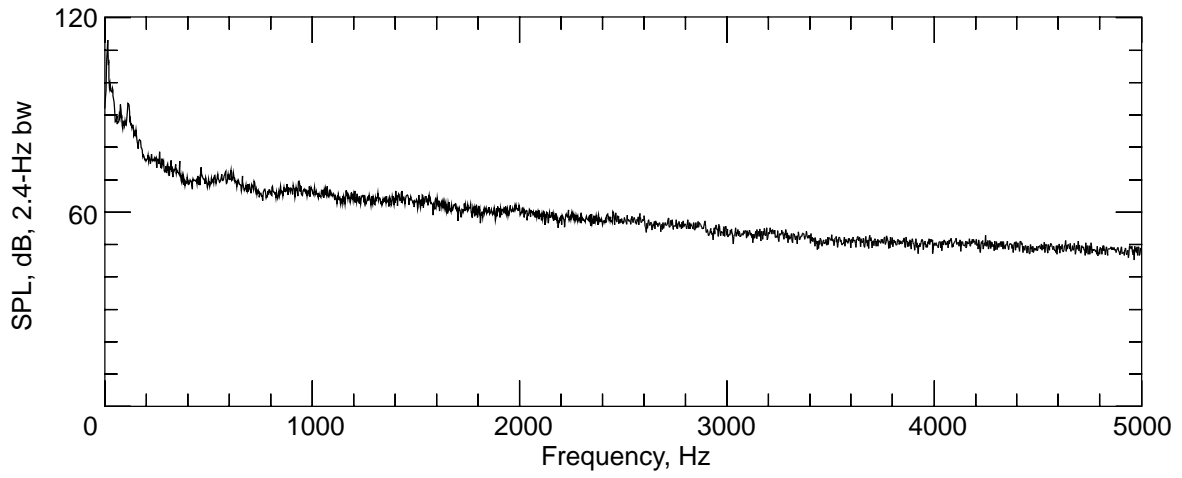
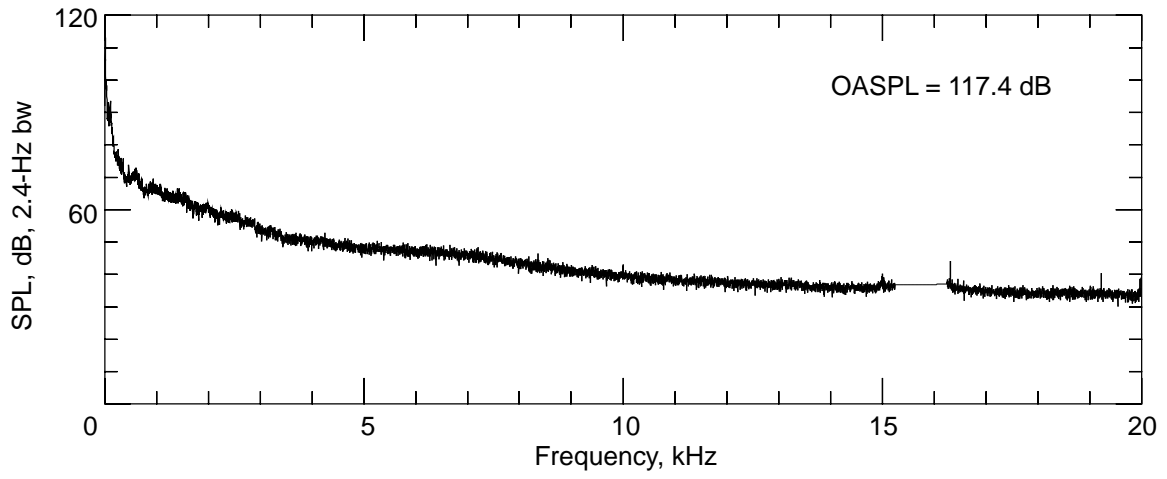
(b) Dynamic pressure = 40 lb/ft<sup>2</sup>.

Figure 29. Continued.



(c) Dynamic pressure = 60 lb/ft<sup>2</sup>.

Figure 29. Continued.



(d) Dynamic pressure = 70 lb/ft<sup>2</sup>.

Figure 29. Concluded.



## REPORT DOCUMENTATION PAGE

*Form Approved*  
*OMB No. 0704-0188*

Public reporting burden for this collection of information is estimated to average 1 hour per response, including the time for reviewing instructions, searching existing data sources, gathering and maintaining the data needed, and completing and reviewing the collection of information. Send comments regarding this burden estimate or any other aspect of this collection of information, including suggestions for reducing this burden, to Washington Headquarters Services, Directorate for Information Operations and Reports, 1215 Jefferson Davis Highway, Suite 1204, Arlington, VA 22202-4302, and to the Office of Management and Budget, Paperwork Reduction Project (0704-0188), Washington, DC 20503.

<b>1. AGENCY USE ONLY</b> <i>(Leave blank)</i>	<b>2. REPORT DATE</b> October 1996	<b>3. REPORT TYPE AND DATES COVERED</b> Technical Memorandum	
<b>4. TITLE AND SUBTITLE</b> Acoustic Survey of a 3/8-Scale Automotive Wind Tunnel		<b>5. FUNDING NUMBERS</b> WU 505-59-52-01	
<b>6. AUTHOR(S)</b> Earl R. Booth, Jr., Gary Romberg, Larry Hansen, and Ron Lutz			
<b>7. PERFORMING ORGANIZATION NAME(S) AND ADDRESS(ES)</b> NASA Langley Research Center Hampton, VA 23681-0001		<b>8. PERFORMING ORGANIZATION REPORT NUMBER</b> L-17487	
<b>9. SPONSORING/MONITORING AGENCY NAME(S) AND ADDRESS(ES)</b> National Aeronautics and Space Administration Washington, DC 20546-0001		<b>10. SPONSORING/MONITORING AGENCY REPORT NUMBER</b> NASA TM-4736	
<b>11. SUPPLEMENTARY NOTES</b> Booth: Langley Research Center, Hampton, VA; Romberg: Chrysler Technology Center, Auburn Hills, MI; Hansen: Enviro-Acoustics Co., Minneapolis, MN; Lutz: Sverdrup Technologies Corp., Tullahoma, TN.			
<b>12a. DISTRIBUTION/AVAILABILITY STATEMENT</b> Unclassified-Unlimited Subject Category 71 Availability: NASA CASI (301) 621-0390		<b>12b. DISTRIBUTION CODE</b>	
<b>13. ABSTRACT</b> <i>(Maximum 200 words)</i> An acoustic survey that consists of insertion loss and flow noise measurements was conducted at key locations around the circuit of a 3/8-scale automotive acoustic wind tunnel. Descriptions of the test, the instrumentation, and the wind tunnel facility are included in the current report, along with data obtained in the test in the form of 1/3-octave-band insertion loss and narrowband flow noise spectral data.			
<b>14. SUBJECT TERMS</b> Acoustic wind tunnel; Background noise level; Noise sources; Acoustic calibration; Open jet section			<b>15. NUMBER OF PAGES</b> 85
			<b>16. PRICE CODE</b> A05
<b>17. SECURITY CLASSIFICATION OF REPORT</b> Unclassified	<b>18. SECURITY CLASSIFICATION OF THIS PAGE</b> Unclassified	<b>19. SECURITY CLASSIFICATION OF ABSTRACT</b> Unclassified	<b>20. LIMITATION OF ABSTRACT</b>